Doctoral Dissertation

Studies on Control of Oxygen-Oxygen Bond Cleavage of Copper-Peroxide Complexes

Tetsuro Tano

January 2014

Department of Material and Life Science

Graduate School of Engineering

Osaka University

Contents

General Introduction

Active-oxygen species of transition-metal ions have attracted much attention in wide variety of research fields. In catalytic and synthetic organic chemistry, for example, first-row transition metal, such as iron and copper, have been recognized as a powerful catalyst in several organic reactions, such as C–C, C–O and C–N bond formation reactions, epoxidation of alkenes, oxidation or polymerization of phenols, and so on.[1,2] In addition, application of transition-metal catalysts for catalytic hydroxylation of alkanes, which is a subject of extensive studies in industrial chemistry, has also been much recent attention. At the present time, however, these reactions are operated at high temperature and high-pressure conditions, with low efficiency and selectivity. In recent years, there has been growing demand for new environmentally-friendly methods for large-scale application of substrate oxidation reactions, which should proceed with high atom-economy using ecologically-benign molecular oxygen or hydrogen peroxide as a terminal oxidant under mild conditions. Although the understanding the activation mechanism of dioxygen or peroxides on the metal center is important to circumvent these problems, the mechanism of many of these reactions is poorly understood to date.

On the other hand, in biological systems, transition-metal active-oxygen species have been invoked as key reactive intermediates in various enzymatic reactions. For example, the iron-oxide species have been widely recognized as the active oxidant in the catalytic substrate-oxidation cycle by heme-containing enzymes, such as cytochrome P450.[3,4] Copper active-oxygen species are also important due to their strong relevance to the reactive intermediates involved in copper monooxygenases, including dopamine β-monooxygenase (DβM), peptidylglycine-α-hydroxylating monooxygenases (PHM), tyrosinase (Tyr), and so on.[5] For instance, X-ray structural analysis by Amzel and his co-workers has recently demonstrated existence of a mononuclear copper-dioxygen adduct (probably copper(II)-superoxide) in the oxy-form of PHM.[6] To evaluate the catalytic mechanisms of these enzymes, much deeper insights into the structure, physicochemical properties, and reactivity of the transition-metal active-oxygen species are required.

The ability of metalloenzyme monooxygenases has inspired chemists to develop small molecule catalysts that can mimic such efficient enzymatic reactivities and can be

adopted to synthetic organic reactions. Recent efforts in synthetic modeling bioinorganic chemistry have focused on heme and non-heme oxo-iron complexes, leading comprehensive understanding of their structure, physicochemical properties, and reactivity. The formation mechasnim of iron-oxide complexes has also been investigated extensively to show that homolytic O–O bond cleavage of a iron(III)-hydroperoxide complex (Fe^{III}-OOH) gives a iron(IV)-oxide (Fe^{IV}=O) complexes, whereas heterolytic O–O bond cleavage of Fe^{III}-OOH generates a iron(V)-oxide complex (Fe^{V}=O).[7] Both iron-oxide complexes have been suggested as the key reactive intermediate in a variety of iron-catalyzed oxidation/oxygenation reactions (Scheme 1).[8,9] So far, several types of supporting ligands including external co-ligand have been examined in order to control not only the O–O bond cleavage process but also the reactivity of the generated iron-oxide complexes. The insights gained from these studies have provided important information for the development of catalytic alkane and aromatic hydroxylation reactions[10] and epoxidation and *cis*-dihydroxylation of olefins.[11]

Scheme 1. O–O bond cleavage pattern of Fe^{III}-OOH producing iron-oxide complexes

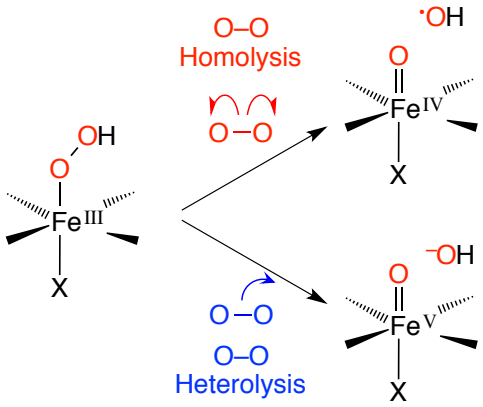

On the other hand, a number of discrete copper active oxygen complexes have also been developed and their structure and physicochemical properties have been well-characterized by X-ray crystallographic analysis and various spectroscopic techniques.[12] As shown in Scheme 2, the reaction of copper(I) complex (LCu^{I}) and dioxygen (O_2) produces a mononuclear copper(II)–superoxide complex ($LCu^{I}O_2$), both

of end-on and side-on binding mode. The binding mode of O_2 has been shown to be controlled by supporting ligands.[13] In many cases, however, the mononuclear copper(II)-superoxide complexes further react with another molecule of copper(I) precursor complex to give end-on and side-on μ-peroxide dicopper(II) complexes.[14,15] Furthermore, from the side-on dicopper(II)-peroxo, homolytic cleavage of the O–O bond takes place in certain ligand systems to provide bis(μ-oxo)dicopper(III) complexes.[16] In this case, two more electrons are injected to the peroxide moiety from each copper(II) ion to induce the O–O bond homolytic cleavage.

Scheme 2

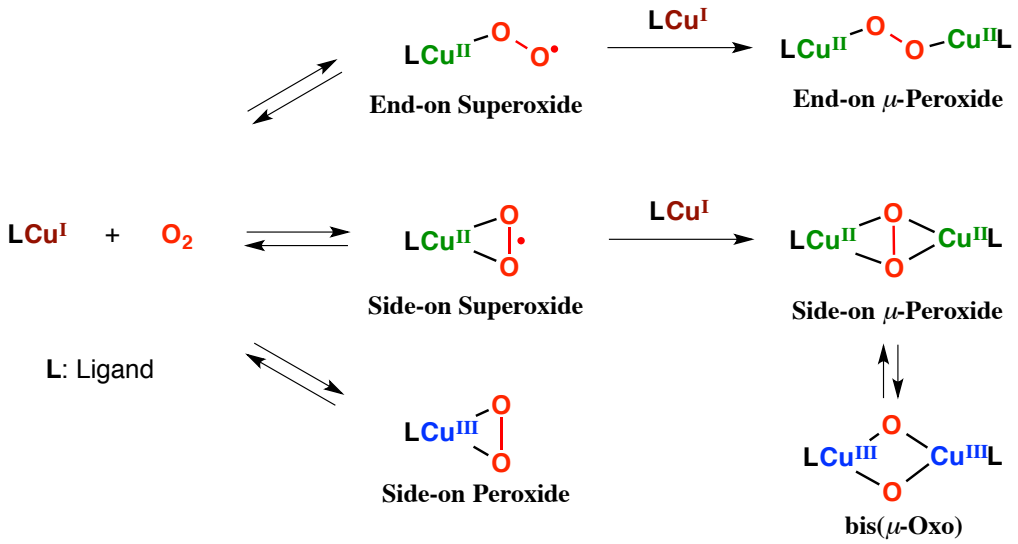

In contrast to the extensive studies on dinuclear dicopper(II)-peroxide complexes, less has been explored about the structures, physicochemical properties, and reactivity of the mononuclear copper active complexes. In principle, one-electron reduction of the superoxide complex and subsequent protonation of the generated copper(II)-peroxide complex or direct hydrogen atom transfer to superoxide species provide a copper(II)-hydroperoxide complex (Scheme 3).[17] Furthermore, O–O bond cleavage of hydroperoxide complex may take place to provide a mononuclear copper(III)-oxide or copper(II)-oxyl radical type complexes, which may have higher reactivity as compared to the superoxide and hydroperoxide complexes.

Scheme 3. Oxygen activation process at mononuclear copper reaction center

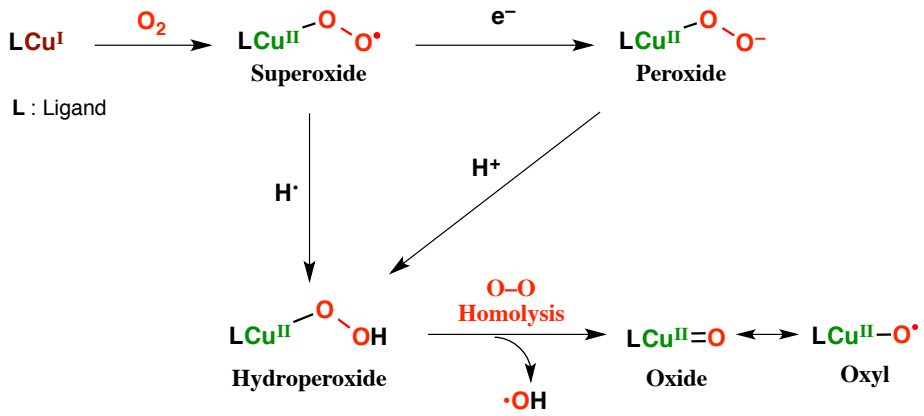

In synthetic modeling studies, however, high reactivity of a mononuclear superoxide species makes it difficult to isolate and characterize the mononuclear copper-active-oxygen complexes. Thus, in order to investigate chemistry of the mononuclear copper(II)-peroxide complexes such as hydroperoxide, alkylperoxide, and acylperoxide complexes, the reactions of copper(II) precursor complexes and hydrogen peroxide (H_2O_2), alkylperoxide (R-OOH), or peracid (RC(O)OOH), so-called shunt pathway, have been employed (Scheme 4).[17] So far, chemical properties of the copper(II)-hydroperoxide complexes have been studied in detail, but the reactivity toward external substrates as well as the O–O bond cleavage process has been less explored. Thus, the studies of this process will give further insights into the catalytic mechanism of copper monooxygenases.

Scheme 4. Generation of mononuclear copper(II) peroxide complexes

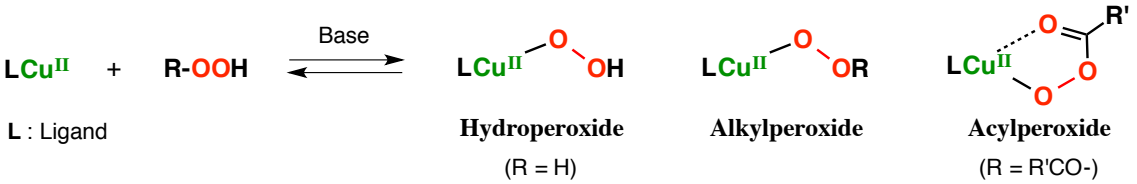

On the basis of these backgrounds, this study is intended to investigate the O–O bond cleavage process of copper(II)-alkylperoxide complexes to find significant ligand effects as well as the importance of oxidation state of the metal center (Cu^{I} vs. Cu^{II}) on the O–O bond cleavage process.

In chapter 1, the author and his co-workers have examined the redox properties of a mononuclear copper(II)-superoxide complex, which exhibits a similar structure as the enzyme active site, toward several types of external substrates in order to get further insights into the intrinsic reactivity of the end-on superoxide copper(II) complex. The author also examined the formation of possible mononuclear copper active-oxygen species such as peroxide and hydroperoxide complex by the reaction with a series of one-electron reductants and hydrogen atom donors, respectively. It has been demonstrated that the redox reactivity of the superoxide complex developed in our research group, exhibiting a four-coordinate distorted tetrahedral geometry, is significantly different from that of the end-on superoxide copper(II) complex, exhibiting a five-coordinate trigonal bipyramidal structure, reported by Schindler et al.[17c,19] Such a difference could be attributed to the different geometry of the superoxide complexes. Reactivity of the generated copper(II)-hydroperoxide complex, however, could not be investigated in detail due to its instability (Scheme 5).

Scheme 5

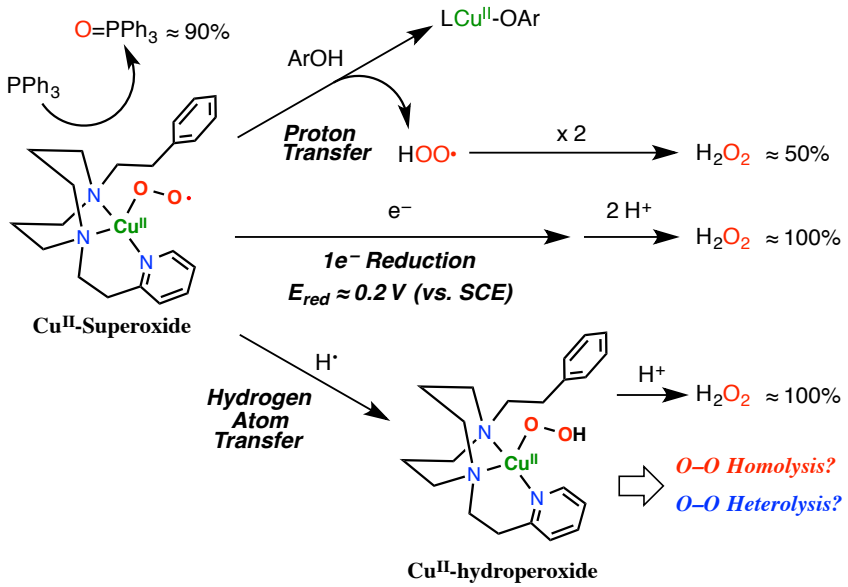

In chapter 2, the author and his co-workers have investigated the reactivity of copper(II)-alkylperoxide complex (LCu^{II}-OOR) supported by simple typical pyridylmethylamine *tridentate* and *tetradentate* ligands in order to gain more insights into ligand effects on the reactivities toward external substrates, paying attention to the oxygen–oxygen bond breaking pattern, of the copper(II)-alkylperoxide complexes. As

a result, it has been demonstrated that the reaction of generated LCu^{II}-OOR complexes with 1,4-cyclohexadiene involves concerted O–O bond homolysis and hydrogen-atom abstraction from the substrate, with the proximal oxygen of the peroxide moiety involved in the C–H bond activation step by detailed product analyses and DFT studies (Scheme 6).

Scheme 6

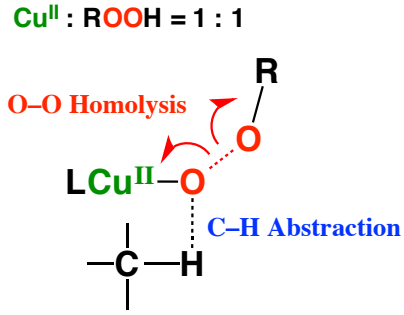

In chapter 3, the author and his co-workers have investigated the reaction of copper(I) complexes supported by similar tridentate ligands used in chapter 2 and cumene hydroperoxide derivatives (^{X}CmOOH; X = Et, Me, H, Br, F, and NO_2) to find that the reaction of the copper(I) complex and ^{X}CmOOH proceeded quite smoothly in a 2 : 1 stoichiometry to give the cumyl alcohol derivatives (^{X}CmOH) as the major product in contrast to the reaction between the copper(II) complexes and ^{X}CmOOH, which gives acetophenone as the major product. The results clearly indicate that the copper(I) complexes induces O–O bond heterolysis, where two electrons are supplied from two molecules of copper(I) complexes (Scheme 7).

Scheme 7

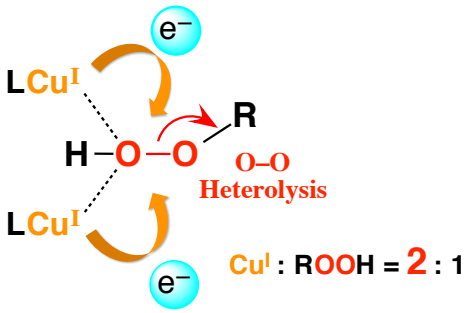

Finally in chapter 4, in order to develop a N_2S coordination environment found in the copper monooxygenases such as PHM and DβM, the author and his co-workers have developed copper complexes supported by a sulphur-containing tridentate ligand

in order to examine the effect of sulfur atom on their structure and redox properties. The copper(I) complex supported by the N_2S ligand exhibits no reactivity toward O_2, being in sharp contrast to the high reactivity of the copper(I) complex supported by the related N_3 ligand used in Chapter 1. Nonetheless, the copper(I) complex of the N_2S ligand shows unique reactivity toward CmOOH to induce efficient heterolytic O–O bond cleavage in a 1 : 1 stoichiometry. This is in contrast to the N_3 tridentate ligand complexes, which react with CmOOH in a 2 : 1 stoichiometry. The authors propose that the sulfur atom acts as an electron donor to induce the O–O bond heterolysis (Scheme 8).

Scheme 8

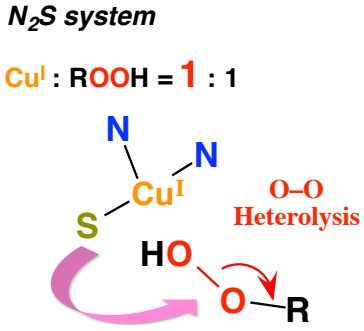

Reference

1. Sun, C. -L.; Li, B. -J.; Shi, Z. -J. *Chem. Rev.* **2011**, *111*, 1293-1314.
2. Allen, S. E.; Walvoord, R. R.; Padilla-Salinas, R.; Kozlowski, M. C. **2013**, *113*, 6234-6458.
3. Meunier, B.; de Visser, S. P.; Shaik, S. *Chem. Rev.* **2004**, *104*, 3947-3980.
4. Denisov, I. G.; Makris, T. M.; Sligar, S. G.; Schlichting, I. *Chem. Rev.* **2005**, *105*, 2253.
5. Klinman, J. P. *Chem. Rev.*, **1996**, *96*, 2541-2562.
6. Prigge, S. T.; Eipper, B. A.; Mains, R. E.; Amzel, L. M. *Science* **2004**, *304*, 864-867.
7. Groves, J. T.; Nemo, T. E.; Myers, R. S. *J. Am. Chem. Soc.* **1979**, *101*, 1032-1033.
8. Nam, W.; Lee, H. L.; Oh, S. –Y; Kim, C.; Jang, H. G. *J. Inorg. Biochem.*

2000, *80*, 219-225.

9. Nam W.; Lim, M. H.; Oh, S. –Y.; Lee, J. H.; Lee, H. J.; Woo, S. K.; Kim, C.; Shin, W. *Angew. Chem., Int. Ed.* **2000**, 39, 3646-3649.
10. Kim, C.; Chen, J.; Kim, L.; Que, L., Jr. *J. Am. Chem. Soc.* **1997**, *119*, 5964-5965.
11. Chen, K.; Costas, M.; Kim, j.; Tipton, A. K.; Que, L., Jr. *J. Am. Chem. Soc.* **2002**, *124*, 3026-3035.
12. 'Copper-Oxygen Chemistry', Eds. Karlin, K. D. & Itoh, S., Wiley Series on Reactive Intermediates in Chemistry and Biology, JOHN WILEY & SONS, INC. **2011**.
13. Itoh, S. Mononuclear copper active-oxygen complexes. *Curr. Opin. Chem. Biol.* **2006**, *10*, 115-122.
14. Mirica, J. M.; Ottenwaelder, X.; Stack, T. D. P. **2004**, *104*, 1013-1045.
15. Lewis, E. A.; Tolman, W. B. *Chem. Rev.* **2004**, *104*, 1047-1076.
16. (a) Tolman, W. B. *Acc. Chem. Res.* **1997**, *30*, 227-237; (b) Holland, P. L.; Tolman, W. B. *Coord. Chem. Rev.* **1999**, *190-192*, 855-869; (c) Blackman, A. G.; Tolman, W. B. In *Metal-Oxo and Metal-Peroxo Species in Catalytic Oxidations*; Springer-Verlag Berlin: Berlin, **2000**; Vol *97*; pp 179-211; (d) Stack, T. D. P. *Dalton trans.* **2003**, 1881-1889; (e) Que, L., Jr.; Tolman, W. B. *Angew. Chem., Int. Ed.* **2002**, *41*, 1114-1137.
17. (a) Fujii, T.; Yamaguchi, S.; Funahashi, Y.; Ozawa, T.; Tosha, T.; Kitagawa, T.; Masuda, H. *Chem. Commun.* **2006**, 4428-4430; (b) Fujii, T.; Yamaguchi, S.; Hirota, S.; Masuda, H. *Dalton Trans.* **2008,** 164-170; (c) Maiti, D.; Lee, D. -H.; Gaoutchenova, K.; Würtele, C.; Holthausen, M. C.; Sarjeant, A. A. N.; Sundermeyer, J.; Schindler, S.; Karlin, K. D. *Angew. Chem., Int. Ed.* **2008**, *47*, 82-85.
18. (a) Kitajima, N.; Fujisawa, K.; Moro-oka, Y. *Inorg. Chem.* **1990**, *29*, 357-358; (b) Kitajima, N.; Katayama, T.; Fujisawa, K.; Iwata, Y.; Moro-oka, Y. *J. Am. Chem. Soc.* **1993**, *115*, 7872-7873; (c) Sanyal, I.; Ghosh, P.; Karlin, K. D. *Inorg. Chem.* **1995**, *34*, 3050-3056; (d) Chen, P.; Fujisawa, K.; Soloman, E. I. *J. Am. Chem. Soc.* **2000**, *122*, 10177-10193; (e) Kunishita, A., Ishimaru, H.; Nakashima, S.; Ogura, T. ; Itoh, S. *J. Am. Chem. Soc.* **2008**, *130*, 4244-4245.

19. Würtele, C.; Gaoutchenova, E.; Harms, K.; Holthausen, M. C.; Sundermeyer, J.; Schindler, S. *Angew. Chem., Int. Ed.* **2006**, *45*, 3867-3869.

Chapter 1 Redox Properties of a Mononuclear Copper(II)-Superoxide Complex

Introduction

Mononuclear copper active-oxygen species are the important reactive intermediates in biological oxygenation reactions.[1-12] Copper monooxygenases such as peptidylglycine α-hydroxylating monooxygenase (PHM), dopamine β-monooxygenase (DβM), and tyramine β-monooxygenase (TβM) have been demonstrated to catalyze aliphatic C–H bond hydroxylation of their respective substrates (dopamine, peptide hormones, and tyramine, respectively) using molecular oxygen (O_2) at a mononuclear copper active site.[1,13-16] It has also been suggested that bacterial depolymerization of polysaccharides is initiated by a class of copper oxygenases (GH61 and CBM33), in which O_2-activation is taking place at a mononuclear copper reaction center for the substrate oxygenation.[17-21] So far, the series of mononuclear copper active-oxygen species such as superoxide (**A**), peroxide (**B**), hydroperoxide (**C**), and oxyl radical (**D**) complexes have been proposed as the key reactive intermediate for the direct aliphatic C–H bond activation both from the enzymatic and computational studies.[1,4,13,15,22-31]

Scheme 1-1

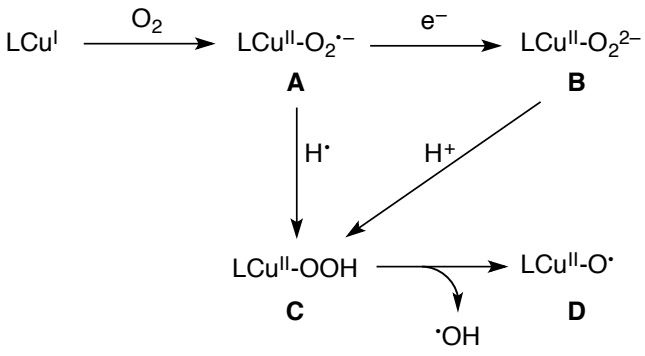

In principle, the reaction of a mononuclear copper(I) complex and O_2 gives a mononuclear copper(II)-superoxide complex **A**, from which a copper(II)-hydroperoxide complex **C** can be generated by the one-electron reduction of **A** and subsequent

protonation of a copper(II)-peroxide complex **B** or direct hydrogen atom transfer to **A** from a substrate. Furthermore, O–O bond homolysis of the hydroperoxide complex **C** may occur to provide a mononuclear copper(II)-oxyl radical species **D** (Scheme 1-1). In synthetic modeling systems, however, copper(II)-superoxide complex **A** tends to react with another molecular of copper(I) starting material to give a dinuclear copper(II)-peroxide complex (not shown in Scheme 1-1), making it difficult to isolate and characterize the mononuclear copper active-oxygen complexes in the reaction of copper(I) complexes and O_2.[2,3,12] Nonetheless, a couple of mononuclear copper(II) end-on superoxide complexes have recently been characterized,[32,33] and one of them, $(TMG_3tren)Cu^{II}$-$OO^{\bullet}$, has been successfully isolated by using the tetramethylguanidine derivative of tripodal *tetradentate* tren ligand (tris(2-aminoethyl)amine) (Chart 1-1),[34] providing important insights into the structure and chemical properties of the proposed reaction intermediate of the mononuclear copper oxygenases.[35-37] We have also studied the reactivity of the end-on superoxide copper(II) complex $\mathbf{2^{O2}}$ generated by using a *tridentate* ligand L (Chart 1-1) to demonstrate that $\mathbf{2^{O2}}$ can directly induce aliphatic hydroxylation at the benzylic position of the ligand sidearm, providing important insight into the catalytic mechanism of PHM and DβM.[38,39] In this study, the author and his co-workers have examined the redox properties of $\mathbf{2^{O2}}$ toward several types of external substrates in order to get further insights into the intrinsic reactivity of the end-on superoxide copper(II) complex and to see how the supporting ligand affects the reactivity of the superoxide complexes. The author has also tried to see the formation of possible mononuclear copper active oxygen species such as peroxide (one-electron reduced product **B**), hydroperoxide (hydrogen atom adduct **C**), and oxyl radical (**D**) complexes, which could be derived from $\mathbf{2^{O2}}$ in the reactions with external substrates (see Scheme 1-1).

Chart 1-1

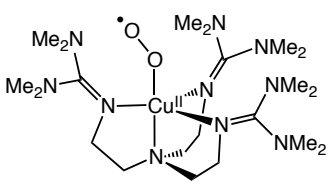

$(TMG_3tren)Cu^{II}$-$OO^{\bullet}$

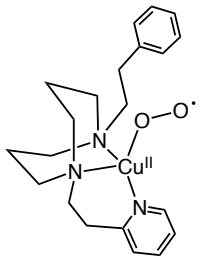

(L)Cu^{II}-$OO^{\bullet}$ ($\mathbf{2^{O2}}$)

Experimental

Materials and Methods. The reagents and the solvents used in this study, except the ligands and the copper complexes, were commercial products of the highest available purity and were further purified by the standard methods, if necessary.[40] The Ligand 1-(2-phenethyl)-5-[2-(2-pyridyl)ethyl]-1,5-diazacyclooctane (**L**) and its copper(I) complex $[(L)Cu^{I}]PF_6$ (**1**) were prepared according to the reported procedures.[38] FT-IR spectra were recorded on a Jasco FTIR-4100, and UV-visible spectra were taken on a Hewlett Packard 8453 photo diode array spectrophotometer. ^{1}H-NMR spectra were recorded on a JEOL LMN–ECP300WB, a JEOL ECP400, a JEOL ECS400, or a Varian UNITY INOVA 600MHz spectrometer. ESI-MS (electrospray ionization mass spectra) measurements were performed on a PerSeptive Biosystems Mariner™ Biospectrometry workstation. Elemental analyses were performed on a Perkin-Elmer or a Fisons instruments EA1108 Elemental Analyzer.

Synthesis.

$[Cu^{II}(L)(OAc)](BF_4)$ ($\mathbf{2^{OAc}}$). Ligand **L** (20 mg, 62 μmol) was treated with an equimolar amount of $Cu^{II}(CH_3COO)_2 \bullet H_2O$ (12 mg, 62 μmol) in CH_2Cl_2 (5.0 mL). After stirring the mixture for 5 min at room temperature, $NaBF_4$ (6.8 mg, 62 μmol) was added to the solution. Insoluble material was then removed by filtration. Addition of *n*-hexane (100 mL) to the filtrate gave a blue powder that was precipitated by standing the mixture for several minutes. The supernatant was then removed by decantation, and the remained blue solid was washed with *n*-hexane three times and dried to give $\mathbf{2^{OAc}}$ in 71 %. FT-IR (KBr) 1610 and 1578 cm^{-1} (OAc^-), 1083 cm^{-1} (BF_4^-); HR-MS (FAB^+) *m*/*z* = 445.1798, calcd for $C_{23}H_{32}N_3O_2Cu$ = 445.1791; Anal. Calcd for $[Cu^{II}(OAc)](BF_4) \bullet 1.5H_2O \bullet 0.1C_6H_{14}$ ($C_{23.6}H_{36.4}BCuF_4N_3O_{3.5}$): C, 49.86; H, 6.45; N, 7.39. Found: C, 49.65; H, 6.39; N, 7.13.

EPR Measurements. The EPR spectrum of the final reaction mixture of copper(II) superoxide complex $\mathbf{2^{O2}}$ and TEMPO-H were recorded on a JEOL X-band spectrometer (JES-RE1XE) with an attached variable temperature apparatus. The EPR spectrum was measured in frozen acetone at 77 K. The magnitude of modulation was chosen to optimize the resolution and the signal-to-noise (S/N) ratio of the observed spectra under non-saturating microwave conditions. The *g* values and the hyperfine coupling constants were calibrated with a Mn^{2+} marker.

Resonance Raman Spectrum. Resonance Raman scattering was excited at 406.7 nm from Kr^+ laser (Spectra Physics, BeamLok 2060). Resonance Raman scattering was dispersed by a single polychromator (Ritsu Oyo Kogaku, MC-100) and was detected by a liquid nitrogen cooled CCD detector (Roper Scientific, LNCCD-1100-PB)The resonance Raman measurements were carried out using a rotated cylindrical cell thermostated at –70 ~ –90 °C by flashing cold liquid nitrogen gas.

Kinetic Measurements. Kinetic measurements for the reactions of copper(II) superoxide complex $\mathbf{2^{O2}}$ with external substrates were performed using a Hewlett Packard 8453 photo diode array spectrophotometer with a Unisoku thermostated cell holder designed for low temperature measurements (USP-203, a desired temperature can be fixed within ± 0.5 °C) in an appropriate solvent (3.0 mL) at a low temperature. For the preparation of the copper(II) superoxide complex $\mathbf{2^{O2}}$, O_2 gas was rapidly introduced to a solution of the copper(I) complex $[(L)Cu^{I}]PF_6$ in a UV cell (1.0 cm path length) through a silicon rubber cap by using a gas-tight syringe, and the increase of the absorption band due to $\mathbf{2^{O2}}$ was monitored. Then, an excess O_2 was removed by flashing Ar gas through a needle for about 5 min, and the substrate was added to start the reactionThe reaction was followed by monitoring the decrease in the LMCT absorption band due to $\mathbf{2^{O2}}$. The pseudo-first-order rate constants for the decay of $\mathbf{2^{O2}}$ were determined from the plots of $\ln(\Delta A)$ *vs*. time based on the time course of the absorption change at λ_{max} due to $\mathbf{2^{O2}}$.

Quantification of H_2O_2. Amount of H_2O_2 was determined by iodometry as follows. A final reaction mixture of $\mathbf{2^{O2}}$ and a substrate was quenched by adding an acetone solution of HPF_6 (2 equiv). Then, the diluted acetone solution (1/10) was treated with an excess NaI. The amount of I_3^- formed was then quantified using its visible spectrum (λ_{max} = 361 nm, ε = 2.5 x 10^4 M^{-1} cm^{-1}).[41]

Results and discussion

Electron-transfer Reduction of $\mathbf{2^{O2}}$. As shown in Scheme 1-1 in Introduction, one-electron reduction of the copper(II)-superoxide complex $\mathbf{2^{O2}}$ may afford a copper(II)-peroxide complex **B**. Thus, the reactions of $\mathbf{2^{O2}}$ with a series of one-electron reductants were examined to search such a possibility. Figure 1-1 shows a typical example of the spectral change for the reaction of $\mathbf{2^{O2}}$ (0.2 mM) with an

equimolar amount of decamethylferrocene ($Me_{10}Fc$) at –85 °C in acetone. The LMCT band at 397 nm due to $\mathbf{2^{O2}}$ gradually decreased with concomitant increase of the absorption band due to the ferrocenium cation ($Me_{10}Fc^+$). The yield of $Me_{10}Fc^+$ was estimated to be 88 % based on the initial concentration of $\mathbf{2^{O2}}$ using intensity of the absorption band due to $Me_{10}Fc^+$ itself (ε = 8.0 x 10^2 M^{-1} cm^{-1} at λ_{max} = 780 nm). This is consistent with a one-electron reduction of the superoxide species. In fact, nearly quantitative formation of H_2O_2 (81 % based on $\mathbf{2^{O2}}$, 92 % based on $Me_{10}Fc^+$ formed) was confirmed by iodometry, and quantitative generation of a copper(II) complex was detected by EPR spectrum. However, all our efforts to isolate the reduced product (type **B** in Scheme 1-1) have been unsuccessful due to its thermal instability, and a complicated mixture of products was obtained, when the reaction mixture was warmed up to room temperature.

The decay of $\mathbf{2^{O2}}$ obeyed second-order kinetics in the presence of the equimolar amount of $Me_{10}Fc$, and the second-order rate constant (k_2) was obtained as 320 ± 2 M^{-1} s^{-1} from the slope of the linear line of the second-order plot shown in the inset of Figure 1-1. The reduction of $\mathbf{2^{O2}}$ also proceeded with octamethylferrocene (Me_8Fc) and *N,N,N'N'*-tetramethylphenylenediamine (TMPD), and the second-order rate constants were determined as 56 ± 0.4 M^{-1} s^{-1} and 9.4 ± 0.06 M^{-1} s^{-1}, (the data are listed in Table 1-1). On the other hand, no reaction took place when weaker reductants such as dimethylferrocene (Me_2Fc) and ferrocene (Fc) were employed under the same experimental conditions (Table 1-1). Based on the one-electron oxidation potentials of TMPD (E_{ox} = 0.12 V vs. SCE) and Me_2Fc (E_{ox} = 0.26 V vs. SCE),[42] the one-electron reduction potential of $\mathbf{2^{O2}}$ was estimated as E_{red} = (0.19 V ± 0.07) vs. SCE. However, the reduction of $\mathbf{2^{O2}}$ was irreversible due to thermal instability of the reduced product; addition of an oxidant such as ferrocenium cation Fc^+ to the final reaction mixture did not reproduce the original superoxide complex $\mathbf{2^{O2}}$. Thus, the estimated E_{red} value is not a true reduction potential.

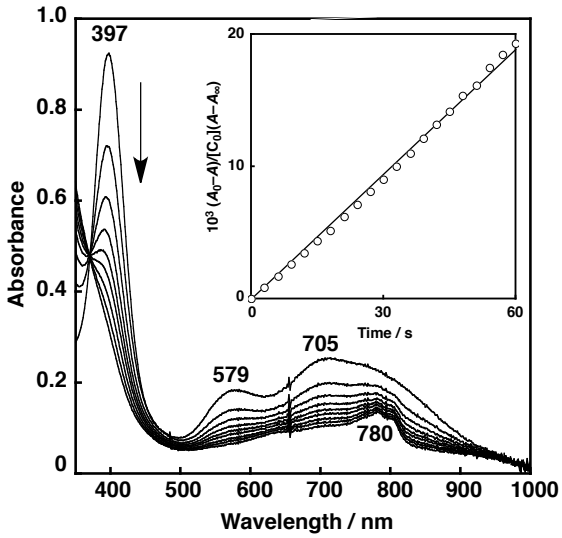

Figure 1-1. The UV-vis spectral change for the reaction of $\mathbf{2^{O2}}$ (0.2 mM) and decamethylferrocene (0.2 mM) in acetone at –85 °C. Inset: Second-order plot based on the absorption change at 397 nm.

Table 1-1. One-electron Oxidation Potential of the Reductants and the Second-order Rate Constants for the Reduction of $\mathbf{2^{O2}}$ in Acetone at –85 °C

	$Me_{10}Fc$	Me_8Fc	TMPD	Me_2Fc	Fc
E^0_{ox} / V vs. SCE[a]	–0.08	–0.04	0.12	0.26	0.37
k_2 / M^{-1} s^{-1}	320 ± 2	56 ± 0.4	9.4 ± 0.06	NR [b]	NR [b]

[a] The data are taken from the literature.[42] [b] No reaction.

Reaction with TEMPO-H (Hydrogen-Atom Donor). Figure 1-2 (left) shows a spectral change for the reaction of $\mathbf{2^{O2}}$ with 2,2,6,6-tetramethylpiperidine-*N*-hydroxide (TEMPO-H) under anaerobic conditions (excess O_2 was removed by flushing Ar gas before the reaction), where the absorption bands due to $\mathbf{2^{O2}}$ decrease to give new absorption bands at 375 nm (ε = 1650 M^{-1} cm^{-1}) and 620 nm (309). The reaction obeyed first-order kinetics in the presence of an excess amount of TEMPO-H (Figure 1-2 (left), Inset), and a plot of the observed pseudo-first-order rate constants against the concentration of TEMPO-H gave a straight line passing through the origin, from which the second rate constant was determined as k_2 = 2.4 ± 0.05 M^{-1} s^{-1} at –85 °C (Figure 1-2,

right).

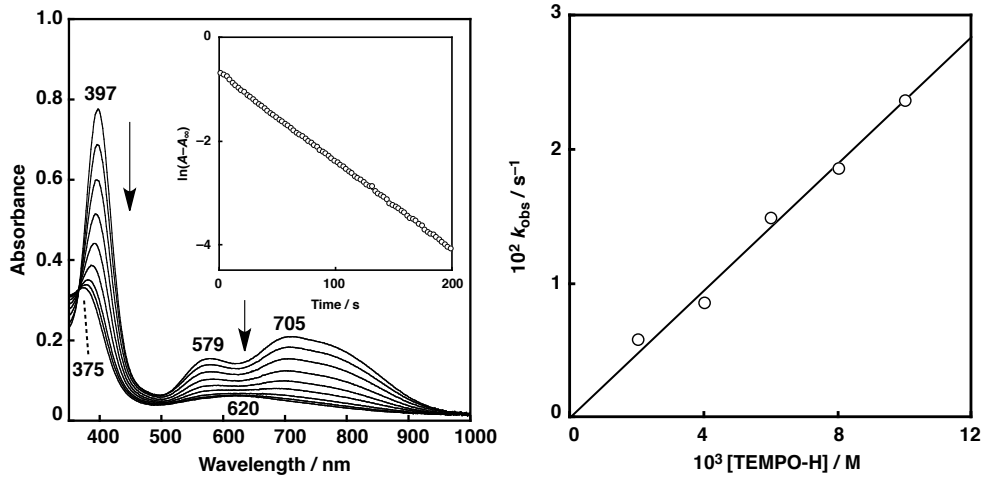

Figure 1-2. Left: The UV-vis spectral change for the reaction of $\mathbf{2}^{\mathbf{O2}}$ (0.2 mM) and TEMPO-H (4.0 mM) in acetone at –85 °C. Inset: Pseudo-first-order plot based on the absorption change at 397 nm. Right: Plot of k_{obs} against the substrate concentration for the reaction of $\mathbf{2}^{\mathbf{O2}}$.

The final spectrum is similar to those of copper(II)-hydroperoxide complexes so far been reported,[43] suggesting the formation of a similar type of copper(II)-hydroperoxide complex $\mathbf{2}^{\mathbf{OOH}}$ (Scheme 1-2), even though resonance Raman data of sufficient quality has yet to be obtained; there is only a very weak Raman band at 831 cm^{-1}, which shifted to 788 cm^{-1}, when the reaction was carried out with ^{18}O-substituted $\mathbf{2}^{\mathbf{O2}}$ (Figure 1-3, left).

Scheme 1-2

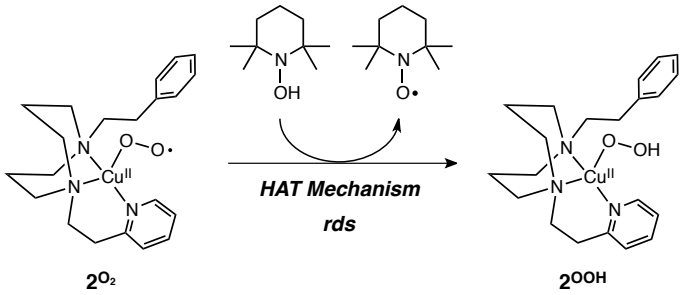

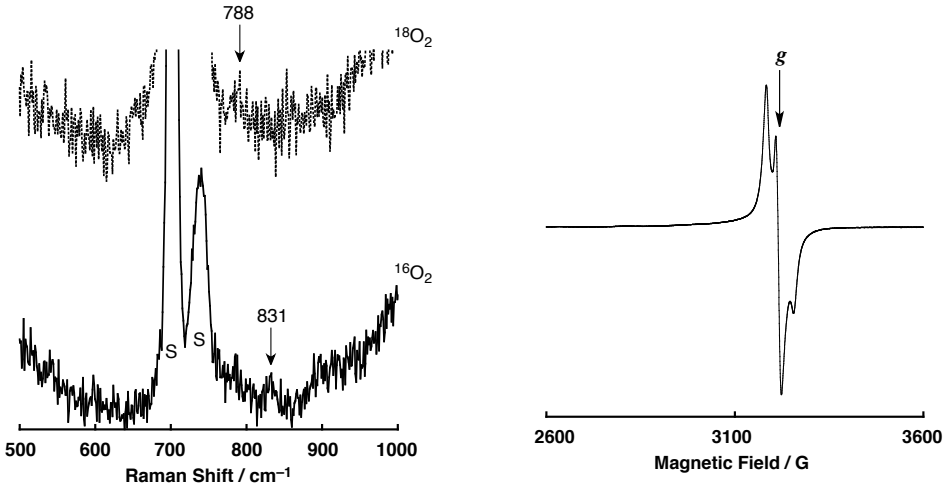

Figure 1-3. Left: Resonance Raman spectra of the reaction mixture of $\mathbf{2}^{\mathbf{O2}}$ (0.2 mM) with TEMPO-H (2.0 mM, solid line, below) and ^{18}O enriched $\mathbf{2}^{\mathbf{O2}}$ (0.2 mM) with TEMPO-H (2.0 mM, doted line, above) obtained with λ_{ex} = 406.7 nm, in CH_2Cl_2 at –85 °C; s denotes the solvent bandRight: EPR spectrum of the final reaction mixture of $\mathbf{2}^{\mathbf{O2}}$ (0.2 mM) with TEMPO-H (0.2 mM) in acetone at 77 K.

The EPR spectrum of the final reaction mixture shown in Figure 1-3 (right) exhibited the typical signal due to TEMPO• free-radical (g = 2.004) (Figure 1-3, right), which is overlapped with a EPR signal of a copper(II) species (Figure 1-3, right). The spin quantification by double integration of the whole EPR signals confirms the existence of two S = 1/2 species corresponding to TEMPO• and copper(II)-hydroperoxide species $\mathbf{2}^{\mathbf{OOH}}$.

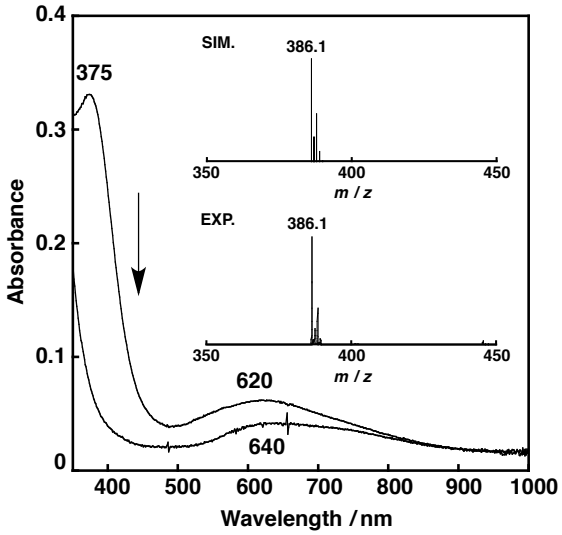

Figure 1-4. The UV-vis spectral change for the self-decomposition of $\mathbf{2}^{\mathbf{OOH}}$ (0.2 mM) in acetone at 30 °C. Inset: Experimental (bottom) and simulated (top) peak envelopes in the positive-ion ESI-MS spectra of the decomposition product of $\mathbf{2}^{\mathbf{OOH}}$ in acetone at 30°C. m/z = 386.1 ($[(\mathbf{L})Cu^{I}]^{+}$).

$\mathbf{2}^{\mathbf{OOH}}$ was relatively stable at –85 °C, but gradually decomposed at room temperature to give a copper(II) complex having a weak d-d band at 640 nm (ε = 210 $M^{-1}cm^{-1}$). In addition, quantitative formation of H_2O_2 (93 % based on the copper complex) was confirmed by iodometry after quenching the final reaction mixture with HPF_6. It should be noted that no ligand hydroxylation product was detected from the final reaction mixture by ESI-MS (Figure 1-4, Inset), and the original ligand was recovered quantitatively by the ordinary work-up treatment (demetallation) of the final reaction mixture using NH_4OH (aq) (Scheme 1-3a). This result is in sharp contrast to the $(TMG_3tren)Cu^{II}$-$OO^{\bullet}$ system, where a ligand hydroxylation took place only after the reaction with hydrogen atom donor such as TEMPO-H or phenols (Scheme 1-3b).[36] The authors concluded that $(TMG_3tren)Cu^{II}$-$OO^{\bullet}$ (type **A** in Scheme 1-1) was not the direct oxidant, but that $(TMG_3tren)Cu^{II}$-$O^{\bullet}$ (type **D**) generated by O–O bond homolysis of $(TMG_3tren)Cu^{II}$-OOH (type **C**), generated by the reaction of **A** and the hydrogen

atom donor, might be the reactive intermediate that induced the ligand methyl hydroxylation.[36] On the other hand, our results clearly indicated that the superoxide complex $\mathbf{2^{O2}}$ (Type **A**), but not the hydroperoxide complex $\mathbf{2^{OOH}}$ (type **C**), directly participates to the aliphatic ligand hydroxylation (Scheme 1-3a).[38,39] Such a difference in reactivity between $\mathbf{2^{O2}}$ and $(TMG_3tren)Cu^{II}$-OO$^{\bullet}$ could be attributed in part to the difference in the coordination number and geometry (four-coordinate/tetrahedral vs. five-coordinate/trigonal bipyramidal) as well as to the difference in the kind of donor atoms (alkylamine and pyridine nitrogen atoms vs. imine (guanidine) nitrogen atoms). It is interesting to note that the proposed geometry (distorted tetrahedral)[38] and observed reactivity (direct C–H bond activation)[38] of $\mathbf{2^{O2}}$ are closer to those of the putative reactive intermediate in the enzymes.[44,45]

Scheme 1-3

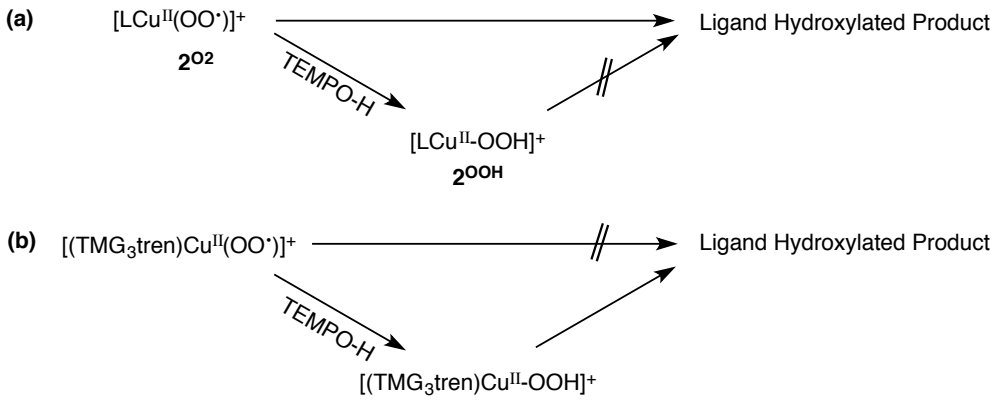

Reaction with Phenol Derivatives. Karlin, Schindler, Sundermeyer, and co-workers reported that the reaction of $(TMG_3tren)Cu^{II}$-OO$^{\bullet}$ and phenols (ArOH) induced hydrogen atom transfer to provide $(TMG_3tren)Cu^{II}$-OOH and phenoxyl radical speceis (ArO$^{\bullet}$), from which the ligand hydroxylation product (Scheme 1-3b) and several phenol oxidation/oxygenation products were produced.[36] Thus, the author and his co-workers also investigated the reaction of $\mathbf{2^{O2}}$ with phenol derivatives to compare the reactivity between $\mathbf{2^{O2}}$ and $(TMG_3tren)Cu^{II}$-OO$^{\bullet}$. Figure 1-5 shows a spectral change for the reaction of $\mathbf{2^{O2}}$ with *p-tert*-butylphenol (^{tBu}ArOH) as a typical example, where the LMCT bands due to $\mathbf{2^{O2}}$ decreases obeying first-order kinetics in the presence of an excess amount of ^{tBu}ArOH.

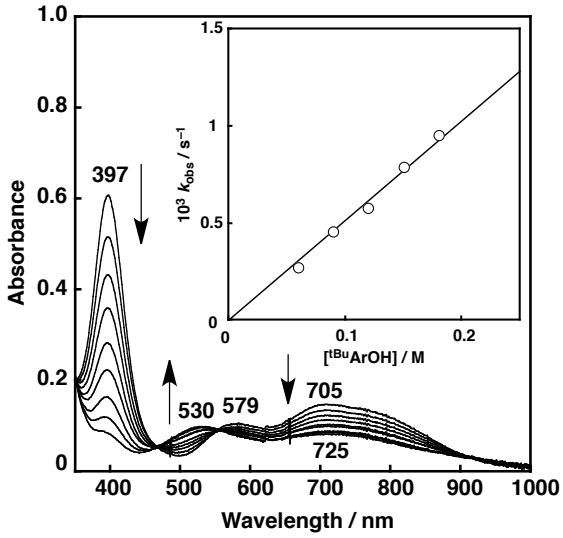

Figure 1-5. The UV-vis spectral change for the reaction of $\mathbf{2^{O2}}$ (0.2 mM) with *p-tert*-butylphenol (180 mM) in acetone at –85 °C. Each spectrum was taken at 500 s intervals. Inset: Plot of k_{obs} against the substrate concentration.

A plot of the pseudo-first-order rate constants (k_{obs}) against the substrate concentration gave a straight line passing through the origin, from which the second-order rate constant k_2 was determined to be (0.68 ± 0.01) x 10^{-2} M^{-1} s^{-1} from the slope (Figure 1-3, Inset). In this case, the spectrum of the final reaction mixture exhibiting weak absorption bands at 530 nm (ε = 485 $M^{-1}\,cm^{-1}$) and 725 nm (ε = 405 $M^{-1}\,cm^{-1}$), which was different from that of $\mathbf{2^{OOH}}$ (see, Figure 1-2) but identical to that of the copper(II)-phenolate complex ($\mathbf{2^{OAr(tBu)}}$) prepared by the reaction of a copper(II) complex $[Cu^{II}(L)(OCOCH_3)]^+$ ($\mathbf{2^{OAc}}$) and lithium *p-tert*-butylphenolate under the same experimental conditions.[46] Thus, the product was not the copper(II)-hydroperoxide complex $\mathbf{2^{OOH}}$, but a copper(II)-phenolate complex $\mathbf{2^{OAr(tBu)}}$. Furthermore, no phenol coupling dimer product was obtained, when the final reaction mixture was quenched with HPF_6 at the low temperature (–85 °C).

The reactions of $\mathbf{2^{O2}}$ with a series of *p*-substituted phenols (^{X}ArOH; X = OPh, Me, H, F, Cl) were also examined under the same experimental conditions to give the corresponding copper(II)-phenolate complexes ($\mathbf{2^{OAr(X)}}$), and the second-order rate constants k_2 for the reactions were determined in the same manner as (0.51 ± 0.01) x

10^{-2} M^{-1} s^{-1}, (0.22 ± 0.01) x 10^{-2} M^{-1} s^{-1}, (0.37 ± 0.3) x 10^{-2} M^{-1} s^{-1}, (0.42 ± 0.02) x 10^{-2} M^{-1} s^{-1}, (0.42 ± 0.01) x 10^{-2} M^{-1} s^{-1}, and (2.0 ± 0.1) x 10^{-3} M^{-1} s^{-1}, respectively, at –85°C. When C_6D_5OD (fully deuterated phenol) was employed instead of C_6H_5OH, there was an appreciable amount of kinetic deuterium isotope effect (KIE = 2.2); $k_{obs(H)}$ = 9.2 x 10^{-4} s^{-1} vs. $k_{obs(D)}$ = 4.2 x 10^{-4} s^{-1} (Figure 1-6).

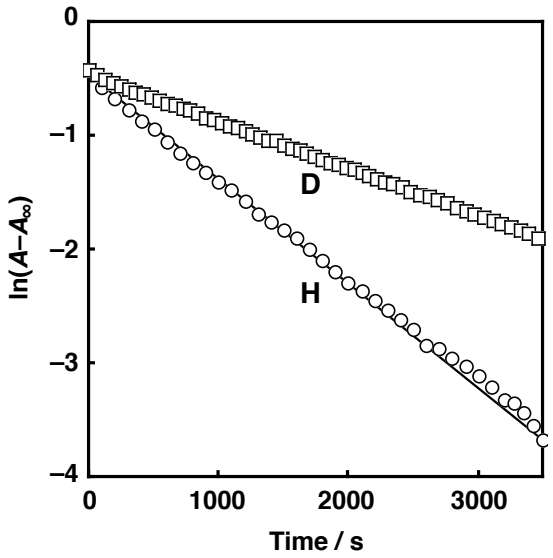

Figure 1-6. Pseudo-first order plots for the reaction of $\mathbf{2^{O2}}$ (0.2 mM) with C_6H_5OH (300 mM, ○) and C_6D_5OD (300 mM, □) in acetone at –85°C.

Formation of the copper(II)-phenolate complexes suggests that the reaction involves a simple acid-base reaction between the phenol substrate ^{X}ArOH and the superoxide ligand ($O_2^{\bullet-}$) in $\mathbf{2^{O2}}$ to generate the copper(II)-phenolate complex, ^{X}ArO-Cu^{II}, and $HO_2^{\bullet}$, the later of which may rapidly disproportionate into (1/2)O_2 and (1/2)H_2O_2 (Scheme 1-4, R = ^{X}Ar). This was confirmed by iodometric detection of H_2O_2 in a 49 % yield based on $\mathbf{2^{O2}}$.

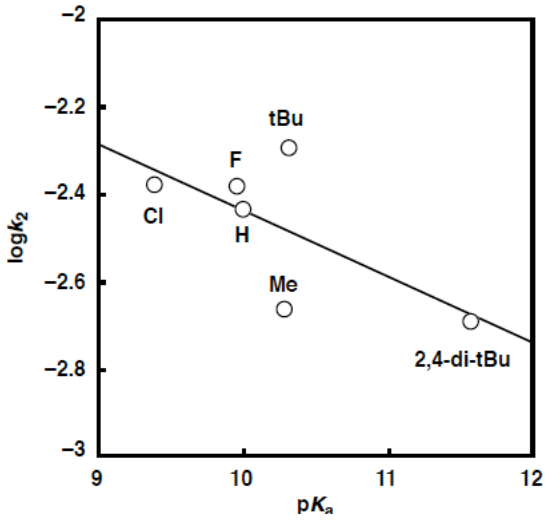

Figure 1-7. Plots of logk_2 against pK_a of ^{X}ArOH (X = Cl, F, ^{t}Bu and 2,4-di ^{t}Bu) for the reactions of $\mathbf{2^{O2}}$ (0.2 mM) with ^{X}ArOH in acetone at –85°C. Slope = –0.18. The pK_a values in H_2O are taken from the literature: *QSAR Comb. Sci.* **2007**, 26, 385–397.

If the proton transfer from the phenol substrate to the superoxide ligand occurs via a simple bimolecular reaction, the rate constant k_2 should increase as the pK_a of phenols decreases (as the acidity of phenols increases). Such a rate-dependence on the pK_a values was actually observed as shown in Figure 1-7, although the correlation is not so good. In support of this mechanism, addition of a stronger acid such as acetic acid (AcOH) to the superoxide complex $\mathbf{2^{O2}}$ rapidly afforded the copper(II)-acetate complex $\mathbf{2^{OAc}}$ and H_2O_2 (~50 %) (Scheme 1-4, R = Ac). Furthermore, a largely negative $\Delta S^{\neq}$ value (–143 ± 3 J K^{-1} mol^{-1}) was obtained in the Eyring plot analysis shown in Figure 1-4, which also supports the bimolecular reaction.

Scheme 1-4

$$\underset{\mathbf{2^{O_2}}}{[LCu^{II}(O_2^{\bullet})]^{+}} + ROH \xrightarrow[(R = {}^{X}Ar \text{ or } Ac)]{} \underset{\mathbf{2^{OR}}}{[LCu^{II}OR)]^{+}} + HO_2^{\bullet}$$

$$HO_2^{\bullet} \longrightarrow 1/2\ O_2 + 1/2\ H_2O_2$$

A simple hydrogen atom transfer (HAT) mechanism from the phenol substrate by the superoxide complex may be ruled out, since the putative copper(II)-hydroperoxide complex $\mathbf{2}^{\mathbf{OOH}}$ was not detected during the course of the reaction, and no phenoxyl radical coupling dimer product was obtained after the reaction (*vide ante*).

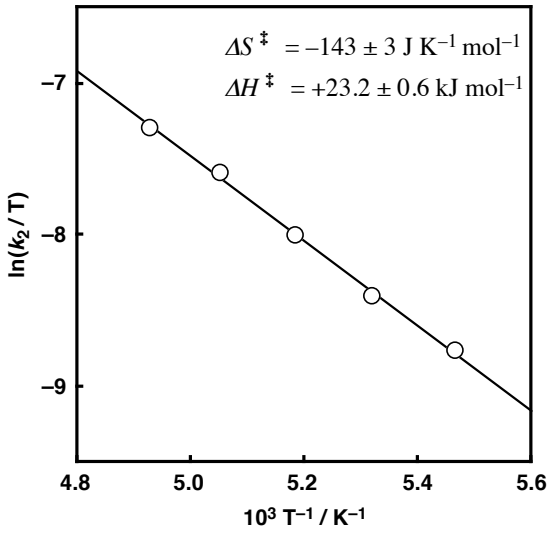

Figure 1-4. Eyring plot for the reaction of $\mathbf{2}^{\mathbf{O2}}$ (0.2 mM) with ^{MeO}ArOH in acetone.

Reaction with Phosphine and Sulfide. The reaction of $\mathbf{2}^{\mathbf{O2}}$ with triphenylphosphine derivatives was studied in order to examine the oxo-transfer ability of the superoxide complex. Figure 1-5 shows a spectrum change for the reaction of $\mathbf{2}^{\mathbf{O2}}$ with tris(4-methylphenyl)phosphine $P(Ar^{Me})_3$ as a typical example, where the decrease of the LMCT bands due to $\mathbf{2}^{\mathbf{O2}}$ obeys first-order kinetics in the presence of a large excess of the substrate.

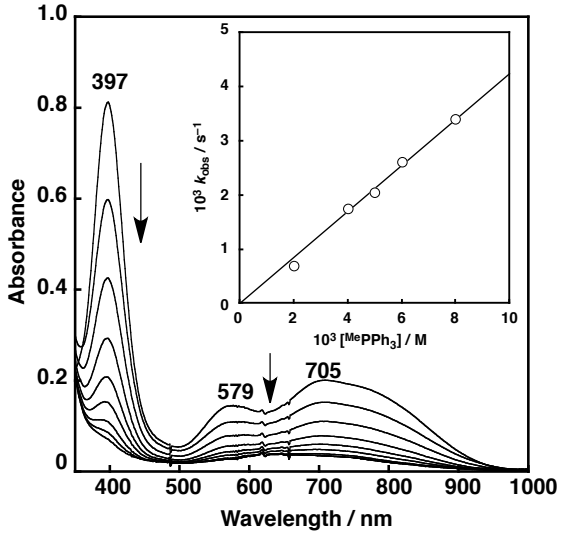

Figure 1-5. The UV-vis spectral change for the reaction of $\mathbf{2^{O2}}$ (0.2 mM) with $P(Ar^{Me})_3$ (4.0 mM) in acetone at –85 °C. Each spectrum was taken at 200 s intervals. Inset: Plot of k_{obs} against the substrate concentration.

A plot of the observed first-order rate constants against the substrate concentration gave a straight line passing through the origin, from which the second-order rate constant was determined from the slope (Figure 1-5, Inset, Table 1-2). In the preparative-scale reaction, the corresponding phosphine oxide was obtained in a 86 % yield based on $\mathbf{2^{O2}}$ (^{1}H-NMR yield). The reactions of a series of *p*-substituted-triphenylphosphine derivatives $P(Ar^Y)_3$ (Y = OMe, H, F, and Cl) were also examined in order to get insight into the reaction mechanism, and the second-order rate constants thus obtained are listed in Table 1-2. In this case, the plot of $\log k_2$ against the Hammett constant σ_p provides a linear correlation with a negative slope (ρ = –4.3, Figure 1-6). This suggests that the superoxide complex also has an electrophilic character in nature.

Table 1-2. The Second-order Rate Constants for the Reaction of $\mathbf{2^{O2}}$ with $\mathbf{P(Ar^Y)_3}$ in Acetone at –85 °C

p-substituent	OMe	Me	H	F	Cl
$10^2 k_2$ / M^{-1} s^{-1}	64 ± 1	42 ± 0.8	7.2 ± 0.1	1.5 ± 0.9	0.67 ± 0.004

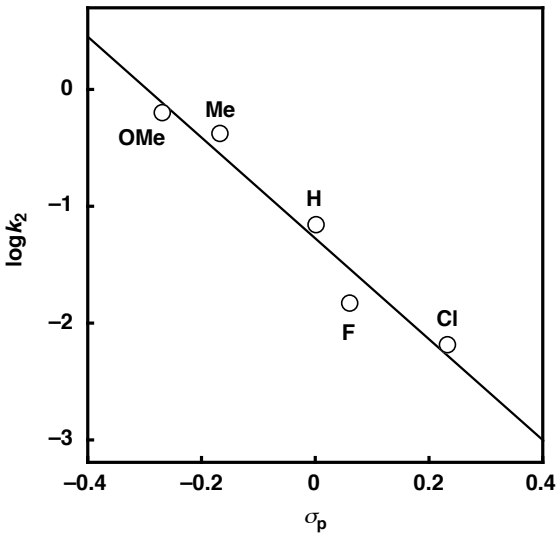

Figure 1-6. Hammett plot for the reaction of $\mathbf{2^{O2}}$ with $P(Ar^Y)_3$ with in acetone at –85 °C.

Recently, Nam and coworkers reported the oxygen atom transfer (OAT) reaction from a chromium(III)-superoxide complex supported by a macrocyclic TMC ligand, $[Cr^{III}(O_2^{\bullet})(TMC)(Cl)]^+$, to triphenylphosphine, where they confirmed generation of $[Cr^{IV}(O)(TMC)(Cl)]^+$ together with triphenylphosphine oxide as the products.[47] These products may be produced by homolytic O–O bond cleavage from a $(TMC)(Cl)Cr^{III}–O–O–^{\bullet+}PPh_3$ adduct intermediate.[47] If the OAT reaction from $\mathbf{2^{O2}}$ to $P(Ar^Y)_3$ proceeds in a similar manner, a $Cu^{II}–O^{\bullet}$ intermediate (Type **D** in Scheme 1-1) might be generated. However, such a reactive intermediate could not be detected in the present reaction.

The reaction of $\mathbf{2^{O2}}$ with thioanisole (PhSMe) was also examined. In this case, however, no oxygenation product (Ph(Me)SO) was obtained, but $\mathbf{2^{O2}}$ was converted to the copper(I) stating material as shown in Figure 1-7. The result can be explained by the mechanism shown in Scheme 1-5. The O_2-bindng to the copper(I) complex **1** is reversible as demonstrated in our previous study,[39] and addition of PhSMe to LCu^I competes with the O_2-bindng. A similar phenomenon was observed in the reaction of a superoxide copper(II) complex supported by $HIPT_3$tren and PhSMe.[48]

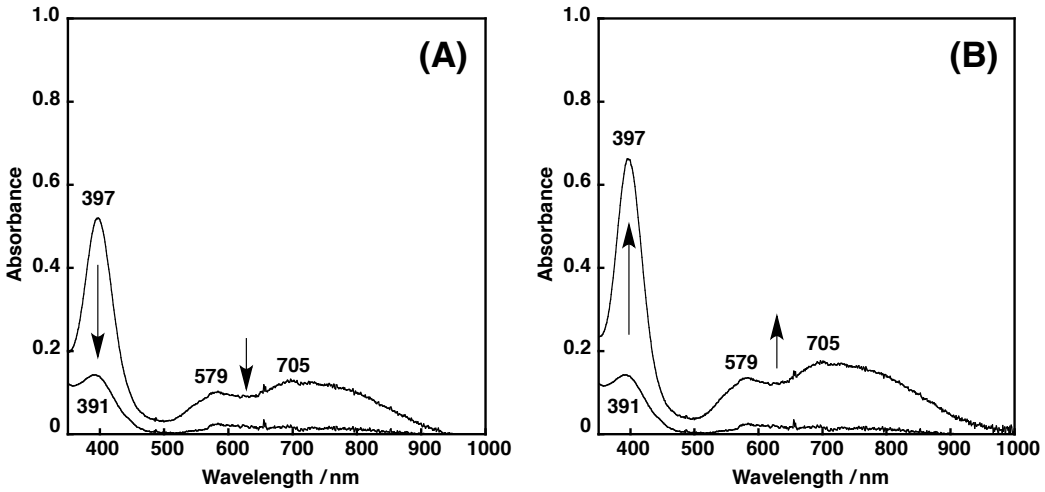

Figure 1-7. (A) The UV-vis spectral change for the reaction of $\mathbf{2}^{\mathbf{O2}}$ (0.2 mM) with thioanisole (100 mM) in acetone at –60 °C. (B) The UV-vis spectral change for the reaction of regeneration of $\mathbf{2}^{\mathbf{O2}}$ (0.2 mM) in acetone containing thioanisole (100 mM) at –85 °C.

Scheme 1-5

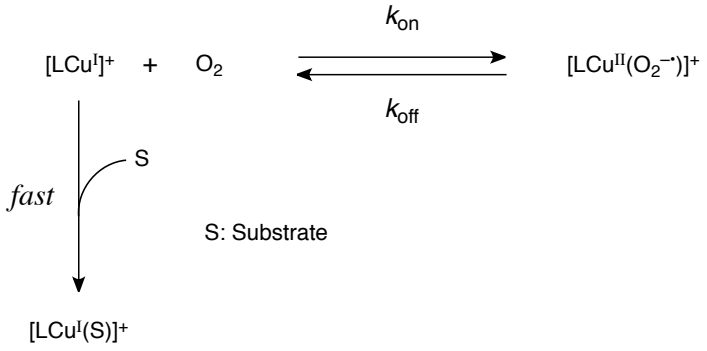

Conclusion

In this study, the reactions of $\mathbf{2}^{\mathbf{O2}}$ with a series of external substrates were examined in order to evaluate the intrinsic reactivity of the superoxide complex supported by the tridentate ligand L (Chart 1-1). Based on the reactivity of $\mathbf{2}^{\mathbf{O2}}$ with a series of one-electron reductants with various E_{ox}, the reduction potential of $\mathbf{2}^{\mathbf{O2}}$ was estimated to be E_{red} = (0.19 ± 0.07) V vs. SCE. In the reaction with hydrogen atom donor such as TEMPO-H, a simple HAT (hydrogen atom transfer) reaction proceeded to give the corresponding hydroperoxide complex LCu^{II}-OOH ($\mathbf{2}^{\mathbf{OOH}}$). In this case, intramolecular

ligand hydroxylation did not proceed. On the other hand, the reaction with phenols (^{X}ArOH) gave the corresponding phenolate adducts LCu^{II}-O^{X}Ar instead of $\mathbf{2}^{\mathbf{OOH}}$. Kinetic analysis has suggested an acid-base reaction between $\mathbf{2}^{\mathbf{O2}}$ and ^{X}ArOH. The reaction of $\mathbf{2}^{\mathbf{O2}}$ with a series of triphenylphosphine derivative gave the corresponding triphenylphosphine oxides via an electrophilic ionic substitution mechanism with a Hammett value $\rho = -4.3$. In this case, Cu^{II}–O$^{\bullet}$ type intermediate may be generated by the O–O bond homolysis from a putative Cu^{II}–O–O-$^{\bullet+}$PPh$_3$ adduct intermediate.

It is interesting to note that the reactivity of $\mathbf{2}^{\mathbf{O2}}$ is quite different from that of (TMG$_3$tren)Cu^{II}-OO$^{\bullet}$. The superoxide complex $\mathbf{2}^{\mathbf{O2}}$ itself can induce intramolecular aliphatic ligand hydroxylation, whereas no ligand hydroxylation product is obtained from the hydroperoxide complex $\mathbf{2}^{\mathbf{OOH}}$ (Scheme 1-3a). On the other hand, the superoxide complex (TMG$_3$tren)Cu^{II}-OO$^{\bullet}$ does not give any ligand hydroxylation products, but the hydroperoxide complex (TMG$_3$tren)Cu^{II}-OOH does (Scheme 1-3b). Furthermore, the reaction of (TMG$_3$tren)Cu^{II}-OO$^{\bullet}$ with phenol derivatives causes HAT reaction to provide several oxidation/oxygenation products from the phenol substrates in addition to the ligand hydroxylation product.[36] On the other hand, the reaction of $\mathbf{2}^{\mathbf{O2}}$ and phenols simply affords the phenolate adducts $\mathbf{2}^{\mathbf{OAr}}$. These differences in reactivity between $\mathbf{2}^{\mathbf{O2}}$ and (TMG$_3$tren)Cu^{II}-OO$^{\bullet}$ could be attributed in part to the difference in the coordination number and geometry (four-coordinate/tetrahedral vs. five-coordinate/trigonal bipyramidal) as well as to the difference in the kind of donor atoms (alkylamine and pyridine nitrogen atoms vs. imine (guanidine) nitrogen atoms). Such ligand effects on the reactivity of the superoxide complexes should be considered in the mechanistic studies of the copper monooxygenases.

References

1. Klinman, J. P. *Chem. Rev.* **1996**, *96*, 2541-2562.
2. Mirica, L. M.; Ottenwaelder, X.; Stack, T. D. P. *Chem. Rev.* **2004**, *104*, 1013-1045.
3. Lewis, E. A.; Tolman, W. B. *Chem. Rev.* **2004**, *104*, 1047-1076.
4. Chen, P.; Solomon, E. I. *Proc. Natl. Acad. Sci. U. S. A.* **2004**, *101*, 13105-13110.
5. Itoh, S. *Curr. Opin. Chem. Biol.* **2006**, *10*, 115-122.
6. Cramer, C. J.; Tolman, W. B. *Acc. Chem. Res.* **2007**, *40*, 601-608.
7. Roth, J. P. *Curr. Opin. Chem. Biol.* **2007**, *11*, 142-150.

8. Rolff, M.; Tuczek, F. *Angew. Chem. Int. Ed.* **2008**, *47*, 2344-2347.
9. Punniyamurthy, T.; Rout, L. *Coord. Chem. Rev.* **2008**, *252*, 134-154.
10. Himes, R. A.; Karlin, K. D. *Curr. Opin. Chem. Biol.* **2009**, *13*, 119-131.
11. Pap, J. S. n.; Kaizer, J.; Speier, G. *Coord. Chem. Rev.* **2010**, *254*, 781-793.
12. Itoh, S. In *Copper-Oxygen Chemistry*; Karlin, K. D., Itoh, S., Eds.; John Wiley & Sons: Hoboken, 2011; Vol. 4, p 225-282.
13. Prigge, S. T.; Mains, R. E.; Eipper, B. A.; Amzel, L. M. *Cell. Mol. Life Sci.* **2000**, *57*, 1236-1259.
14. Halcrow, M. A. In *Comprehensive Coordination Chemistry II*; Que, J., L., Tolman, W. B., Eds.; Elsevier: Amsterdam, **2004**, pp 395-436.
15. Klinman, J. P. *J. Biol. Chem.* **2006**, *281*, 3013-3016.
16. Hess, C. R.; Wu, Z.; Ng, A.; Gray, E. E.; McGuirl, M. A.; Klinman, J. P. *J. Am. Chem. Soc.* **2008**, *130*, 11939-11944.
17. Vaaje-Kolstad, G.; Westereng, B.; Horn, S. J.; Liu, Z.; Zhai, H.; Sørlie, M.; Eijsink, V. G. H. *Science* **2010**, *330*, 219-222.
18. Harris, P. V.; Welner, D.; McFarland, K. C.; Re, E.; Navarro Poulsen, J.-C.; Brown, K.; Salbo, R.; Ding, H.; Vlasenko, E.; Merino, S.; Xu, F.; Cherry, J.; Larsen, S.; Lo Leggio, L. *Biochemistry* **2010**, *49*, 3305-3316.
19. Quinlan, R. J.; Sweeney, M. D.; Lo Leggio, L.; Otten, H.; Poulsen, J.-C. N.; Johansen, K. S.; Krogh, K. B. R. M.; Jørgensen, C. I.; Tovborg, M.; Anthonsen, A.; Tryfona, T.; Walter, C. P.; Dupree, P.; Xu, F.; Davies, G. J.; Walton, P. H. *Proceedings of the National Academy of Sciences* **2011**, *108*, 15079-15084.
20. Phillips, C. M.; Beeson, W. T.; Cate, J. H.; Marletta, M. A. *ACS Chem. Biol.* **2011**, *6*, 1399-1406.
21. Hemsworth, G. R.; Taylor, E. J.; Kim, R. Q.; Gregory, R. C.; Lewis, S. J.; Turkenburg, J. P.; Parkin, A.; Davies, G. J.; Walton, P. H. *J. Am. Chem. Soc.* **2013**, *135*, 6069-6077.
22. Bollinger, J., J Martin; Krebs, C. *Curr. Opin. Chem. Biol.* **2007**, *11*, 151-158.
23. Chen, P.; Bell, J.; Eipper, B. A.; Solomon, E. I. *Biochemistry* **2004**, *43*, 5735-5747.
24. Chen, P.; Solomon, E. I. *J. Am. Chem. Soc.* **2004**, *126*, 4991-5000.
25. Kamachi, T.; Kihara, N.; Shiota, Y.; Yoshizawa, K. *Inorg. Chem.* **2005**, *44*, 4226-4236.

26. Crespo, A.; Marti, M. A.; Roitberg, A. E.; Amzel, L. M.; Estrin, D. A. *J. Am. Chem. Soc.* **2006**, *128*, 12817-12828.
27. de la Lande, A.; Gérard, H.; Moliner, V.; Izzet, G.; Reinaud, O.; Parisel, O. *J. Biol. Inorg. Chem.* **2006**, *11*, 593-608.
28. Gherman, B.; Heppner, D.; Tolman, W.; Cramer, C. *J. Biol. Inorg. Chem.* **2006**, *11*, 197-205.
29. Yoshizawa, K.; Kihara, N.; Kamachi, T.; Shiota, Y. *Inorg. Chem.* **2006**, *45*, 3034-3041.
30. de la Lande, A.; Parisel, O.; Gérard, H.; Moliner, V.; Reinaud, O. *Chem. Eur. J.* **2008**, *14*, 6465-6473.
31. Poater, A.; Cavallo, L. *Inorg. Chem.* **2009**, *48*, 4062-4066.
32. Maiti, D.; Fry, H. C.; Woertink, J. S.; Vance, M. A.; Solomon, E. I.; Karlin, K. D. *J. Am. Chem. Soc.* **2007**, *129*, 264-265.
33. Peterson, R. L.; Himes, R. A.; Kotani, H.; Suenobu, T.; Tian, L.; Siegler, M. A.; Solomon, E. I.; Fukuzumi, S.; Karlin, K. D. *J. Am. Chem. Soc.* **2011**, *133*, 1702-1705.
34. Würtele, C.; Gaoutchenova, E.; Harms, K.; Holthausen, M. C.; Sundermeyer, J.; Schindler, S. *Angew. Chem. Int. Ed.* **2006**, *45*, 3867-3869.
35. Lanci, M. P.; Smirnov, V. V.; Cramer, C. J.; Gauchenova, E. V.; Sundermeyer, J.; Roth, J. P. *J. Am. Chem. Soc.* **2007**, *129*, 14697-14709.
36. Maiti, D.; Lee, D. H.; Gaoutchenova, K.; Wurtele, C.; Holthausen, M. C.; Sarjeant, A. A. N.; Sundermeyer, J.; Schindler, S.; Karlin, K. D. *Angew. Chem. Int. Ed.* **2008**, *47*, 82-85.
37. Maiti, D.; Lee, D.-H.; Narducci Sarjeant, A. A.; Pau, M. Y. M.; Solomon, E. I.; Gaoutchenova, K.; Sundermeyer, J. r.; Karlin, K. D. *J. Am. Chem. Soc.* **2008**, *130*, 6700-6701.
38. Kunishita, A.; Kubo, M.; Sugimoto, H.; Ogura, T.; Sato, K.; Takui, T.; Itoh, S. *J. Am. Chem. Soc.* **2009**, *131*, 2788-2789.
39. Kunishita, A.; Ertem, M. Z.; Okubo, Y.; Tano, T.; Sugimoto, H.; Ohkubo, K.; Fujieda, N.; Fukuzumi, S.; Cramer, C. J.; Itoh, S. *Inorg. Chem.* **2012**, *51*, 9465-9480.
40. Perrin, D. D.; Armarego, W. L. F.; Perrin, D. R. *Purification of Laboratory Chemicals 4th Edition*; 4th ed.; Pergamon Press: Elmsford, NY, 1996.

41. Fukuzumi, S.; Kuroda, S.; Tanaka, T. *J. Am. Chem. Soc.* **1985**, *107*, 3020-3027.
42. Tahsini, L.; Kotani, H.; Lee, Y.-M.; Cho, J.; Nam, W.; Karlin, K. D.; Fukuzumi, S. *Chem. Eur. J.* **2012**, *18*, 1084-1093.
43. Kunishita, A.; Kubo, M.; Ishimaru, H.; Ogura, T.; Sugimoto, H.; Itoh, S. *Inorg. Chem.* **2008**, *47*, 12032-12039.
44. Prigge, S. T.; Eipper, B. A.; Mains, R. E.; Amzel, L. M. *Science* **2004**, *304*, 864-867.
45. Evans, J. P.; Ahn, K.; Klinman, J. P. *J. Biol. Chem.* **2003**, *278*, 49691-49698.
46. The copper(II)-phenolate complex could not be isolated due to its thermal instability.
47. Cho, J.; Woo, J.; Nam, W. *J. Am. Chem. Soc.* **2012**, *134*, 11112-11115.
48. Kobayashi, Y.; Ohkubo, K.; Nomura, T.; Kubo, M.; Fujieda, N.; Sugimoto, H.; Fukuzumi, S.; Goto, K.; Ogura, T.; Itoh, S. *Eur. J. Inorg. Chem.* **2012**, *2012*, 4574-4578.

Chapter 2 Reactivity of Copper(II)–Alkylperoxide Complexes

Introduction

Alkylperoxide complexes of transition-metal ions (M-OOR; M = transition-metal ion, R = alkyl group) have attracted much attention due to their strong relevance to biological and catalytic oxidation reactions.[1,2,3] Among the series of M-OOR, the non-heme iron complexes have been extensively studied by Que and coworkers [4] and by other research groups, [5] providing profound insights into the catalytic mechanism of iron-containing monooxygenases and iron-catalyzed hydrocarbon oxygenation reactions.[6,7] In most cases, Fe^{IV}=O and/or Fe^{V}=O species generated by homolytic or heterolytic O–O bond cleavage of Fe^{III}-OOR have been invoked as the key reactive intermediate. Thus, Fe^{III}-OOR has been considered as a precursor of reactive iron-oxo species but not itself actively responsible for hydrocarbon oxidation.

Alkylperoxide complexes of copper may also be important active-oxygen species because copper ions are widely used to initiate lipid peroxidation in model systems, particularly for the study of low density lipoprotein (LDL) oxidation.[8] In the presence of a suitable reducing agent for Cu^{II}, such as ascorbic acid or α-tocopherol, peroxidation is believed to involve the reductive decomposition of preformed lipid hydroperoxides (ROOH) to alkoxyl radicals (RO•) by the reduced metal ion (eqn 1). Peroxidation of the parent polyunsaturated fatty acid (RH) is then initiated by hydrogen atom abstraction, the process being propagated through oxygenation reactions (eqns 2-4).

$$Cu^{I} + ROOH \rightarrow Cu^{II} + RO\bullet + OH^{-} \quad (1)$$

$$RO\bullet + RH \rightarrow ROH + R\bullet \quad (2)$$

$$R\bullet + O_2 \rightarrow ROO\bullet \quad (3)$$

$$ROO\bullet + RH \rightarrow ROOH + R\bullet \quad (4)$$

Copper(II) ions can also induce lipid peroxidation in the absence of an additional reducing agent. It has often been assumed that this involves the reduction of Cu^{II} by a

preformed lipid hydroperoxide (eqn 5), resulting in the generation of a peroxyl radical (ROO•), which may then initiate further cycles of peroxidation (eqn 4).[8] An alternative explanation for the ability of Cu^{II} to induce lipid peroxidation in the presence of a lipid hydroperoxide, but not a reducing agent, involves the oxidation of Cu^{II} by the hydroperoxide, forming Cu^{III} and an alkoxyl radical (eqn 6).[9] However, the likelihoods of these reactions (eqns 5 and 6) have only been discussed from the viewpoint of outer sphere electron/proton-transfers based on the redox potentials of the metal ions and ROOH; no attention has been paid to inner sphere redox reactions involving adducts between Cu^{II} and ROOH.[8]

$$Cu^{II} + ROOH \rightarrow Cu^{I} + ROO\bullet + H^{+} \quad (5)$$

$$Cu^{II} + ROOH \rightarrow Cu^{III} + RO\bullet + OH^{-} \quad (6)$$

Copper has long been recognized as a key element in oxygen activation chemistry both in biological and catalytic oxidation reactions.[10,11] The structures, physicochemical properties, and reactivities of a variety of mononuclear, dinuclear, and multinuclear copper active-oxygen complexes have been explored in detail to date, shedding light on the mechanism of copper monooxygenases and copper-catalyzed oxidation reactions.[12] Among copper active-oxygen complexes, however, little has been explored with respect to the physicochemical properties and reactivities of copper(II)-alkylperoxide complexes, which could be key reactive intermediates in the above reactions (eqns 1, 5 and 6). Copper(II)-alkylperoxide complexes could also be precursors of mononuclear Cu^{II}–O• species, which have been invoked as key reactive intermediates in many biological and industrial oxygenation reactions.[13]

Structural and spectroscopic characterization of a copper(II)-alkylperoxide complex LCu^{II}-OOR was first accomplished by Kitajima and coworkers using hydrotris(pyrazolyl)borate ligand, L = $HB(3,5\text{-}i\text{-}Prpz)_3^-$.[14] The reactivity of the *tert*-butyl-hydroperoxide derivative (R = ^{t}Bu) toward some organic substrates was briefly examined to demonstrate that the reactions mostly involved an auto-oxidation-type free-radical mechanism induced by the Cu–O and O–O bond homolytic cleavage of LCu^{II}-OO^{t}Bu.[14a] However, further studies on the intrinsic reactivity of copper(II)-alkylperoxide complexes with different supporting ligands had not been reported until recently. In this respect, we have recently investigated the

reactivity of the mononuclear copper(II)-cumylperoxide complex (R = $C(Me)_2Ph$ (Cm)) supported by a bis(pyridin-2-ylmethyl)amine tridentate ligand (L) to demonstrate that C–H bond activation of external substrates could occur via O–O bond homolysis of the cumylperoxide species.[15] In this study, the author and his co-workers have further investigated the reactivity of LCu^{II}-OOR supported by the bis(pyridin-2-ylmethyl)amine (bpa) *tridentate* and tris(pyridin-2-ylmethyl)amine (tpa) *tetradentate* ligands (Chart 2-1) to gain more insights into ligand effects on the reactivities of the copper(II)-alkylperoxide species.

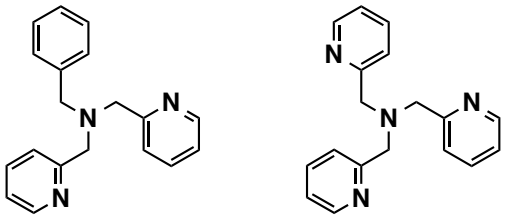

Chart 2-1. Structures of bpa and tpa ligands

Experimental

Reagents

The reagents and the solvents used in this study, except the ligands and the copper complexes, were commercial products of the highest available purity and were further purified by standard methods, when necessary.[16] Ligands bpa and tpa,[17] and their copper(II) complexes $[Cu^{II}(bpa)(CH_3CN)_2](ClO_4)_2$ (**1a**)[18] and $[Cu^{II}(tpa)(CH_3CN)](ClO_4)_2$ (**1b**),[19] were prepared according to the reported procedures. Cumene hydroperoxide (CmOOH) used in this study was prepared by a reported procedure[20] and purified by silica gel column chromatography (eluent: AcOEt–Hexane). ^{18}O-labeled ($Cm^{18}O^{18}OH$) was synthesized using $^{18}O_2$ instead of $^{16}O_2$ by the same procedure.[20]

Physical methods

UV-visible spectra were taken in acetonitrile or in propionitrile on a Hewlett Packard 8453 photodiode array spectrophotometer equipped with a Unisoku thermostated cell holder designed for low temperature measurements (USP-203). ^1H-NMR spectra were

recorded on a JEOL ECP 400, a JEOL ECS 400 or a Varian UNITY INOVA 600MHz. EPR spectra were recorded on a BRUKER E-500 spectrometer at –196 °C equipped with a variable temperature cell holder or a JEOL JES–FA100. A Mn^{II}-maker was used as the reference, and experimental errors in the EPR parameters (*g* values) is ±0.001. Mass spectra were recorded with a JEOL JMS–700T Tandem MS station or a JEOL JMS–700. ESI-MS (electrospray ionization mass spectra) measurements were performed on a PE SCIEX API 150EX. Resonance Raman scattering was excited at 406.7 nm from Kr^+ laser (Spectra Physics, BeamLok 2060), or 441.6 nm from He-Cd laser (KIMMON KOHA, K5651R). Resonance Raman scattering was dispersed by a single polychromator (Ritsu Oyo Kogaku, MC-100) and was detected by a liquid nitrogen cooled CCD detector (HORIBA JOBIN YVON, Symphony 1024 x 128 Cryogenic Front Illuminated CCD Detector). The resonance Raman measurements were carried out using a rotated cylindrical cell thermostated at –80°C or a rotating NMR tube (outer diameter = 5 mm) thermostated at –40 °C by flashing cold nitrogen gas. A 135° back-scattering geometry was used.

Kinetic measurements

Kinetic measurements for the reaction of copper(II) complexes **1a** and **1b** with cumene hydroperoxide were performed using a Hewlett Packard 8453 photodiode array spectrophotometer equipped with a Unisoku thermostated cell holder designed for low temperature measurements (USP-203, a desired temperature can be fixed within ± 0.5 °C) in acetonitrile at –40 °C. To an acetonitrile solution of the copper(II) complex (1.0 mM) in a 1.0 cm path length UV-vis cell closed with a rubber septum cap, an acetonitrile solution of CmOOH was added using a microsyringe through the rubber septum cap. Then, an acetonitrile solution of Et_3N was added using a microsyringe under anaerobic conditions to initiate the reaction. The reaction was monitored by following an increase of the characteristic absorption band due to the Cu^{II}-cumylperoxide complex LCu^{II}-OOCm (**2a** and **2b**). The pseudo-first-order rate constants for the formation and decomposition processes of LCu^{II}-OOCm were determined from the plots of $\ln(\Delta A)$ vs. time based on the time course of the absorption change at the λ_{max} of LCu^{II}-OOCm. The self-decomposition of **2a** and **2b** was examined at 60 °C.

The reactions of LCu^{II}-OOCm with external substrates were examined at 30 °C. Thus, the cumylperoxide copper(II) complex (**2a** or **2b**) was first generated *in situ* at

–40 °C as described above, and then the solution was warmed up to 30 °C. The reaction of LCu^{II}-OOCm and the external substrate was initiated by adding an excess amount of 1,4-cyclohexadiene (CHD) using a microsyringe under anaerobic conditions. The first-order rate constants (k_{obs}) were determined by following a decrease in the absorption band due to the peroxide complex.

Product analysis

Decomposition products derived from cumene hydroperoxide and oxidation products of the substrates were analyzed by using a HPLC system consisting of a Shimadzu LC-6A chromatographic pump and an on-line Shimadzu UV-vis spectrophotometric detector. Reverse phase chromatography was performed on an ODS column (Cosmosil $5C_{18}$-AR-II, 250 mm x 4.6 mm, Nacalai tesque) at room temperature with an acetonitrile-water (60 : 40) mixed solvent as mobile phase at a constant flow rate of 0.5 mL min^{-1}. The yields of products were determined by comparing the integrated peak areas of the products with that of the internal standard (anisole) using calibration lines.

Self-decomposition. Cumylperoxide copper(II) complex **2a** or **2b** was generated *in situ* in a UV-vis cell by the consecutive addition of cumene hydroperoxide (1.0 mM) and Et_3N (1.0 mM) to an acetonitrile solution of **1a** or **1b** (1.0 mM) at –40 °C, and the mixture was warmed up to 60 °C. Then, the self-decomposition reaction was followed by monitoring the decrease in the LMCT absorption bands due to **2a** or **2b**. After cooling the solution to room temperature, anisole (1.0 mM) was added as an internal standard, and then the products from CmOOH were analyzed using the HPLC sysetm mentioned above.

Oxidation of CHD. Cumylperoxide copper(II) complex **2a** or **2b** was generated *in situ* in a UV-vis cell (1.0 cm path length) by the consecutive addition of cumene hydroperoxide (1.0 mM) and Et_3N (1.0 mM) to an acetonitrile solution of **1a** or **1b** (1.0 mM) at –40 °C, and then solution was warmed to 30 °C. An excess amount of substrate was added to the solution, and the reaction was followed by monitoring the decrease in the LMCT absorption band due to **2a** or **2b**. After cooling the solution to room temperature, anisole (1.0 mM) was added as an internal standard, and the products from CmOOH and CHD were analyzed by using the HPLC system mentioned above.

Computational methods

All geometries were fully optimized at the M06-L level of density functional theory[21] using the Stuttgart [8s7p6d | 6s5p3d] ECP10MWB contracted pseudopotential basis set

on Cu[22] and the 6-31G(d) basis set[23] on all other atoms. In addition, 3 uncontracted f functions having exponents 5.100, 1.275, and 0.320 were placed on Cu. The grid = ultrafine option (in Gaussian 09[24]) was chosen for integral evaluation and an automatically generated density-fitting basis set was used within the resolution-of-the-identity approximation for the evaluation of Coulomb integrals. The nature of all stationary points was verified by analytic computation of vibrational frequencies, which were also used for the computation of zero-point vibrational energies, molecular partition functions (with all frequencies below 50 cm^{-1} replaced by 50 cm^{-1} when computing free energies), and for determining the reactants and products associated with each transition-state structure (by following the normal modes associated with imaginary frequencies). Partition functions were used in the computation of 298 K thermal contributions to free energy employing the usual ideal-gas, rigid-rotator, harmonic oscillator approximation.[25] Solvation effects associated with acetonitrile as solvent were accounted for by using the SMD continuum solvation model.[26] Free energy contributions were added to single-point M06-L electronic energies computed with the SDD basis set on Cu and the 6-311+G(2df, p) basis set on all other atoms to arrive at final, composite free energies. Standard-state free energies for complexes including explicit MeCN solvent molecules include a correction for the molarity of liquid acetonitrile.

The O-O bond cleavage transition state geometries are associated with electronic structures that are not well described by a single determinant. In such instances, standard Kohn-Sham DFT is not directly applicable,[25,27] and the author and his co-workers adopt the Yamaguchi broken-spin-symmetry (BS) procedure[28] to compute the energy of the spin-purified low-spin (LS) state as

$$ {}^{LS}E = \frac{{}^{BS}E\left({}^{HS}\left\langle S^2 \right\rangle - {}^{LS}\left\langle S^2 \right\rangle \right) - {}^{HS}E\left({}^{BS}\left\langle S^2 \right\rangle - {}^{LS}\left\langle S^2 \right\rangle \right)}{{}^{HS}\left\langle S^2 \right\rangle - {}^{BS}\left\langle S^2 \right\rangle} \qquad (7) $$

where HS refers to the single-determinantal high-spin coupled state that is related to the low-spin state by spin flip(s) and $< S^2 >$ is the expectation value of the total spin operator applied to the appropriate determinant. This broken-symmetry DFT approach has routinely proven effective for the prediction of state-energy splittings in metal

coordination compounds.[29] Time-dependent density functional theory (TDDFT) calculations were performed to predict the UV/visible electronic excitations of postulated intermediates. The B98 density functional,[30] the Stuttgart [8s7p6d | 6s5p3d] ECP10MWB contracted pseudopotential basis set on Cu, and the 6-311+G(d) basis set[23] on all other atoms were used for the TDDFT calculations with non-equilibrium solvation effects computed using the SMD continuum solvation model for acetonitrile as solvent.[31]

Results and discussion

Characterization of copper(II) alkylperoxide complexes.

The bpa ligand system

The alkylperoxide copper(II) complexes were generated in situ by the reaction of copper(II) precursor complexes with cumene hydroperoxide ($PhC(Me)_2OOH$; CmOOH). Figure 2-1a shows the spectral change for the reaction of $[Cu^{II}(bpa)(CH_3CN)_2](ClO_4)_2$ (**1a**, 1.0 mM) and CmOOH (4 eq) in CH_3CN at –40 °C in the presence of 10 equiv of triethylamine (Et_3N), where a characteristic absorption band at 388 nm (ε = 1530 M^{-1} cm^{-1}) due to ligand to metal charge transfer (LMCT) transition and a relatively weak band at 560 nm (ε = 178 M^{-1} cm^{-1})[32] appear together with a d-d band at 700 nm (ε = 123 M^{-1} cm^{-1}). The generated species was stable for several hours even at room temperature. The apparent binding constant K_{app} of CmOOH to **1a** was determined by the titration in CH_3CN at –40 °C in the presence of Et_3N (10 mM) as shown in Figure 2-S1b, and a plot of $(A - A_0)/(A_\infty - A)$ against $[[CmOOH]_0–[Cu]_0(A - A_0) /(A_\infty - A_0)]$ based on the absorption change at 388 nm gave a linear correlation, from which K_{app} was determined to be 7.1 x 10^3 M^{-1} as the slope (Figure 2-1b, Inset).[33]

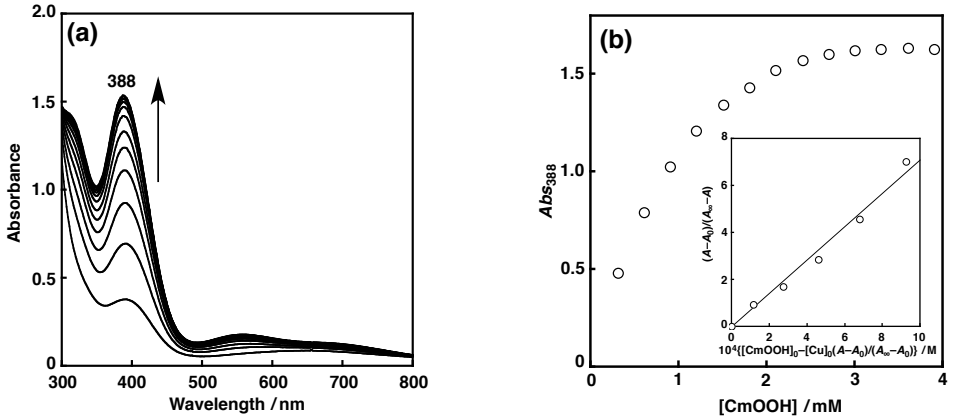

Figure 2-1. (a) Spectral change for the reaction of **1a** (1.0 mM) with CmOOH (4.0 mM) in the presence of Et_3N (10 mM) in CH_3CN at –40ºC. (b) Spectrophotometric titration for the formation of cumylperoxide copper(II) complex from the reaction of **1a** (1.0 mM) and CmOOH in the presence of Et_3N (10 mM) in CH_3CN at –40ºC. Inset: Plot of $(A - A_0)/(A_\infty - A)$ against $[CmOOH]_0 - [Cu]_0(A - A_0)/(A_\infty - A_0)]$.

The ESI-MS (electrospray ionization mass spectrum) of the solution exhibited a prominent ion peak at a mass-to-charge (m/z) ratio of 503.3 (Figure 2-2a, EXP), whose mass and isotope distribution pattern were consistent with the chemical formula of $[Cu(bpa)(O_2Cm)]^+$ (calculated m/z = 503.3) (Figure 2-2a, SIM). When $Cm^{18}O_2H$ was used instead of $Cm^{16}O_2H$, the peak position shifted to 507.3 (4 mass unit shift) as shown in Figure 2-2b. These results unambiguously indicate the formation of cumylperoxide copper(II) complex **2a** (Scheme 2-1).

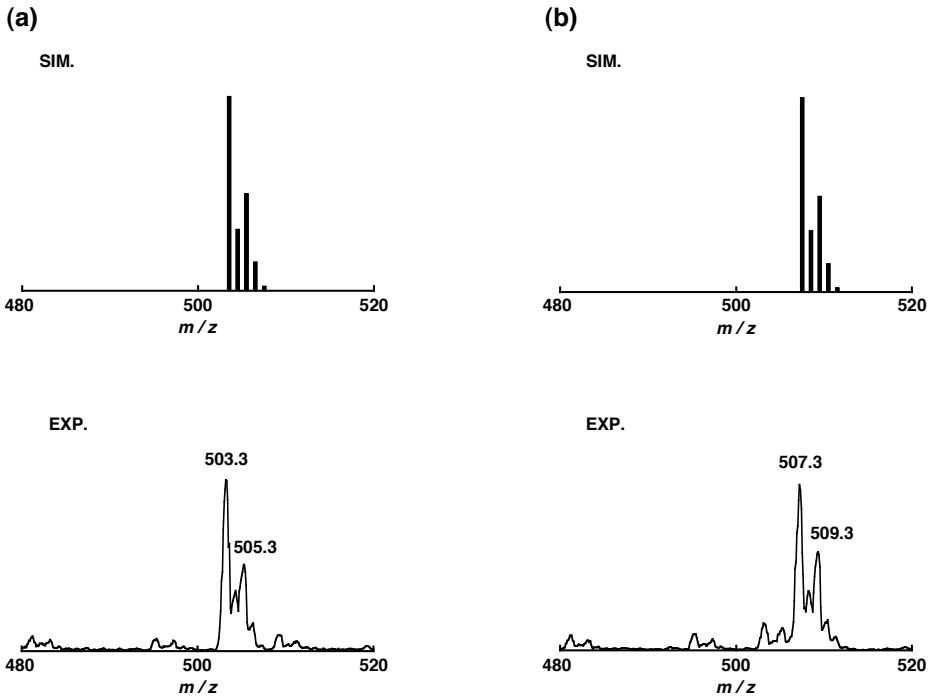

Figure 2-2. Experimental (EXP, bottom) and simulated (SIM, top) peak envelopes in the positive-ion ESI-MS spectra of the product derived from the reaction of **1a** (1.0 mM) with CmOOH (1.0 mM) in the presence of Et_3N (1.0 mM) in CH_3CN at –40ºC, (a) with $Cm^{16}O_2H$ and (b) with $Cm^{18}O_2H$.

Scheme 2-1

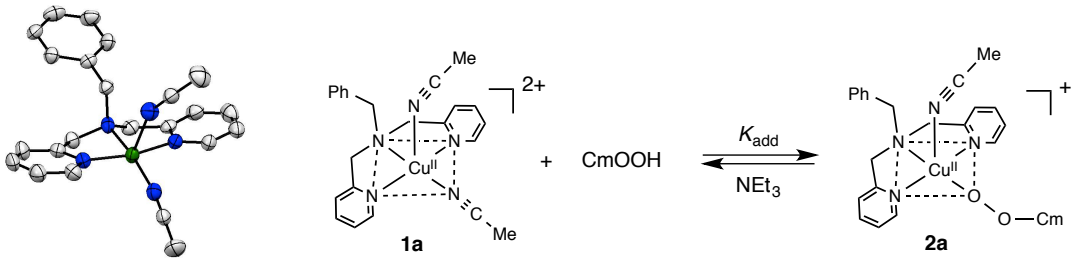

In the resonance Raman spectrum shown in Figure 2-3, there are isotope sensitive Raman bands at 864, 828, 588, and 526 cm^{-1}, which shifted to 842, 793, 581, and 508 cm^{-1}, respectively, upon ^{18}O-substitution using $Cm^{18}O^{18}OH$. Appearance of the multiple resonance Raman bands and their associated isotope shifts ($\Delta\nu$ = 22, 35, 7, and

18 cm^{-1}) are similar to those reported from the resonance Raman studies of the cumylperoxide copper(II) complex supported by the bis(2-pyridinylmethyl)amine tridentate ligand and the hydrotrispyrazolylborate ligand.[14b,15] By analogy to those detailed Raman studies and based on comparisons to vibrational spectra computed for $[Cu(bpa)(O_2Cm)]^+$, the bands in the 800 cm^{-1} region of **2a** can be assigned to mixed O–O/C–O/C–C vibrations of the cumylperoxide group, the band at 508 cm^{-1} to the Cu–O stretching vibration, and the additional 581 cm^{-1} bands of **2a** can be assigned to the C–C–O deformation mode of the alkylperoxide moiety.

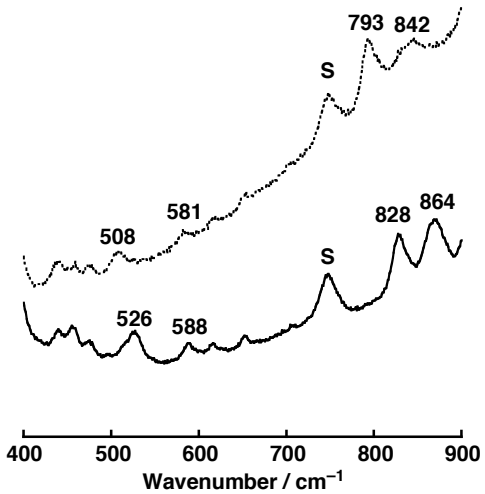

Figure 2-3. Resonance Raman spectra of **2a** derived from the reaction of **1a** (4.0 mM) with CmOOH (12 mM) in the presence of Et_3N (4.0 mM) generated by using $Cm^{16}O_2H$ (solid line, below) and $Cm^{18}O_2H$ (doted line, above) obtained with λ_{ex} = 441.6 nm in CH_3CN –40°C; s denotes the solvent band.

The EPR spectrum of **2a** is shown in Figure 2-4b, which clearly indicates a tetragonal geometry of the copper(II) center ($g_{//}$ = 2.226, $g_{\perp}$ = 2.064, $A_{//}$ = 192 G). We have already determined the crystal structure of the starting material $[Cu^{II}(bpa)(CH_3CN)_2](ClO_4)_2$ (**1a**), which exhibits a five coordinate square pyramidal geometry (τ = 0.07) (see left Figure in Scheme 2-1, for detailed crystal structure, see reference paper[18]). Judging from the EPR data shown in Figure 2-4a ($g_{//}$ = 2.222, $g_{\perp}$ = 2.071, $A_{//}$ = 176 G), complex **1a** may have a similar square pyramidal structure having two solvent molecules as the external co-ligands in the axial and equatorial positions in

CH_3CN. In **2a**, the solvent molecule in the equatorial position may be replaced by the peroxide ligand to form a five coordinate square pyramidal structure (Scheme 2-1). The mononuclearity of **2a** was confirmed by spin quantification using EPR spectrum (98 % spin remained). In spite of our great efforts, however, single crystal of **2a** has yet to be obtained.

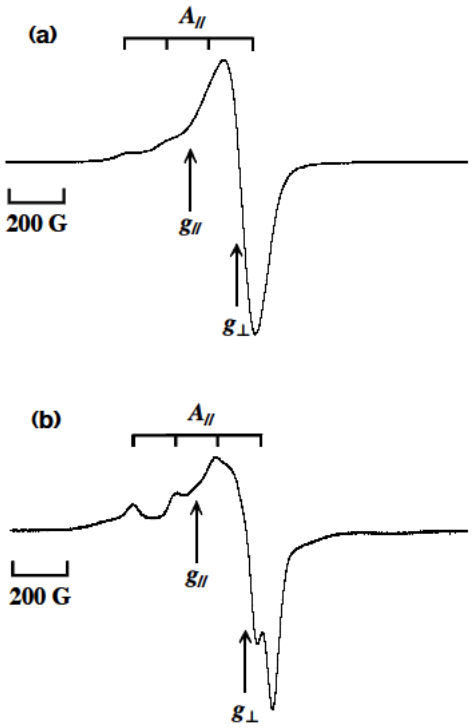

Figure 2-4. (a) EPR spectrum of **1a** (starting material) (2.0 mM) in CH_3CN at –196°C. EPR parameter $g_{//} = 2.222$, $g_{\perp} = 2.071$, $A_{//} = 176$ G. (b) EPR spectrum of **2a** generated by the reaction of **1a** (2.0×10^{-3} M) and CmOOH (2.0×10^{-2} M) in the presence of Et_3N (2.0×10^{-3} M) in CH_3CN at –196°C. EPR parameters $g_{//} = 2.216$, $g_{\perp} = 2.064$, $A_{//} = 192$ G.

It is interesting to note that the UV-vis spectrum of **2a** changes dramatically depending on the temperature as shown in Figure 2-5. The λ_{max} at –90 °C is 380 nm and shifts gradually to 405 nm as the temperature goes up to 10 °C (the spectral measurement was carried out in propionitrile instead of acetonitrile, since the melting point of the former solvent is much lower than that of the latter one). Simultaneously, the absorption at 560 nm becomes more intense and that at 700 nm becomes less intense. This temperature dependent spectral change is reversible.

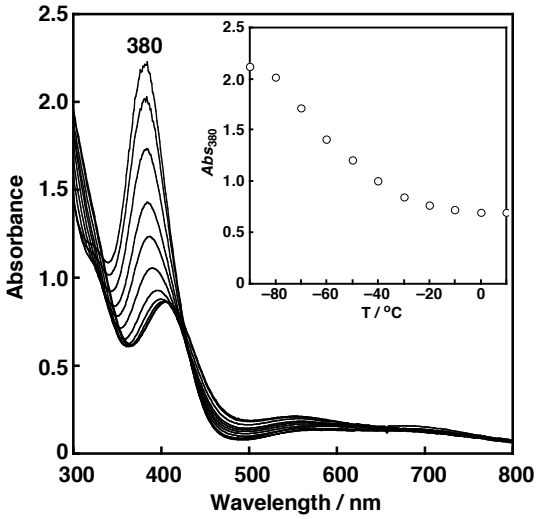

Figure 2-5. Temperature dependent UV-vis spectral change of **2a** (1.0 mM) in propionitrile from –90 °C to 10 °C. Inset: temperature dependent absorption change at 380 nm.

Scheme 2-2

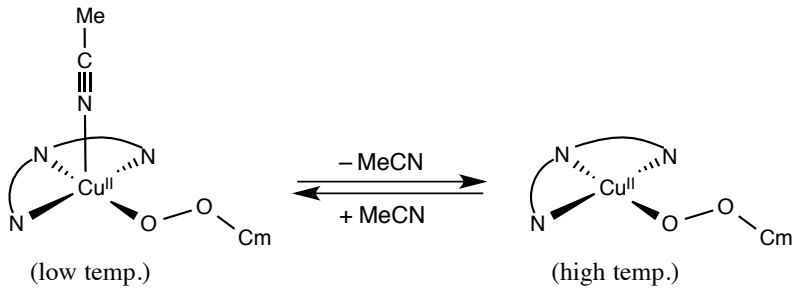

The author and his co-workers attribute this spectral change to an equilibrium association/dissociation of a MeCN solvent molecule as illustrated in Scheme 2-2. At lower temperature, the 5-coordinate square pyramidal structure having an η^1-alklyperoxide ligand at the equatorial position and the solvent molecule as an axial ligand predominates as illustrated in Scheme 2-2. When the temperature is raised, the coordinated MeCN dissociates from the complex to give a 4-coordinate cumylperoxide copper(II) complex. DFT calculations indicate that at –90˚C (lower temperature) the two structures have approximately equal free energies whereas at 10˚C (higher temperature) the 4-coordinate cumylperoxide copper(II) complex with a square planer

structure and free MeCN is preferred by about 4 kcal/mol. Consistent with this analysis, TDDFT calculations indicate an LMCT transition at 561 nm for the 4-coordinate complex, but no absorption in the 700 nm region, while for the 5-coordinate acetonitrile complex an absorption is predicted at 716 nm with no predicted transition in the 560 nm region having any significant intensity. Both structures are also predicted to have intense LMCT transitions near 400 nm, but that for the 5-coordinate complex is predicted to be 30 nm to the red of the 4-coordinate complex, which is contrary to what is observed experimentally. However, it must be noted that the positions of the λ_{max} values in the experimental spectra may be influenced by the tails of very intense absorptions further to the blue that are not practical to include in the TDDFT calculations. Because it is much easier to distinguish accurately between the behavior of the 560 nm and 700 nm peaks than between peaks having a nominal separation of 25 nm in the blue region of the spectrum, the author and his c0-workers consider their invocation of a solvent coordination equilibrium to be reasonably secure.

The larger $A_{//}$ value of **2a** in the EPR spectrum may also support our proposal. Namely, the large $A_{//}$ value of **2a** (192 G) as compared to that of **1a** (176 G) can be attributed to the partial dissociation of the solvent molecule MeCN, making the contribution of d_{x2-y2} ground state larger.

The tpa ligand system

Cumylperoxide copper(II) complexes **2b** of the tetradentate ligands tpa can be generated in a similar manner, and the spectral data such as UV-vis and resonance Raman are summarized in Table 2-1. The UV-vis, resonance Raman and EPR spectra themselves are presented in Figures S1~S4.

Table 2-1. The apparent formation constant K_{app} and UV-vis and resonance Raman data of the cumylperoxide copper(II) complexes

Complex	UV-vis λ_{max}, nm (ε, M^{-1} cm^{-1})	Resonance Raman ν ($\Delta\nu(^{16}O–^{18}O)$), cm^{-1}
2a	388 (1530), 560 (178), 700 (123)	526 (18), 588 (7), 828 (35), 864 (22)
2b	430 (617), 690 (173), 790 (169)	535 (7), 607 (18), 832 (35), 879 (21)

The copper(II) complex **2b** supported by the tetradentate ligand (tpa) gave an alkylperoxide-to-copper(II) charge transfer (LMCT) band at 430 nm (ε = 617 M^{-1} cm^{-1}) and d-d bands at 690 nm (ε = 173 M^{-1} cm^{-1}) and at 790 nm (ε = 169 M^{-1} cm^{-1}) (Figure 2-S2; TDDFT predicts separate absorptions at 708 and 734 nm).[32] The two distinct d-d bands at the longer wavelength region are a typical spectral feature of the copper(II) complexes having a trigonal bipyramidal structure. Thus, **2b** may also have a trigonal bipyramidal structure as in the case of the starting copper(II) complex (Scheme 2-3).

Scheme 2-3

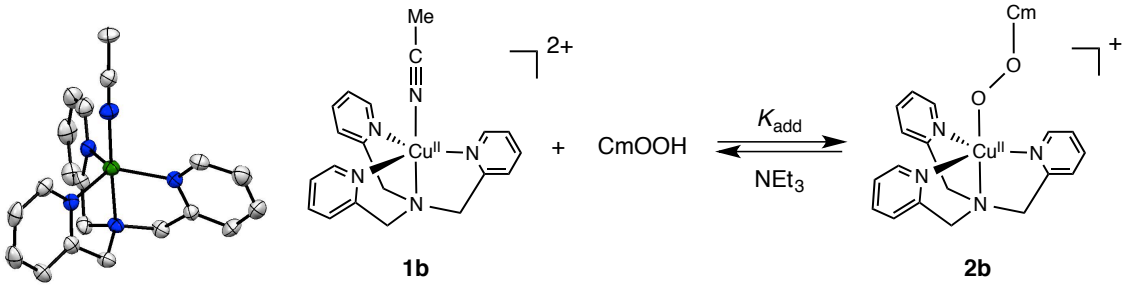

The generated cumylperoxide complex **2b** was also stable for several hours even at room temperature. Then, the apparent binding constant K_{app} of CmOOH to **1b** was determined as 7.5 x 10^4 M^{-1} by the titration in CH_3CN at –40 °C in the presence of Et_3N (10 mM) as shown in Figure 2-S1.[33] In this case, no temperature dependent spectral change was evident in the UV/Vis absorption spectra. This result also supports our interpretation of the temperature dependent solvent association/dissociation equilibrium in the tridentate bpa ligand system shown in Scheme 2-2, since in the tetradentate tpa system there is no vacant coordination site for MeCN solvent binding.

The ESI-MS of the titration solution exhibited a prominent ion peak at a mass-to-charge (m/z) ratio of 504.2 (Figure 2-S2a, EXP), whose mass and isotope distribution pattern were consistent with the chemical formula of $[Cu(tpa)(O_2Cm)]^+$ (calculated m/z = 504.2) (Figure 2-S2a, SIM). When $Cm^{18}O^{18}OH$ was used instead of $Cm^{16}O^{16}OH$, the peak position shifted to 508.2 (4 mass unit shift) (Figure 2-S2b). These results unambiguously confirmed the formation of cumylperoxide copper(II) complex **2b**.

In the resonance Raman spectrum shown in Figure 2-S3, there are isotope sensitive Raman bands at 879, 832, 607, and 535 cm^{-1}, which shifted to 858, 797, 589, and 528 cm^{-1} upon ^{18}O-substitution using $Cm^{18}O^{18}OH$. Judging from the resonance Raman band abound 850 cm^{-1}, the O–O bond in the tetradentate tpa ligand system is somewhat stronger than that in the tridentate bpa ligand system (see Table 2-1). This is also reflected in the lower reactivity of **2b** as compared to **2a** as discussed below.

Complex **2b** exhibited a rather featureless isotropic EPR spectrum as shown in Figure 2-S4b, which is nearly identical to the EPR spectrum of **1b** (starting material, Figure 2-S4a). Thus, the trigonal bipyramidal structure of **1b** is maintained in the cumylperoxide complex **2b** as indicated in Scheme 2-3. In spite of our great efforts, however, single crystal of **2b** has yet to be obtained. The mononuclearity of **2b** was also confirmed by spin quantification using EPR spectrum (100 % spin remained).

Recently, Nam and coworkers reported a similar cumylperoxide copper(II) complex supported by hexamethyl-tren ligand (Me_6-tren).[34] The complex exhibits similar spectroscopic characteristics (UV-vis, ESI-MS and resonance Raman) to those of **2b**, suggesting a similar trigonal bipyramidal structure. However, their alkylperoxide complex does not exhibit any reactivity toward external substrates, being in sharp contrast to our complex **2b** (see below).[34]

Reactivity of the copper(II) alkylperoxide complexes.

Self-decomposition in CH_3CN

The cumylperoxide copper(II) complexes were relatively stable at room temperature but gradually decomposed at higher temperature (Table 2-2). Figure 2-6 shows the spectral change of the self-decomposition of **2a** in CH_3CN at 60 °C to give a copper(II) compound having a weak band at 580 nm (ε = 118 M^{-1} cm^{-1}). The reaction obeys first-order kinetics as shown in the inset of Figure 2-6 ($k_{dec(2a)}$ = 9.6 x 10^{-3} s^{-1}). ESI-MS analysis of the final reaction solution indicated formation of $[Cu^{II}(bpa)(CN)]^+$ as a major product complex as shown in Figure 2-S5; HPLC analysis of the organic products demonstrated formation of acetophenone (PhCOMe) and cumyl alcohol (CmOH) in 76 % and 15 % yields, respectively.

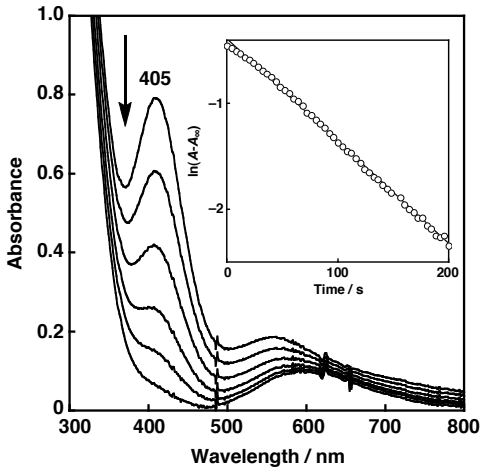

Figure 2-6. Spectral change for the self-decomposition of **2a** in acetonitrile (1.0 mM) at 60°C. Inset: first-order plot based on the absorption change at 405 nm.

It has been reported that the products obtained from a cumylperoxide complex largely depend on the O–O bond cleavage pattern (Scheme 2-4). If homolytic O–O bond cleavage occurs (path a), acetophenone (PhCOMe) is produced from cumyloxyl radical via β-scission releasing methyl radical (CH_3•). In contrast, heterolytic O–O bond cleavage (path b) gives cumyl alcohol (CmOH) after oxyanion protonation.[35] Thus, formation of PhCOMe as the major product (76 %) suggests that self-decomposition of **2a** mainly involves O–O bond homolysis (path a). However, the formation of CmOH as the minor product (15 %) could be interpreted to indicate that the heterolytic O–O bond cleavage (path b) might also occur as a minor pathway. However, one would expect O–O bond heterolysis to be thermodynamically unfavorable due to instability of the generated LCu^{II}–O^+ species.

Scheme 2-4

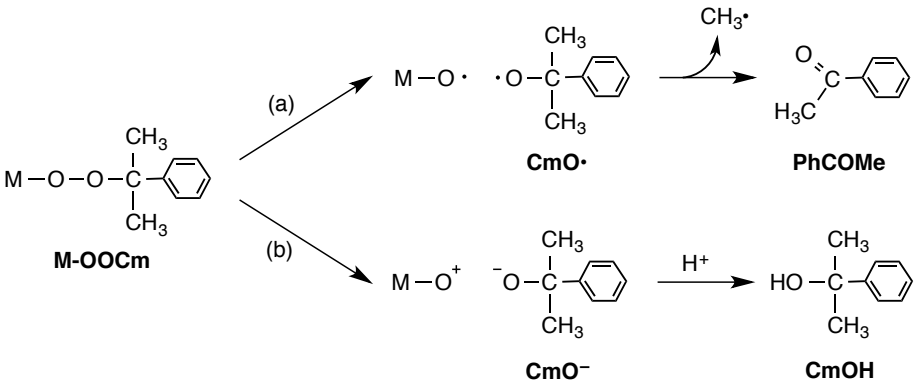

Scheme 2-5

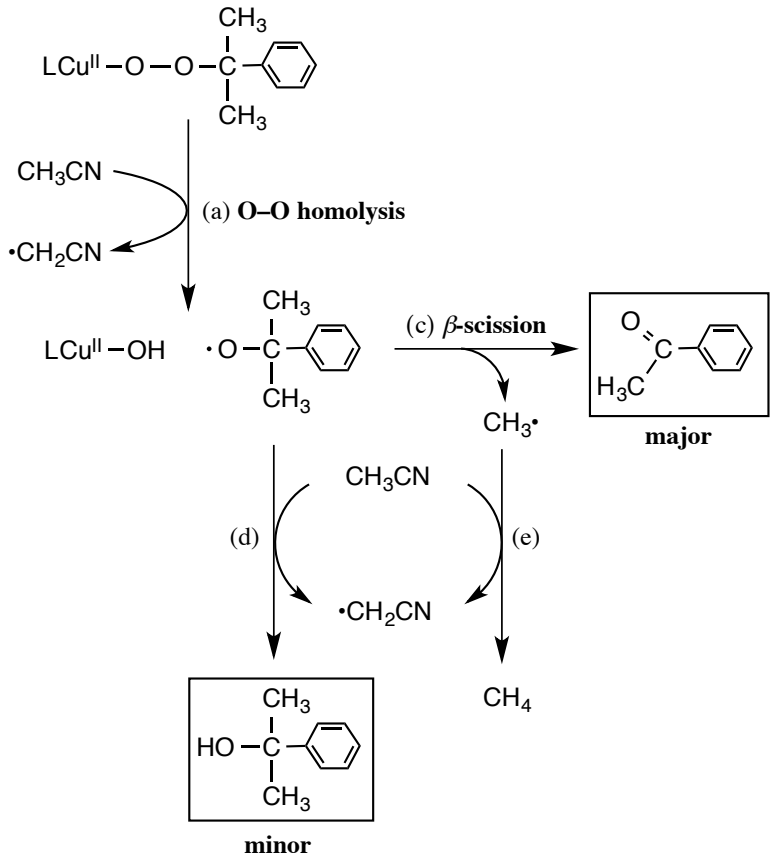

An alternative interpretation is that CmOH is produced from cumyloxyl radical (CmO•) via direct hydrogen atom abstraction from the solvent (path d, Scheme 2-5), which may compete with the β-scission of CH_3• (path c). It should be mentioned here that the decay process of **2a** exhibited a distinct solvent kinetic deuterium isotope effect (KIE) of 2.9 (k_{dec}^{H} = 9.6 x 10^{-3} s^{-1}, k_{dec}^{D} = 3.3 x 10^{-3} s^{-1}), when the reaction was carried out in CD_3CN. Thus, the O–O bond homolysis (path a) might be associated with the hydrogen atom abstraction from the solvent as indicated in Scheme 2-5. Generated solvent radical •CH_2CN may be trapped by the generated LCu^{II}-OH to give LCu^{II}-OCH_2CN, which is further converted to LCu^{II}-CN (as detected by ESI-MS) and HCHO. The author and his co-workers examine these issues in additional detail below in our DFT-based mechanistic analysis.

The cumylperoxide copper(II) complex **2b** also decomposed at 60 °C to give PhCOMe as the major product (~85 %) together with CmOH as the minor one (~15 %). In these cases as well, the cyano complex $[Cu^{II}(tpa)(CN)]^+$ was detected from the final

reaction mixture by ESI-MS. The decomposition rate $k_{dec(2b)}$ of **2b** (3.5 x 10^{-3} s^{-1}) was smaller than that of **2a** (9.6 x 10^{-3} s^{-1}), which is consistent with the fact that the O–O bond of the former is stronger than that in the later as suggested by the resonance Raman data shown in Table 2-1. In this case as well, a solvent KIE of 2.1 (k_{dec}^{D} = 1.7 x 10^{-3} s^{-1}) was obtained, suggesting a similar hydrogen atom abstraction from the solvent concomitant with the O–O bond homolysis.

Table 2-2. Rate constant (k_{dec}) and products of self-decomposition of cumylperoxide copper(II) complexes in CH_3CN at 60°C

Complex	K_{dec}, s^{-1}	CmOH	PhCOMe
2a	9.6 x 10^{-3}	15 %	76 %
2b	3.5 x 10^{-3}	15 %	83 %

Reaction with 1,4-cyclohexadiene (CHD)

Reactivity of the alkylperoxide copper(II) complexes toward external substrates was then examined in order to gain more insight into the roles of copper(II)-alkylperoxide complexes in the initial steps of lipid peroxidation (eqns 1, 5, and 6). In this study, 1,4-cyclohexadiene (CHD) was employed as a model substrate. Addition of CHD into the acetonitrile solution of **2a** at 30 ºC under anaerobic conditions (**2a** was generated at –40 ºC and then warmed up to 30 ºC) resulted in a decrease of the characteristic absorption band at 405 nm assigned to **2a** as shown in Figure 2-7a. The reaction obeyed first-order kinetics in the presence of an excess amount of CHD as shown in the inset Figure 2-7a. A plot of the first-order rate constant k_{obs} against the substrate concentration gave a linear correlation, from which the second-order rate constant k_2 was determined as 4.9 x 10^{-2} M^{-1} s^{-1} (Figure 2-7b). Since the reaction of **2a** with CHD was much faster than the self-decomposition at 30°C and the first-order rate constant k_{obs} exhibited first-order dependence on the CHD concentration, O–O bond cleavage of **2a** is not the rate-determining step, as discussed further below.

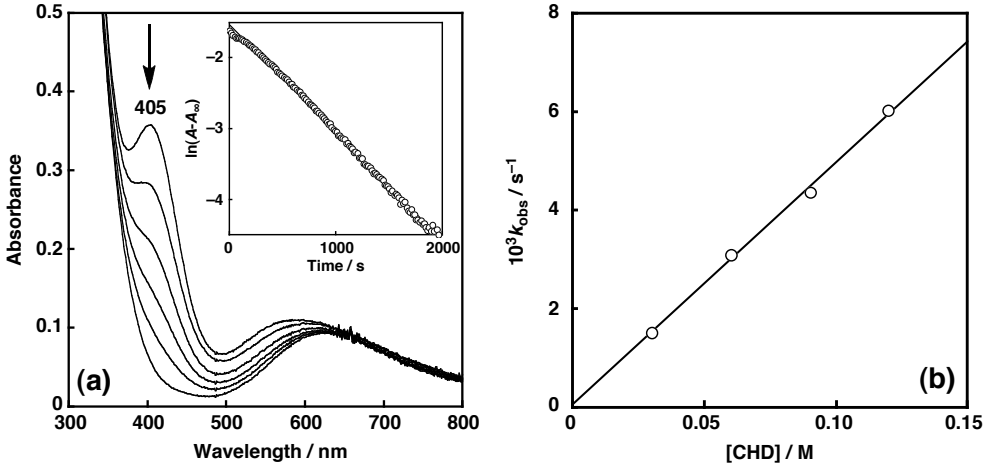

Figure 2-7. (a) Spectral change for the reaction of **2a** (1.0 mM) and CHD (30 mM) in CH_3CN at 30 °C under anaerobic conditions; Inset: the pseudo-first-order plot based on the absorption change at 405 nm. (b) Plot of k_{obs} vs substrate concentration for the reaction of **2a** with CHD.

ESI-MS analysis on the final reaction solution indicated formation of $[Cu^{II}(bpa)(OH)]^+$ as a major copper(II) product complex as shown in Figure 2-S6, which was in contrast to the case of self-decomposition of **2a** where $[Cu^{II}(bpa)(CN)]^+$ was a major product. The product distribution pattern of the organic products was also different from that of the self-decomposition reaction. Namely, cumyl alcohol (CmOH) became a major product (64 %), whereas acetophenone (PhCOMe) was a minor one (32 %). Quantitative formation of benzene as the oxidation product of CHD was also confirmed by HPLC (98 % based on **2a**). In the absence of **2a**, no such reaction took place between CHD and CmOOH, confirming the participation of the copper(II) complex to the oxidation of CHD by CmOOH. These results suggest that neither LCu^{II}–O• nor cumyloxyl radical CmO• are fully generated by complete O–O bond homolysis of **2a** (path a) prior to possibly concerted hydrogen-atom abstraction(s) from the substrate (CHD) (paths f and g) to give LCu^{II}-OH and CmOH together with benzene product (Scheme 2-6). Formation of PhCOMe as the minor product (32 %) may also indicate that the hydrogen atom abstraction by CmO• (path g) competes to some extent with the β-scission (path c) in CmO•. In this case as well, generated CH_3• may also abstract hydrogen atom from CHD (path h).

Scheme 2-6

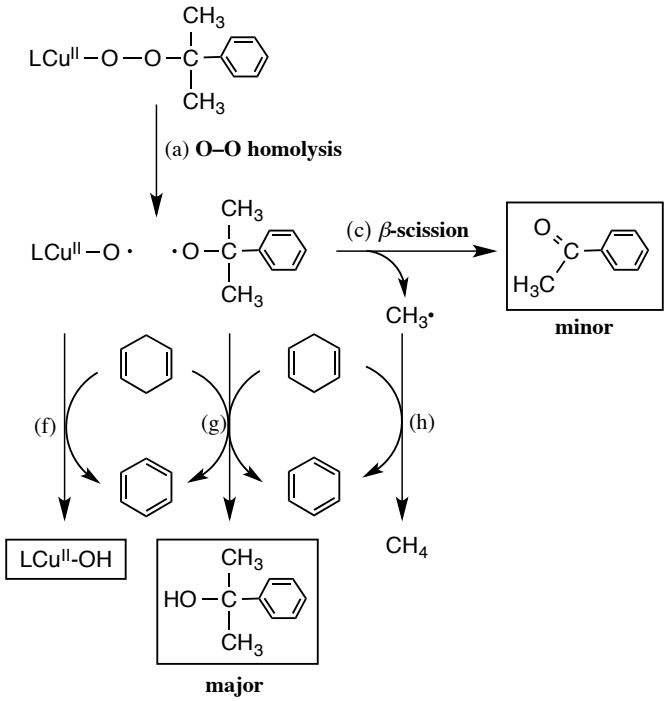

It has been reported that the rate of β-scission of cumyloxyl radical CmO• is ~7.5 x 10^5 s^{-1} in CH_3CN at room temperature.[35b] Then, the rate constant for the hydrogen atom abstraction from CHD by CmO• under the present reaction conditions can be estimated as ~1.5 x 10^6 s^{-1} from the product ratio of CmOH/PhCOMe = 2 (64%/32%). Since the concentration of CHD used was 3 x 10^{-2} M, the second-order rate constant for the hydrogen atom abstraction from CHD by CmO• is calculated to be ~5 x 10^7 M^{-1} s^{-1}. The calculated second-order rate constant is very close to the reported value of ~6 x 10^7 M^{-1} s^{-1}.[36]

It should be noted that the observed second-order rate constant k_2 = 4.9 x 10^{-2} M^{-1} s^{-1} is much smaller than that of the second-order rate constant for the hydrogen atom abstraction from CHD by CmO• (~5 x 10^7 M^{-1} s^{-1}). This unambiguously indicates that the rate-determining step in the oxidation of CHD by LCu^{II}-OOCm involves some degree of O–O bond homolysis. Were the O–O bond homolysis to be the only component of the rate-limiting step, with hydrogen atom abstraction occurring after complete O–O bond homolysis (Scheme 2-6 in the limit of a fully *stepwise* mechanism), the rate constant k_2 would perforce be the same as the self-decomposition rate and be independent of the CHD concentration. However, this is not the case for the present

reaction as indicated in Figure 2-7b, where k_2 was much faster than the self-decomposition at 30°C and showed a first-order dependence on CHD concentration. Thus, it can be concluded that the O–O bond homolysis of LCu^{II}-OOCm occurs concomitantly with the hydrogen atom abstraction as illustrated in Scheme 2-7 (concerted mechanism). This conclusion is further supported by DFT calculations (see below).

Scheme 2-7

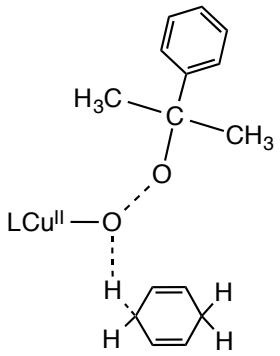

The cumylperoxide copper(II) complex **2b** supported by the tetradentate ligand tpa also reacted with a CHD, obeying first-order kinetics at 30 °C (Figure 2-S7a), to give CmOH as the major product (71 %) together with PhCOMe as the minor one (29 %). The product distribution in this reaction is similar to that of **2a**. The second-order rate k_2 for **2b** was determined as 7.9 x 10^{-3} M^{-1} s^{-1} (Figure 2-S7b), which was smaller than that for **2a** (4.9 x 10^{-2} $M^{-1}s^{-1}$). This may be due to a stronger O–O bond in **2b** as compared to **2a** as suggested by the resonance Raman data shown in Table 2-1.

Theoretical Modeling

Density functional theory (DFT) calculations were employed in order to assess the structural and energetic details associated with specific microscopic steps suggested in our various mechanistic analyses above. As noted previously, the author and his co-workers evaluated the tendency of MeCN solvent to occupy an open coordination site in otherwise tetracoordinate $[Cu^{II}(OOCm)bpa]^+$ (cf. ***i*** and ***ii*** in Figure 2-8), and they find that at 25 °C entropy effects favor free solvent and the 4-coordinated $[Cu^{II}(OOCm)bpa]^+$ by about 5.1 kcal/mol, although ***i*** and ***ii*** + separated MeCN become isoergonic at about –90 °C.

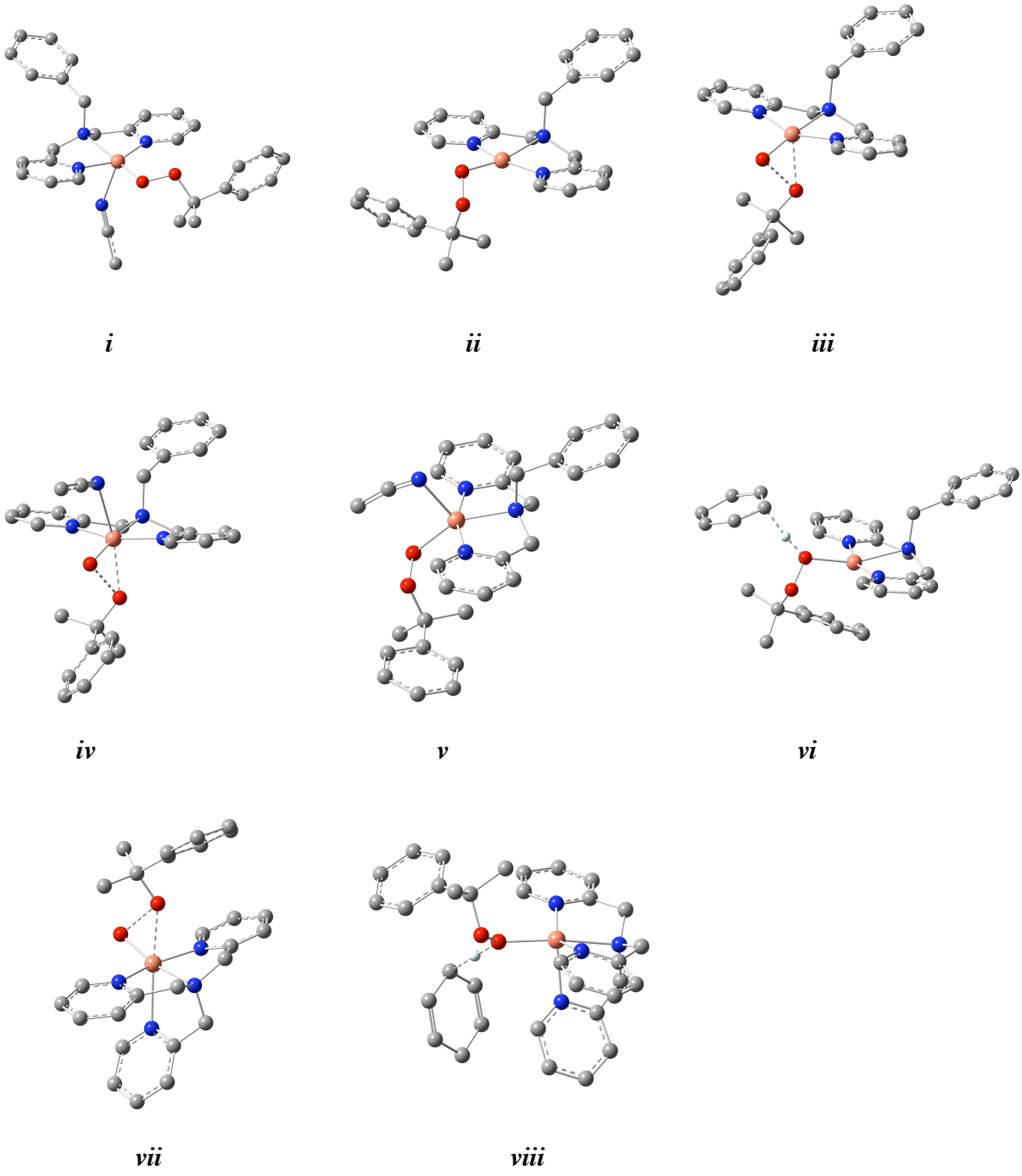

Figure 2-8. Ball-and-stick stereostructures for selected stationary points on the mechanistic pathway leading to O-O bond cleavage as computed at the M06-L level of theory. For clarity, hydrogen atoms are not shown other than those transferred from CHD to a peroxyl O atom. Hydrogen atoms are white, carbon atoms are gray, nitrogen atoms are blue, oxygen atoms are red, and copper atoms are latte.

The author and his co-workers next considered the unimolecular O–O bond scission mechanism implicated for the self-decomposition of ***ii***. Transition-state (TS) structure ***iii*** exhibits O–O bond breakage with migration of the newly forming Cm-O• radical to the copper center. An analogous structure ***iv*** was also located that involves the same reaction coordinate but includes a coordinated CH_3CN molecule (included to assess its influence on the reaction energetics). Finally, with inclusion of a molecule of solvent CH_3CN it is possible to characterize a TS structure ***v*** that involves H atom abstraction from the CH_3CN methyl group concomitant with O–O bond breakage (the H-atom transfer takes place to the O atom of the peroxyl fragment coordinated to the Cu atom). All three TS structures lead to the same supported copper product, $[Cu^{II}(OH)•OCm]bpa]^+$. The free energies of activation associated with the TS structures ***iii***, ***iv***, and ***v*** are all very close: 30.9, 32.1 and 32.2 kcal/mol, respectively. This small span of activation free energies suggests that O–O bond scission and H-atom abstraction from solvent acetonitrile should be competitive with one another, consistent with the mixtures of cumyloxyl decomposition products described above. Providing additional support for these two reaction paths being simultaneous, the author and his co-workers note that they predict the semi-classical primary kinetic isotope effect (KIE) for (H/D)-atom abstraction from CH_3CN to be 5.6. This value is larger than the observed value of 2.9, and inclusion of quantum mechanical tunneling would be likely to make the computed value larger still. The smaller observed KIE value may thus be associated with substantial reactivity occurring through the O–O bond scission step, which is insensitive to solvent isotopic composition.

With respect to the reaction of $[Cu^{II}(OOCm)bpa]^+$ with CHD, a TS structure ***vi***, similar to the one depicted in Scheme 2-7, was located having a free energy of activation of 24.7 kcal/mol. Comparing the $\Delta G^{\ddagger}$ values of ***iii***-***v*** with that for ***vi*** indicates that the concerted nature of the H atom abstraction from CHD reduces the barrier associated with O–O bond scission. It also suggests that C–H bonds stronger than that in CHD by more than 10 kcal/mol or so would be unlikely to participate in the concerted reaction, as simple O–O bond scission would be more energetically favorable.

Similar TS structures (***vii***, ***viii***) were found for the analogous tpa-supported compounds with corresponding free energies of activation slightly higher (~ 1.0 kcal/mol) than the ones in the bpa series. This observation agrees well with the experimental reactivity observations.

Conclusion

In this study, the spectroscopy and reactivity of copper(II)-alkylperoxide complexes supported by the tridentate and tetradentate 2-pyridylmethylamine ligands (bpa and tpa) have been explored in detail. Both complexes exhibit an intense LMCT band around 400 nm together with d-d band(s) associated with tetragonal and trigonal bipyramidal structures, respectively (Table 2-1). The complexes also provide multiple resonance Raman bands as indicated in Table 2-1, which have been assigned to mixed O–O/C–O/C–C and Cu–O vibrations and a C–C–O deformation mode of the alkylperoxide moiety. Interestingly, the cumylperoxide copper(II) complex **2a** supported by the tridentate bpa ligand shows thermochromic solvent association/dissociation behavior (Figure 2-5 and Scheme 2-2).

Both cumylperoxide copper(II) complexes **2a** and **2b** are fairly stable at ambient temperature, but both decompose at a higher temperature (60 °C) in CH_3CN. Detailed product analyses and DFT studies indicate that the self-decomposition reaction involves homolytic O–O bond cleavage of the peroxide moiety, where concomitant C–H bond abstraction from the solvent molecule is partially involved (Scheme 2-5).

The cumylperoxide complexes react with 1,4-cyclohexadiene (CHD) to give benzene at 30 °C. Detailed product analyses and DFT studies indicate that this reaction involves concerted homolytic cleavage of the O–O bond and hydrogen-atom abstraction from CHD (Scheme 2-6). DFT calculations indicate that the oxygen atom directly bonded to the copper(II) ion (proximal oxygen) is the one involved in the C–H bond activation process, as illustrated in Scheme 2-7, and this prediction is consistent with the observed distribution of possible copper and cumylperoxide products. In both the self-decomposition and the CHD-oxidation reactions, the reactivity of **2a** is higher than that of **2b**, which could be attributed to a weaker O–O bond in **2a** compared to **2b,** an hypothesis further supported by the resonance Raman data (Table 2-1).

To date, alkylperoxide complexes of transition-metal ions M-OOR have been considered as precursors of reactive metal-oxo species, but not themselves actively responsible for hydrocarbon oxidation. However, the present study demonstrates that C–H bond activations of solvent molecules (CH_3CN) and substrates (CHD) can occur in a concerted manner with O–O bond cleavage. This suggests that Cu^{II}-OOR itself can be an oxidant for hydrocarbons when the C–H bonds are sufficiently reactive.

Acknowledgment

This chapter was reproduced from Dalton Transactions, 2011, 40, 10326-10336, with permission from the Royal Society of Chemistry.

References

1. (a) Girerd, J.-J.; Banse, F.; Simaan, A. in *Structure and Bonding*, Springer: Berlin, Heidelberg, **2000**, vol. *97*, pp 145-177; (b) Costas, M.; Mehn, M. P.; Jensen, M. P.; Que, L., Jr. *Chem. Rev.* **2004**, *104*, 939-986.
2. Chavez, F. A.; Mascharak, P. K. *Acc. Chem. Res.* **2000**, *33*, 539-545.
3. (a) Hikichi, S.; Akita, M.; Moro-Oka, Y. *Coord. Chem. Rev.* **2000**, *198*, 61-87; (b) Akita, M.; Hikichi, S. *Bull. Chem. Soc. Jpn.* **2002**, *75*, 1657-1679.
4. (a) Zang, Y.; Elgren, T. E.; Dong, Y.; Que, L., Jr. *J. Am. Chem. Soc.* **1993**, *115*, 811-813; (b) Ménage, S.; Wilkinson, E. C.; Que, L., Jr.; Fontecave, M. *Angew. Chem., Int. Ed.* **1995**, *34*, 203-205; (c) Kim, J.; Larka, E.; E. C. Wilkinson; Que, L., Jr. *Angew. Chem., Int. Ed.* **1995**, *34*, 2048-2051; (d) Lange, S. J.; Miyake, H.; Que, L., Jr. *J. Am. Chem. Soc.* **1999**, *121*, 6330-6331; (e) Lehnert, N.; Ho, R. Y. N.; Que, L., Jr.; Solomon, E. I. *J. Am. Chem. Soc.* **2001**, *123*, 8271-8290; (f) Lehnert, N.; Ho, R. Y. N.; Que, L., Jr.; Solomon, E. I. *J. Am. Chem. Soc.* **2001**, *123*, 12802-12816; (g) Miyake, H.; Chen, K.; Lange, S. J.; Que, L., Jr. *Inorg. Chem.* **2001**, *40*, 3534-3538; (h) Kim, J.; Zang, Y.; Costas, M.; Harrison, R. G.; Wilkinson, E. C.; Que, L., Jr. *J. Biol. Inorg. Chem.* **2001**, *6*, 275-284; (i) Jensen, M. P.; Lange, S. J.; Mehn, M. P.; Que, E. L.; Que, L., Jr. *J. Am. Chem. Soc.* **2003**, *125*, 2113-2128; (j) Kaizer, J.; Costas, M.; Que, L., Jr. *Angew. Chem., Int. Ed.* **2003**, *42*, 3671-3673; (k) M. i. Payeras, A.; Ho, R. Y. N.; Fujita, M.; Que, L., Jr. *Chem.–Eur. J.* **2004**, *10,* 4944-4953. (l) Rohde, J.-U.; Torelli, S.; Shan, X.; Lim, M. H.; Klinker, E. J.; Kaizer, J.; Chen, K.; Nam, W.; Que, L., Jr. *J. Am. Chem. Soc.* **2004**, *126*, 16750-16761; (m) Bukowski, M. R.; Halfen, H. L.; van den Berg, T. A.; Halfen, J. A.; Que, L., Jr. *Angew. Chem., Int. Ed.* **2005**, *44*, 584-587; (n) Jensen, M. P.; Costas, M.; Ho, R. Y. N.; Kaizer, J.; M. i. Payeras, A.; Munck, E.; Que, L., Jr.; Rohde, J. -U. and Stubna, A. *J. Am. Chem. Soc.* **2005**, *127*, 10512-10525; (o) Bautz, J.; Comba, P.; Que, L., Jr. *Inorg. Chem.* **2006**, *45*, 7077-7082; (p) Jensen, M. P.; M. i. Payeras, A.; Fiedler, A. T.; Costas, M.;

Kaizer, J.; Stubna, A.; Munck, E.; Que, L., Jr. *Inorg. Chem.* **2007**, *46*, 2398-2408; (q) Shan, X.; Rohde, J. -U.; Koehntop, K. D.; Zhou, Y.; Bukowski, M. R.; Costas, M.; Fujisawa, K.; Que, L., Jr. *Inorg. Chem.* **2007**, *46*, 8410-8417; (r) Fiedler, A. T.; Que, L., Jr. *Inorg. Chem.* **2009**, *48*, 11038-11047.

5. (a) MacFaul, P. A.; Arends, I. W. C. E.; Ingold, K. U.; Wayner, D. D. M. *J. Chem. Soc., Perkin Trans. 2* **1997**, 135-146; (b) Wada, A.; Ogo, S.; Watanabe, Y.; Mukai, M.; Kitagawa, T.; Jitsukawa, K.; Masuda, H.; Einaga, H. *Inorg. Chem.* **1999**, *38*, 3592-3593; (c) Sobolev, A. P.; Babushkin, D. E.; Talsi, E. P. *J. Mol. Catal. A-Chem.* **2000**, *159*, 233-245; (d) Ogihara, T.; Hikichi, S.; Akita, M.; Uchida, T.; Kitagawa, T.; Moro-oka, Y. *Inorg. Chim. Acta* **2000**, *297*, 162-170; (e) Lobanova, M. V.; Bryliakov, K. P.; Duban, E. A.; Taksum, E. P. *Mendeleev Commun.* **2003**, 175-177; (f) Lehnert, N.; Fujisawa, K.; Solomon, E. I. *Inorg. Chem.* **2003**, *42*, 469-481; (g) Krishnamurthy, D.; Kasper, G. D.; Namuswe, F.; Kerber, W. D.; Sarjeant, A. A. N.; Moenne-Loccoz, P.; Goldberg, D. P. *J. Am. Chem. Soc.* **2006**, *128*, 14222-14223; (h) Gosiewska, S.; Permentier, H. P.; Bruins, A. P.; van Koten, G.; Gebbink, R. *Dalton Trans.* **2007**, 3365-3368; (i) Seo, M. S.; Kamachi, T.; Kouno, T.; Murata, K.; Park, M. J.; Yoshizawa, K.; Nam, W. *Angew. Chem., Int. Ed.* **2007**, *46*, 2291-2294; (j) Namuswe, F.; Kasper, G. D.; Sarjeant, A. A. N.; Hayashi, T., Krest, C. M.; Green, M. T.; Moenne-Loccoz, P.; Goldberg, D. P. *J. Am. Chem. Soc.* **2008**, *130*, 14189-14200; (k) Namuswe, F.; Hayashi, T.; Jiang, Y. B.; Kasper, G. D.; Sarjeant, A. A. N.; Moenne-Loccoz, P.; Goldberg, D. P. *J. Am. Chem. Soc.* **2010**, *132*, 157-167; (l) Stasser, J.; Namuswe, F.; Kasper, G. D.; Jiang, Y.; Krest, C. M.; Green, M. T.; Penner-Hahn, J.; Goldberg, D. P. *Inorg. Chem.* **2010**, *49*, 9178-9190.

6. Kovaleva, E. G.; Lipscomb, J. D. *Science* **2007**, *316*, 453-457.

7. Costas, M.; Chen, K.; Que, L., Jr. *Coord. Chem. Rev.* **2000**, *200-202*, 517-544.

8. Burkitt, M. J. *Arch. Biochem. Biophys.* **2001**, *394*, 117-135.

9. Jones, C. M.; Burkitt, M. J. *J. Am. Chem. Soc.* **2003**, *125*, 6946-6954.

10. (a) Halcrow, M. A. in *Comprehensive Coordination Chemistry II*, eds. Que, L., Jr. and Tolman, W. B. Elsevier: Amsterdam, **2004**, pp 395-436; (b) Itoh, S. in *Comprehensive Coordination Chemistry II*, eds. Que, L., Jr. and Tolman, W. B. Elsevier: Amsterdam, **2004**, pp 369-393.

11. Punniyamurthy, T.; Rout, L. *Coord. Chem. Rev.* **2008**, *252*, 134-154.
12. (a) Mirica, L. M.; Ottenwaelder, X.; Stack, T. D. P. *Chem. Rev.* **2004**, *104*, 1013-1045; (b) Lewis, E. A.; Tolman, W. B. *Chem. Rev.* **2004**, *104*, 1047-1076; (c) Himes, R. A.; Karlin, K. D. *Curr. Opin. Chem. Biol.* **2009**, *13*, 119-131.
13. Itoh, S. *Curr. Opin. Chem. Biol.* **2006**, *10*, 115-122.
14. (a) Kitajima, N.; Katayama, T.; Fujisawa, K.; Iwata, Y.; Moro-oka, Y. *J. Am. Chem. Soc.* **1993**, *115*, 7872-7873; (b) Chen, P.; Fujisawa, K.; Solomon, E. I. *J. Am. Chem. Soc.* **2000**, *122*, 10177-10193.
15. Kunishita, A.; Ishimaru, H.; Nakashima, S.; Ogura, T.; Itoh, S. *J. Am. Chem. Soc.* **2008**, *130*, 4244-4245.
16. Perrin, D. D.; Armarego, W. L. F.; Perrin, D. R. *Purification of Laboratory Chemicals,* 4th Ed.: Pergamon Press: Elmsford, NY, **1996**.
17. (a) Kawahara, S.-i.; Uchimaru, T. *Eur. J. Inorg. Chem.* **2001**, 2437-2442; (b) Tyeklar, Z.; Jacobson, R. R.; Wei, N.; Murthy, N. N.; Zubieta, J.; Karlin, K. D. *J. Am. Chem. Soc.* **1993**, *115*, 2677-2689.
18. Kunishita, A.; Scanlon, J. D.; Ishimaru, H.; Honda, K.; Ogura, T.; Suzuki, M.; Cramer, C. J.; Itoh, S. *Inorg. Chem.* **2008**, *47*, 8222-8232.
19. Fox, S.; Nanthakumar, A.; Wikstrom, M.; Karlin, K. D.; Blackburn, N. J. *J. Am. Chem. Soc.* **1996**, *118*, 24-34.
20. Finn, M. G.; Sharpless, K. B. *J. Am. Chem. Soc.* **1991**, *113*, 113-126.
21. Zhao, Y.; Truhlar, D. G. *J. Chem. Phys.* **2006**, *125*, 194101-194118.
22. Dolg, M.; Wedig, U.; Stoll, H.; Preuss, H. *J. Chem. Phys.* **1987**, *86*, 866-872.
23. Hehre, W. J.; Radom, L.; Schleyer, P. v. R.; Pople, J. A. *Ab Initio Molecular Orbital Theory*, Wiley: New York, **1986**.
24. Frisch, M. J.; Trucks, G. W.; Schlegel, H. B.; Scuseria, G. E.; Robb, M. A.; Cheeseman, J. R.; Scalmani, G.; Barone, V.; Mennucci, B.; Petersson, G. A.; Nakatsuji, H.; Caricato, M.; Li, X.; Hratchian, H. P.; Izmaylov, A. F.; Bloino, J.; Zheng, G.; Sonnenberg, J. L.; Hada, M.; Ehara, M.; Toyota, K.; Fukuda, R.; Hasegawa, J.; Ishida, M.; Nakajima, T.; Honda, Y.; Kitao, O.; Nakai, H.; Vreven, T.; Montgomery, J. A., Jr.; Peralta, J. E.; Ogliaro, F.; Bearpark, M.; Heyd, J. J.; Brothers, E.; Kudin, K. N.; Staroverov, V. N.; Kobayashi, R.; Normand, J.; Raghavachari, K.; Rendell, A.; Burant, J. C.; Iyengar, S. S.; Tomasi, J.; Cossi, M.; Rega, N.; Millam, J. M.; Klene, M.; Knox, J. E.; Cross, J. B.; Bakken, V.;

Adamo, C.; Jaramillo, J.; Gomperts, R.; Stratmann, R. E.; Yazyev, O.; Austin, A. J.; Cammi, R.; Pomelli, C.; Ochterski, J. W.; Martin, R. L.; Morokuma, K.; Zakrzewski, V. G.; Voth, G. A.; Salvador, P.; Dannenberg, J. J.; Dapprich, S.; Daniels, A. D.; Farkas, O.; Foresman, J. B.; Ortiz, J. V.; Cioslowski, J.; Fox, D. J. Gaussian 09, Revision A.02; Gaussian, Inc.: Wallingford, CT, **2009**.

25. Cramer, C. J. *Essentials of Computational Chemistry: Theories and Models*, John Wiley & Sons: Chichester, **2004**.
26. Marenich, A. V.; Cramer, C. J.; Truhlar, D. G. *J. Phys. Chem. B*, **2009**, *113*, 6378-6396.
27. (a) Ziegler, T.; Rauk, A.; Baerends, E. J. *Theor. Chim. Acta* **1977**, *43*, 261-271; (b) Noodleman, L. *J. Chem. Phys.* **1981**, *74*, 5737-5743; (c) Cramer, C. J.; Truhlar, D. G. *Phys. Chem. Chem. Phys.* **2009**, *11*, 10757-10816.
28. (a) Yamaguchi, K.; Jensen, F.; Dorigo, A.; Houk, K. N. *Chem. Phys. Lett.* **1988**, *149*, 537-542; (b) Soda, T.; Kitagawa, Y.; Onishi, T.; Takano, Y.; Shigeta, Y.; Nagao, H.; Yoshioka, Y.; Yamaguchi, K. *Chem. Phys. Lett.* **2000**, *319*, 223-230.
29. (a) Noodleman, L.; Peng, C. Y.; Case, D. A.; Mouesca, J.-M. *Coord. Chem. Rev.* **1995**, *144*, 199-244; (b) Neese, F. *Coord. Chem. Rev.* **2009**, *253*, 526-563; (c) Ciofini, I.; Daul, C. A. *Coord. Chem. Rev.* **2003**, *238*, 187-209; (d) Harvey, J. N. *Struct. Bond.* **2004**, *112*, 151-183.
30. Schmider, H. L.; Becke, A. D. *J. Chem. Phys.* **1998**, *108*, 9624-9631.
31. Improta, R.; Barone, V.; Scalmani, G.; Frisch, M. J. *J. Chem. Phys.* **2006**, *125*, 054103.
32. TD-DFT calculations have clearly indicated that the 388 nm absorption band (for **2a**) and the 430 nm band (for **2b**) are due to the charge-transfer from π^* of peroxide fragment to d_{x2-y2} of Cu. However, the 560 nm band of **2a** is a bit more complicated. The acceptor orbital is still the same d_{x2-y2}, but the excitation is about equal parts the d_{z2} of Cu and an O_2 π orbital. That mixing of d-d character with CT character is presumably responsible for the rather low extinction coefficient.
33. Itoh, S.; Kawakami, H.; Fukuzumi, S. *Biochemistry* **1998**, *37*, 6562-6571.
34. Choi, Y. J.; Cho, K.-B.; Kubo, M.; Ogura, T.; Karlin, K. D.; Cho, J.; Nam, W. *Dalton Trans.* **2011**, *40*, 2234-2241.

35. (a) Adachi, S.; Nagano, S.; Ishimori, K.; Watanabe, Y.; Morishima, I.; Egawa, T.; Kitagawa, T.; Makino, R. *Biochemistry* **1993**, *32*, 241-252; (b) Avila, D. V.; Brown, C. E.; Ingold, K. U.; Lusztyk, J. *J. Am. Chem. Soc.* **1993**, *115*, 466-470; (c) Baciocchi, E.; Bietti, M.; Salamone, M.; Steenken, S. *J. Org. Chem.* **2002**, *67*, 2266-2270.

36. Salamone, M.; Anastasi, G.; Bietti, M.; DiLabio, G. A. *Org. Lett.* **2011**, *13*, 260-263.

Supporting Information

For Chapter 2

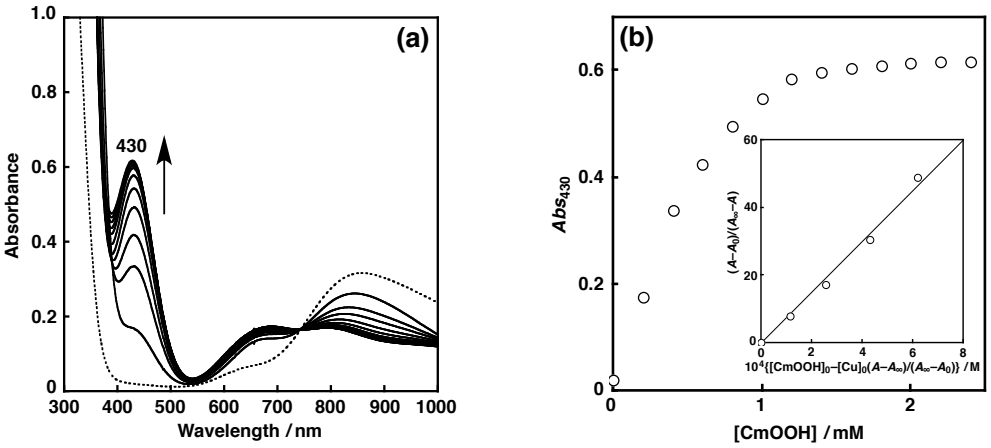

Figure 2-S1. (a) Spectral change for the reaction of **1b** (1.0 mM) with CmOOH (2.5 mM) in the presence of Et_3N (10 mM) in CH_3CN at –40ºC. (b) Spectrophotometric titration for the formation of cumylperoxide copper(II) complex from the reaction of **1b** (1.0 mM) and CmOOH in the presence of Et_3N (10 mM) in CH_3CN at –40ºC. Inset: Plot of $(A - A_0)/(A_\infty - A)$ against $[CmOOH]_0 - [Cu]_0(A - A_0)/(A_\infty - A_0)]$.

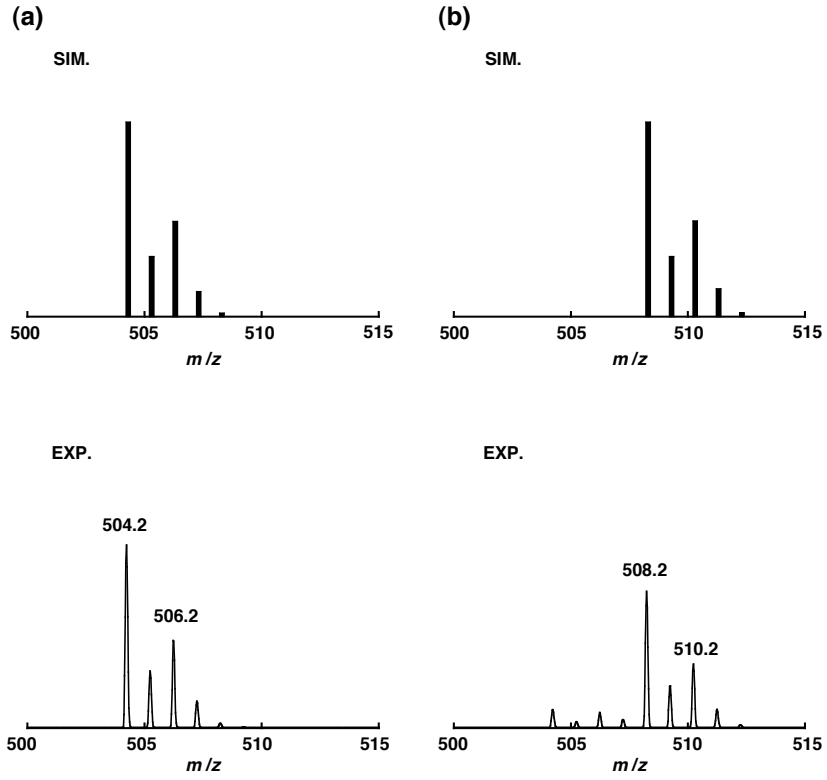

Figure 2-S2. Experimental (bottom) and simulated (top) peak envelopes in the positive-ion ESI-MS spectra of the product derived from the reaction of **1b** (1.0 mM) with CmOOH (1.0 mM) in the presence of Et_3N (1.0 mM) in CH_3CN at –40ºC; (a) with $Cm^{16}O_2H$ and (b) with $Cm^{18}O_2H$.

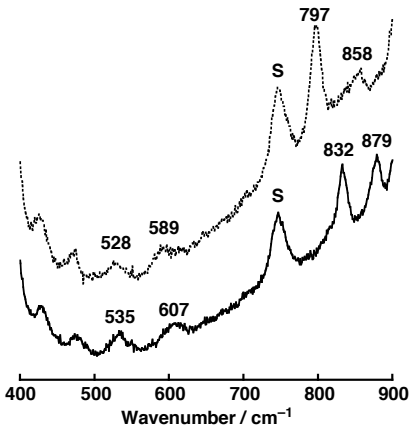

Figure 2-S3. Resonance Raman spectra of the product derived from the reaction of **1b** (4.0 mM) with CmOOH (12 mM) in the presence of Et_3N (40 mM) generated by using $Cm^{16}O_2H$ (solid line, below) and $Cm^{18}O_2H$ (doted line, above) obtained with λ_{ex} = 441.6 nm in CH_3CN –40°C; s denotes the solvent band.

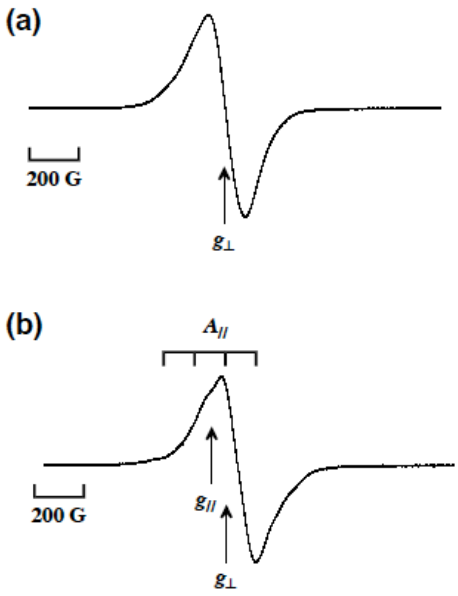

Figure 2-S4. (a) EPR spectrum of **1b** (starting material) (2.0 x 10^{-3} M) in CH_3CN at –196°C. EPR parameter $g_{\perp}$ = 2.112. Low resolution of the spectrum prohibits precise assignment of the $g_{//}$ value. (b) EPR spectrum of the **2b** generated in the reaction of 1b (2.0 x 10^{-3} M) and CmOOH (1.0 x 10^{-2} M) in the presence of Et_3N (2.0 x 10^{-3} M) in CH_3CN at –196°C. EPR parameters $g_{//} = 2.198$, $g_{\perp} = 2.118$, $A_{//} = 147$ G.

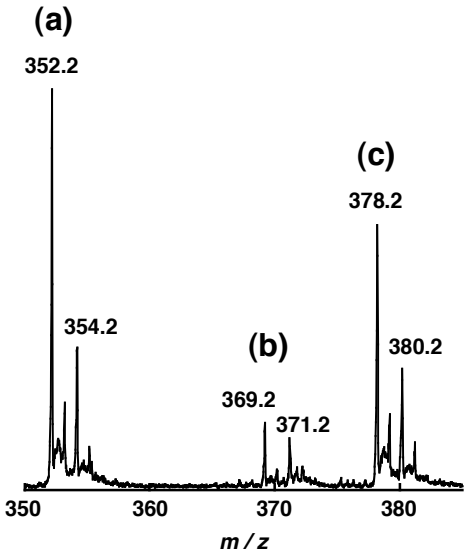

Figure 2-S5. ESI-MS (pos.) spectrum after the self-decomposition of **2a** in CH_3CN. (a) m/z = 352.2 ($[Cu^{I}(bpa^{H})]^{+}$), (b) m/z = 369.2 ($[Cu^{II}(bpa^{H})(OH)]^{+}$), (c) m/z = 378.2 ($[Cu^{II}(bpa^{H})(CN)]^{+}$).

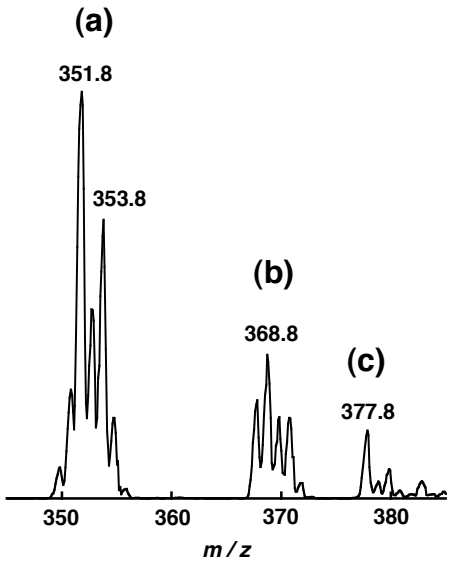

Figure 2-S6. ESI-MS (pos.) spectrum of the final reaction mixture of **2a** and CHD. (a) m/z = 351.8 ($[Cu^{I}(bpa)]^{+}$), (b) m/z = 368.8 ($[Cu^{II}(bpa)(OH)]^{+}$), (c) m/z = 377.8 ($[Cu^{II}(bpa)(CN)]^{+}$).

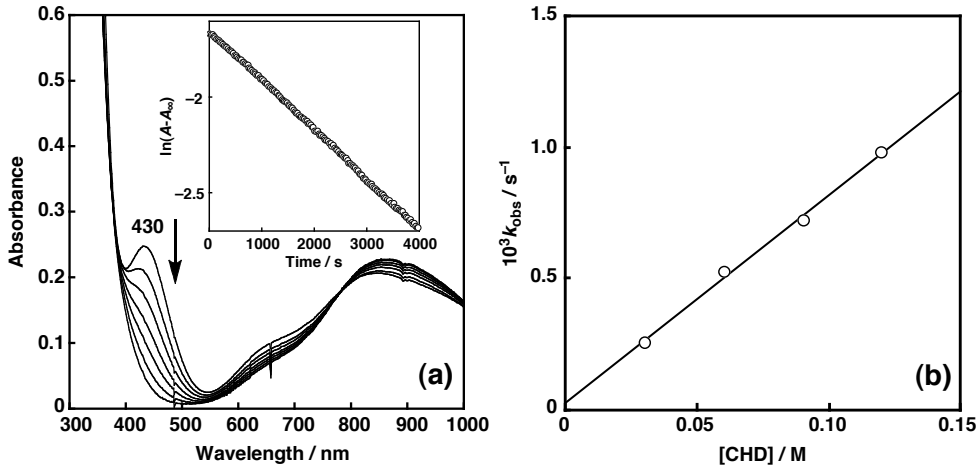

Figure 2-S7. (a) Spectral change for the reaction of **2b** (1.0 mM) and CHD (30 mM) in CH_3CN at 30 °C under anaerobic conditions; Inset: the pseudo-first-order plot based on the absorption change at 430 nm. (b) Plots of k_{obs} vs substrate concentration for the reaction of **2b** with CHD.

Chapter 3 Heterolytic Alkyl Hydroperoxide O–O Bond Cleavage by Copper(I) Complexes

Introduction

The alkylperoxide complexes (M-OOR) of transition-metal ions have been long-standing research objectives because of their strong relevance to biological and catalytic oxidation reactions.[1] Among them, the non-heme iron complexes have been studied most extensively[2,3] to provide profound insights into the catalytic mechanism of iron-containing monooxygenases and iron-catalyzed hydrocarbon oxygenation reactions.[4,5] Homolytic cleavage of O–O bond of Fe^{III}-OOR provides Fe^{IV}=O, whereas O–O bond heterolysis gives Fe^{V}=O species, both of which have been invoked as key reactive intermediates in the oxygenation reactions. However, little attention has been focused on alkylperoxo complexes of copper.[6] In this respect, the author and his co-workers have recently investigated the reaction of cumene hydroperoxide (^{H}CmOOH) and a copper(II) complex supported by *N*,*N*-di(2-pyridylmethyl)benzylamine tridentate ligand (L^{a}, Figure 3-1) to find that the generated cumylperoxo copper(II) complex $L^{a}Cu^{II}(OO^{H}Cm)$ undergoes *homolytic* O–O bond cleavage inducing C–H bond activation of an external substrate such as 1,4-cyclohexadiene.[7] The results provided important insights into the dioxygen-activation mechanism by mononuclear copper complexes in biological and catalytic oxygenation reactions.[8]

In this study, the author and his co-workers have investigated the reaction of *copper(I)* complexes of similar tridentate ligands (L^{a} and L^{b}) and cumene hydroperoxide derivatives (^{X}CmOOH; X = Et, Me, H, Br, F, and NO_2) to find that the copper(I) complexes induce *heterolytic* O–O bond breaking of the alkyl hydroperoxides in contrast to the case of former copper(II)/^{H}CmOOH system.

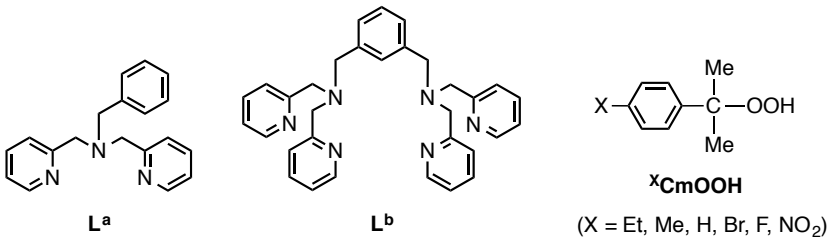

Figure 3-1. Ligands (L^a and L^b) and cumene hydroperoxide derivatives (^{X}CmOOH).

Experimental

Reagents

The reagents and solvents used in this study, except *p*-substituted cumene hydroperoxide derivatives (^{X}CmOOH), were commercial products of the highest available purity and were further purified by the standard methods, if necessary.[14] Ligands L^a (*N*,*N*-di(2-pyridylmethyl)benzylamine) and L^b (*N*,*N*,*N*',*N*'-tetra(2-pyridylmethyl)-*m*-xylylenediamine) and copper(I) complex of L^a, $[Cu^{I}(L^a)(CH_3CN)](PF_6)$ (**1a**), were prepared according to the reported procedures.[11,15] Cumene hydroperoxide (^{H}CmOOH) and 8-hydroperoxy-*p*-cymene (^{Me}CmOOH) were prepared by the reported procedures.[16]

Synthesis of Cumene Hydroperoxide Derivatives ^{X}CmOOH (X = Br, F, Et and NO_2).

1-(4-Bromophenyl)-1-methylethyl hydroperoxide (^{Br}CmOOH). This compound was synthesized by a similar method described in the literature for the synthesis of 8-hydroperoxy-*p*-cymene (^{Me}CmOOH) using 2-(4-bromophenyl)-2-propanol instead of 8-hydroxy-*p*-cymene [T. Ueno, H. Masuda, C.-T. Ho, *Journal of Agricultural and Food Chemistry*, *52* (**2004**) 5677-5684.]. Thus, a solution of 2-(4-bromophenyl)-2-propanol (0.5 g, 2.3 μmol) in ethanol (5 mL) was added dropwise to a stirred mixture of 30% hydrogen peroxide (150 mL) and 2.5 % (w/v) sulfuric acid (15 mL). After stirring for 1 h at room temperature, the reaction mixture was extracted with 250 mL of dichloromethane, washed with water (100 mL x 2), dried over sodium sulfate. After removal of sodium sulfate by filtration, concentration of solvent gave colorless oil, from which 1-(4-bromophenyl)-1-methylethyl hydroperoxide was isolated by silica gel column

chromatography (eluent: hexane/EtOAc = 5/1) in 12 %. HRMS (EI^+) *m/z* = 229.9941 (M^+), calcd for $C_9H_{11}BrO_2$ = 229.9942. ^{1}H-NMR (400 MHz, $CDCl_3$) δ 1.59 (6 H, s, -C*H*$_3$), 7.34 (2 H, d, *J* = 8.8 Hz, Ar*H*), 7.50 (2 H, d, *J* = 8.4 Hz, Ar*H*).

1-(4-Fluorophenyl)-1-methylethyl hydroperoxide (^{F}CmOOH). This compound was prepared by the same procedure described for the synthesis of ^{Br}CmOOH using 2-(4-fluorophenyl)-2-propanol instead of 2-(4-bromophenyl)-2-propanol. Yield: 62 %. HRMS (EI^+) *m/z* = 170.0744 (M^+), calcd for $C_9H_{11}FO_2$ = 170.0743. ^{1}H-NMR (400 MHz, $CDCl_3$) δ 1.60 (6 H, s, -C*H*$_3$), 7.06 (2 H, m, Ar*H*), 7.44 (2 H, m, Ar*H*).

1-(4-Ethylphenyl)-1-methylethyl hydroperoxide (^{Et}CmOOH). This compound was prepared by the same procedure described for the synthesis of ^{Br}CmOOH using 2-(4-ethylphenyl)-2-propanol instead of 2-(4-bromophenyl)-2-propanol. Yield: 70 %. HRMS (EI^+) *m/z* = 180.1148 (M^+), calcd for $C_{11}H_{16}O_2$ = 180.1150. ^{1}H-NMR (400 MHz, $CDCl_3$) δ 1.25 (3 H, t, -CH_2CH_3), 1.61 (6 H, s, -C*H*$_3$), 2.66 (2 H, q, *J* = 7.2 Hz, -C*H*$_2$CH$_3$), 7.22 (2 H, d, *J* = 8.8 Hz, Ar*H*), 7.39 (2 H, d, *J* = 8.4 Hz, Ar*H*).

1-(4-Nitrophenyl)-1-methylethyl hydroperoxide (^{NO2}CmOOH). This compound was prepared according to the method for the synthesis of cumene hydroperoxide (^{H}CmOOH) using 4-nitrocumene instead of cumene [M.G. Finn, K.B. Sharpless, *J. Am. Chem. Soc.*, *113* (**1991**) 113-126]. A 50-mL round bottom flask was charged with 4-nitrocumene (2.0 g, 12 mmol) and stirred for 40 h at 80°C under O_2 atmosphere. 1-(4-nitrophenyl)-1-methylethyl hydroperoxide was isolated by silica gel column chromatography (eluent: hexane/EtOAc = 5/1) in 25 % conversion yield (~80 % of starting material was recovered.). HRMS (CI^+) *m/z* = 198.0762 ($[M + H]^+$), calcd for $C_9H_{12}NO_4$ = 198.0766. ^{1}H-NMR (400 MHz, $CDCl_3$) δ 1.64 (6 H, s, -C*H*$_3$), 7.64 (2 H, d, *J* = 9.2 Hz, Ar*H*), 8.24 (2 H, d, *J* = 8.4 Hz, Ar*H*).

Synthesis of Copper Complexes (1b and 3b').

$[Cu^I_2(L^b)(CH_3CN)_2](PF_6)_2$ (1b). Ligand L^b (30 mg, 60 μmol) was treated with two equimolar amount of $[Cu^I(CH_3CN)_4](PF_6)$ (45 mg, 120 μmol) in CH_2Cl_2 (1 mL) under N_2 atmosphere in a glovebox (Miwa MFG Co., Ltd. DB0-1KP). After stirring the mixture for 30 min at room temperature, insoluble material was removed by filtration. Addition of ether (30 mL) to the filtrate gave a pale yellow powder that was precipitated by standing the mixture for 10 min. The supernatant was then removed by

decantation, and the remained pale yellow solid was washed with ether three times and dried to give complex **1b** in 67 %. Single crystals of **1b** were obtained by vapor diffusion of ether into an acetonitrile solution of the complex. FT-IR (KBr) 843 cm^{-1} (PF_6^-); Anal. Calcd for $C_{36}H_{38}Cu_2F_{12}N_8P_2$ $[Cu^I_2(L^b)(CH_3CN)_2]$ $(PF_6)_2$: C, 43.25; H, 3.83; N, 11.21. Found: C, 43.31; H, 4.04; N, 11.45.

$[Cu^{II}_2(L^b)(\mu\text{-}OMe)_2](PF_6)_2(Et_2O)$ (3b'). An acetonitrile solution (1.0 mL) of **1b** (12 mg, 12 μmol) was prepared in a glovebox at room temperature. The solution was cooled to –40ºC, and an acetonitrile solution (100 mL) of ^{H}CmOOH (240 mM) was added by using a microsyringe through the rubber septum cap. After stirring the mixture for 10 min, an excess amount of pre-cooled ether was poured into the solution to give a blue powder that was precipitated by standing the mixture for several minutes. The supernatant was removed by filtration to give **3b'** as a blue powder in 81 %. Single crystals of **3b'** were obtained by vapor diffusion of ether into CH_3CN/MeOH (v/v = 1:1) solution of the complex. FT-IR (KBr) 842 cm^{-1} (PF_6^-); Anal. Calcd for $C_{38}H_{48}Cu_2F_{12}N_6O_3P_2$ $[Cu^{II}_2(L^b)(\mu\text{-}OMe)_2](PF_6)_2(Et_2O)$: C,42.31; H, 4.59; N, 7.97. Found: C, 42.02; H, 4.61; N, 8.05.

Physical measurements

FT-IR spectra were recorded on a Jasco FTIR-4100, and UV–visible spectra were taken on a Jasco V–570 or a Hewlett Packard 8453 photo diode array spectrophotometer equipped with a Unisoku thermostated cell holder designed for low temperature measurements (USP-203). ^{1}H-NMR spectra were recorded on a JEOL FT-NMR GX-400 spectrometer. ESI-MS (electrospray ionization mass spectra) measurements were performed on a Mariner ESI-TOF instrument. Elemental analyses were recorded with a Perkin-Elmer or a Fisons instruments EA1108 Elemental Analyzer.

Crystallography

Each single crystal obtained was mounted on a CryoLoop (Hampton Research Co.) with a mineral oil, and all data of X-ray diffraction were collected at –170 ºC on a Rigaku RAXIS-RAPID diffractmeter using filtered Mo-Kα radiation. The structures were solved by direct methods SIR 92 or SIR 2008 and expanded using Fourier techniques [A. Altomare, G. Cascarano, C. Giacovazzo, A. Guagliardi, M. Burla, G. Polidori, M. Camalli, *J. Appl. Crystallogr*, *27* (**1994**) 435-436; M.C. Burla, R. Caliandro, M. Camalli, B. Carrozzini, G.L. Cascarano, L.D. Caro, C. Giacovazzo, G. Polidori, D. Siliqi, R. Spagna, *J. Appl. Crystallogr.*, *40* (**2007**) 609-613.]. The non-hydrogen atoms were

refined anisotropically by full-matrix least-squares on F^2. The hydrogen atoms were attached at idealized positions on carbon atoms and were not refined. All structures in the final stages of refinement showed no movement in the atom positions. The calculations were performed using Single-Crystal Structure Analysis Software, version 4.0.

Low temperature UV-vis measurements

Kinetic measurements for the reaction of copper(I) complexes with cumene hydroperoxides (^{X}CmOOHs) were performed in acetonitrile at –40 ºC. To an acetonitrile solution of the copper(I) complex (0.5 mM) in a 1.0 cm path length UV-vis cell closed with a rubber cap, an acetonitrile solution of ^{X}CmOOH was added using a microsyringe through the rubber septum cap under anaerobic conditions to initiate the reaction. The reaction was monitored by following an increase of the characteristic absorption band due to the product.

Product analysis

Decomposition products derived from ^{X}CmOOH were analyzed by using a HPLC system consisting of a Shimadzu LC-6A chromatographic pump and an on-line Shimadzu UV-vis spectrophotometric detector. Reverse phase chromatography was performed on an ODS column (Cosmosil 5C_{18}-AR-II, 250 mm × 4.6 mm, Nacalai tesque) at room temperature with an acetonitrile-water (40 : 60) mixed solvent as mobile phase at a constant flow rate of 0.5 mL min^{-1}. The yield of products was determined by comparing the integrated peak areas of the products with that of the internal standard (anisole or nitrobenzene) using calibration lines. The intermediate was generated *in situ* in a UV-vis cell by the addition of ^{X}CmOOH (0.5 mM) to an acetonitrile solution of copper(I) complexes (0.5 mM) at –40ºC, and the mixture was warmed up to room temperature. Then, the decomposition reaction was followed by monitoring the decrease in the LMCT absorption bands due to the intermediate.

Results and Discussion

The reaction of [$Cu^{I}(L^{a})(CH_3CN)$](PF_6) (**1a**) (0.5 mM) and the equimolar amount of ^{H}CmOOH was first examined in acetonitrile. The HPLC analysis of the organic products derived from ^{H}CmOOH demonstrated that cumyl alcohol (^{H}CmOH) was formed in 43 % together with a small amount of acetophenone (PhCOMe, 7 %). In

this case, however, almost 50 % of the starting material, ^{H}CmOOH, was recovered. The result indicates that the stoichiometry of copper(I) complex **1a** and ^{H}CmOOH was 2 : 1. In fact, the reaction of **1a** (0.5 mM) with 0.5 equivalent of ^{H}CmOOH (0.25 mM) under otherwise the same experimental conditions consumed almost all the substrate (^{H}CmOOH) to give ^{H}CmOH and PhCOMe in 93 % and 7 %, respectively. The formation of ^{H}CmOH (alcohol) as the major product is in sharp contrast to the product distribution in the reaction of copper(II) complex of the same ligand L^{a} and ^{H}CmOOH, where PhCOMe (ketone) was the major product; PhCOMe 76 % and ^{H}CmOH 15 %.[7]

It has been reported that the products obtained from a cumylperoxo complex largely depend on the O–O bond cleavage pattern as indicated in Scheme 3-1. Namely, if homolytic O–O bond cleavage occurs (path a), acetophenone (PhCOMe) is produced from cumyloxyl radical via β-scission releasing methyl radical ($CH_3^{\bullet}$). On the other hand, heterolytic O–O bond cleavage (path b) gives cumyl alcohol (^{H}CmOH) after oxyanion protonation.[9] Thus, formation of ^{H}CmOH as the major product (93 %) in the present system suggests that the reaction of copper(I) complex **1a** and ^{H}CmOOH mainly involves O–O bond heterolysis (path b).

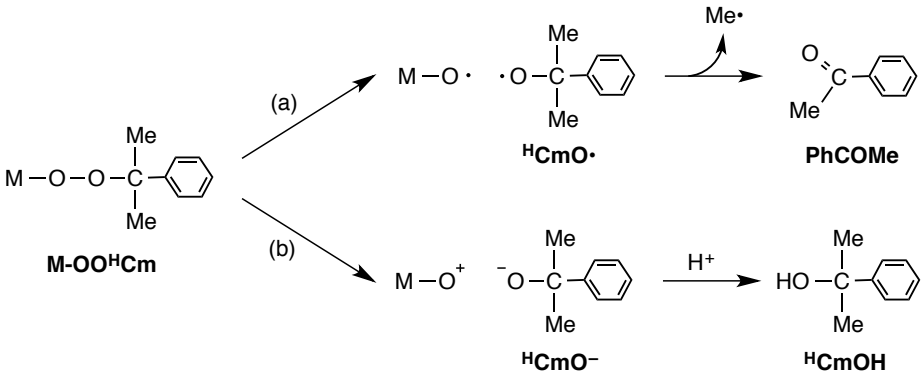

Scheme 3-1. Possible decomposition pathways of cumylperoxo complex M-OO^{H}Cm.

Since the stoichiometry of the reaction between mononuclear copper(I) complex **1a** and ^{H}CmOOH was 2 : 1, the author and his co-workers also examined the reaction of a dinuclear copper(I) complex and cumene hydroperoxide to get more insight into the reaction intermediate and products. Dicopper(I) complex **1b** was prepared by treating the dinucleating ligand L^{b} and 2 equivalent of $[Cu^{I}(CH_3CN)_4](PF_6)$ in acetonitrile, the crystal structure of which is shown in Figure 3-2. The crystallographic data and the

selected bond lengths and angles of **1b** are presented in Tables 3-1 and 3-2. Each copper(I) ion is ligated by three nitrogen atoms of one of the tridentate metal-binding moieties of L^b and one acetonitrile co-ligand, exhibiting a highly distorted tetrahedral geometry. The τ_4 values for Cu(1) and Cu(2) are 0.69 and 0.62, respectively; τ_4 value is a simple geometry index for four-coordinate complexes proposed by Houser and his coworkers defined as $\tau_4 = [360° - (a + b)]/141$, where a and b are the two largest θ angles in the four-coordinate species.[10] The τ_4 value will range from 1.0 for a perfect tetrahedral geometry to zero for a perfect square planar geometry. Thus, the structure of the copper(I) center of **1b** is similar to that of the reported mononuclear copper(I) complex $[Cu^I(L^a)(CH_3CN)]B(C_6F_5)_4$, which exhibits a τ_4 value of 0.72.[11]

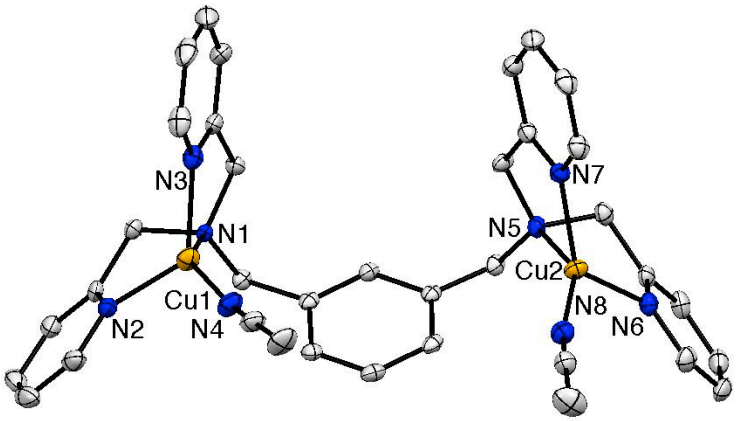

Figure 3-2. ORTEP diagram of $[Cu^I_2(L^b)(CH_3CN)_2](PF_6)_2$ (**1b**) with 50% ellipsoid probability. The counter anions and the hydrogen atoms are omitted for clarity.

Table 3-1. Summary of the X-ray Crystallographic Data of **1b**

Compound	**1b**
formula	$C_{36}H_{38}Cu_2F_{12}N_8P_2$
formula weight	999.77
crystal system	monoclinic
space group	$P2_1/n$ (#14)
a, Å	14.9249(7)
b, Å	20.748(2)
c, Å	15.2283(7)
α, deg	90.000
β, deg	118.425
γ, deg	90.000
V, Å^3	4147.1(4)
Z	4
F(000)	2024.00
D_{calcd}, g/cm^{-3}	1.601
T, K	103
crystal size, mm	0.30 x 0.30 x 0.20
μ (Mo$K\alpha$), cm^{-1}	11.953
$2\theta_{max}$, deg	55.0
no. of reflns measd	38252
no. of reflns obsd	9239 ([$I > 2.00\sigma(I)$])
no. of variables	579
R1 [a]	0.0732
wR2 [b]	0.1751
GOF	0.889

[a] $R1 = \Sigma \, ||F_o| - |F_c|| \, / \, \Sigma \, |F_o|$. [b] $wR2 = [\, \Sigma \, w \, (|F_o| - |F_c|)^2 \, / \, \Sigma \, w \, (F_o^2)^2]^{1/2}$

Table 3-2. Selected Bond Lengths (Å) and Angles (deg) of **1b**

Cu(1)–N(1)	2.240(3)	Cu(2)–N(5)	2.293(3)
Cu(1)–N(2)	2.037(4)	Cu(2)–N(6)	2.030(4)
Cu(1)–N(3)	2.026(5)	Cu(2)–N(7)	2.007(4)
Cu(1)–N(4)	1.903(3)	Cu(2)–N(8)	1.918(4)
N(1)–Cu(1)–N(2)	80.93(12)	N(5)–Cu(2)–N(6)	80.47(11)
N(1)–Cu(1)–N(3)	79.76(13)	N(5)–Cu(2)–N(7)	79.21(13)
N(1)–Cu(1)–N(4)	141.10(13)	N(5)–Cu(2)–N(8)	146.91(13)
N(2)–Cu(1)–N(3)	122.26(13)	N(6)–Cu(2)–N(7)	126.16(15)
N(2)–Cu(1)–N(4)	115.33(16)	N(6)–Cu(2)–N(8)	109.82(15)
N(3)–Cu(1)–N(4)	113.67(16)	N(7)–Cu(2)–N(8)	114.26(15)

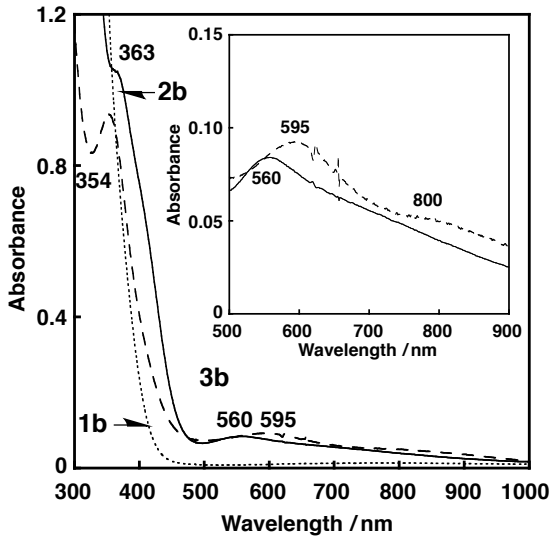

Figure 3-3. UV-vis spectrum of **2b** (solid line) generated by the reaction of **1b** (0.5 mM, dotted line) with ^{H}CmOOH (0.5 mM) in CH_3CN at –40°C under anaerobic conditions and its decomposition product **3b** (dashed line) generated by the addition of H_2O at –40°C. Inset: Expanded UV-vis spectra at 500–900 nm region.

The reaction of dicopper(I) complex **1b** with an equimolar amount of ^{H}CmOOH (molar ratio of Cu^{I} : ^{H}CmOOH = 2 : 1) was then examined. In this case as well, cumyl alcohol (^{H}CmOH) was obtained as the major product (95 %) together with a small amount of acetophenone (5 %), indicating that the reaction also involves heterolytic O–O bond cleavage of ^{H}CmOOH. Figure 3-3 shows the UV-vis spectral change for the reaction at –40°C. Upon addition of equimolar amount of ^{H}CmOOH to an acetonitrile solution of **1b** initially gave a spectrum having an intense absorption band at 363 nm (ε = 2045 $M^{-1}\,cm^{-1}$) together with a weak band at 560 nm (ε = 168 $M^{-1}\,cm^{-1}$) (solid line).[12] This species, designated as **2b**, gradually decomposed even at the low temperature to provide another copper(II) species **3b**. The same species **3b** was generated rapidly, when a small amount of H_2O (0.5 mL) was added to the solution of **2b**, suggesting that **3b** is produced by hydrolysis of **2b**. ESI-MS analysis of the final reaction mixture exhibited a prominent ion peak cluster at m/z = 330.2, whose mass and isotope distribution pattern were consistent with the chemical formula of di(μ-hydroxo)dicopper(II) complex $[Cu^{II}_2(L^b)(\mu\text{-}OH)_2]^{2+}$ (m/z = 330.1) (Figure 3-4).

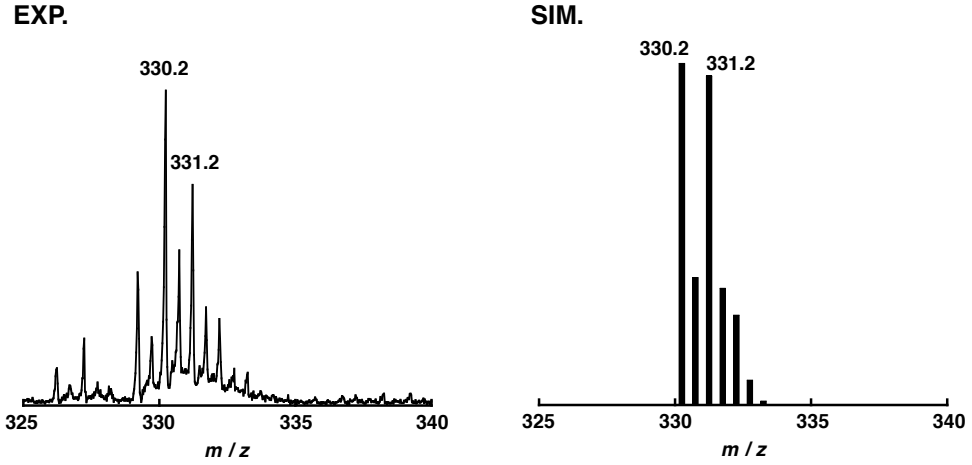

Figure 3-4. Experimental (EXP, left) and simulated (SIM, right) peak envelopes in the positive-ion ESI-MS spectra of the product **3b** derived from the decomposition of intermediate **2a** in CH_3CN at 30°C.

In spite of our great efforts, pure sample of **3b** could not be isolated, but its di(μ-methoxo) variant **3b'** was successfully obtained in a 81% yield by recrystallization of **3b** from methanol. In Figure 3-5 is shown the crystal structure of **3b'**. The

crystallographic data and the selected bond lengths and angles are presented in Tables 3-3 and 3-4. Each copper(II) ion has a largely distorted square-pyramidal geometry consisting of two pyridine nitrogen atoms and two bridging methoxide oxygen atoms in a basal plane and the tertiary amine nitrogen atom in the apical position, where no ligand modification took place. Similarity of the absorption spectrum of isolated **3b'** to that of **3b** also support the di(μ-hydroxo)dicopper(II) core structure in the latter.

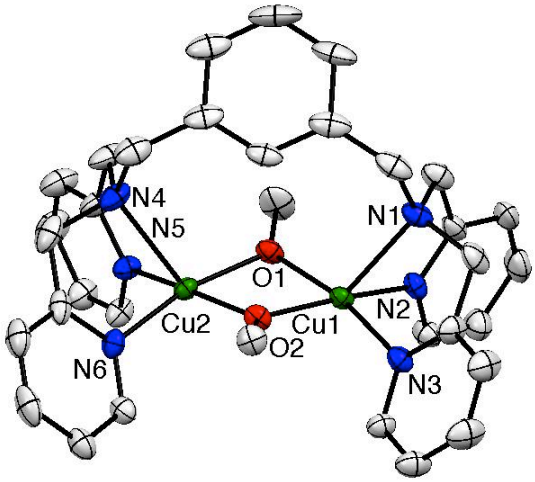

Figure 3-5. ORTEP diagram of $[Cu^{II}_2(L^b)(\mu\text{-}OCH_3)_2](PF_6)_2$ (**3b'**) with 50% ellipsoid probability. The counter anions and the hydrogen atoms are omitted for clarity.

Table 3-3. Summary of the X-ray Crystallographic Data of **3b'**

Compound	**3b'**
formula	$C_{38}H_{48}Cu_2F_{12}N_6O_3P_2$
formula weight	1053.86
crystal system	orthorhombic
space group	*P*na2_1(#33)
a, Å	11.0085(5)
b, Å	31.848(2)
c, Å	12.7919(6)
α, deg	90.000
β, deg	90.000
γ, deg	90.000
V, Å^3	484.8(4)
Z	4
F(000)	2152.00
D_{calcd}, g/cm^{-3}	1.561
T, K	103
crystal size, mm	0.30 x 0.30 x 0.30
μ (Mo$K\alpha$), cm^{-1}	11.131
$2\theta_{max}$, deg	55.0
no. of reflns measd	41634
no. of reflns obsd	9388 ([$I > 2.00\sigma(I)$])
no. of variables	616
R1 [a]	0.0572
wR2 [b]	0.1390
GOF	1.202

[a] $R1 = \Sigma \, ||F_o| - |F_c|| \, / \, \Sigma \, |F_o|$. [b] $wR2 = [\, \Sigma \, w \, (|F_o| - |F_c|)^2 \, / \, \Sigma \, w \, (F_o^2)^2 \,]^{1/2}$

Table 3-4. Selected Bond Lengths (Å) and Angles (deg) of **3b'**

Compound **3b'**			
Cu(1)–Cu(2)	2.9957(13)	Cu(2)–O(1)	1.928(4)
Cu(1)–O(1)	1.925(4)	Cu(2)–O(2)	1.9333(4)
Cu(1)–O(2)	1.933(4)	Cu(2)–N(4)	2.353(5)
Cu(1)–N(1)	1.900(6)	Cu(2)–N(6)	1.870(4)
Cu(1)–N(2)	1.970(4)	Cu(2)–N(6)	2.001(4)
Cu(1)–N(3)	2.008(4)		
Cu(2)–Cu(1)–O(1)	38.99(10)	Cu(1)–Cu(2)–O(1)	38.93(10)
Cu(2)–Cu(1)–O(2)	39.21(11)	Cu(1)–Cu(2)–O(2)	39.21(10)
Cu(2)–Cu(1)–N(1)	127.21(11)	Cu(1)–Cu(2)–N(4)	126.45(11)
Cu(2)–Cu(1)–N(2)	129.92(12)	Cu(1)–Cu(2)–N(5)	129.51(13)
Cu(2)–Cu(1)–N(3)	129.54(12)	Cu(1)–Cu(2)–N(6)	128.31(12)
O(1)–Cu(1)–O(2)	76.97(14)	O(1)–Cu(2)–O(2)	76.91(14)
O(1)–Cu(1)–N(1)	110.12(14)	O(1)–Cu(2)–N(4)	109.86(14)
O(1)–Cu(1)–N(2)	94.60(15)	O(1)–Cu(2)–N(5)	94.02(16)
O(1)–Cu(1)–N(3)	168.16(15)	O(1)–Cu(2)–N(6)	166.85(15)
O(2)–Cu(1)–N(1)	115.44(14)	O(2)–Cu(2)–N(4)	114.73(14)
O(2)–Cu(1)–N(2)	166.67(15)	O(2)–Cu(2)–N(5)	166.70(16)
O(2)–Cu(1)–N(3)	92.55(16)	O(2)–Cu(2)–N(6)	91.39(15)
N(1)–Cu(1)–N(2)	77.00(15)	N(4)–Cu(2)–N(5)	77.32(16)
N(1)–Cu(1)–N(3)	79.20(16)	N(4)–Cu(2)–N(6)	80.32(16)
N(2)–Cu(1)–N(3)	94.67(17)	N(5)–Cu(2)–N(6)	96.42(17)

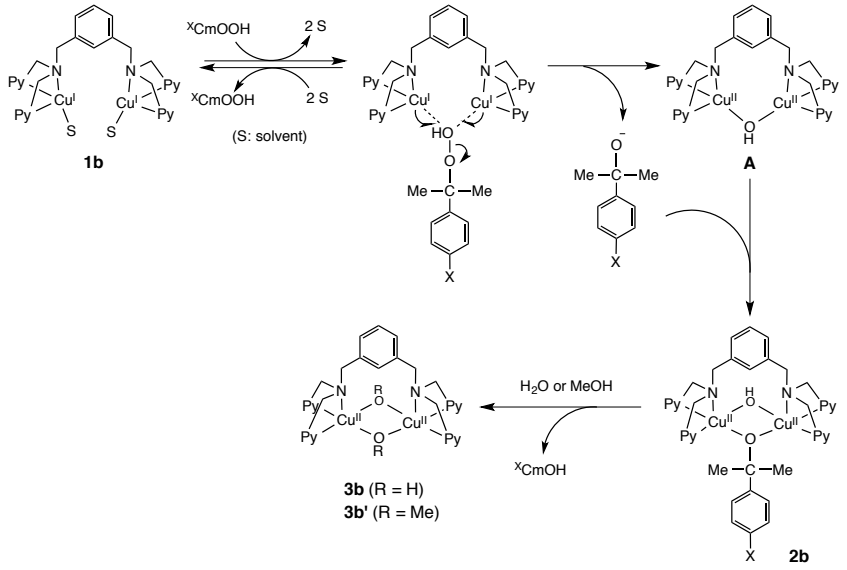

Scheme 3-2. Proposed mechanism of the reaction of **1b** and ^{X}CmOOH.

Possible mechanism for the reaction of **1b** and cumene hydroperoxide generating **3b** is shown in Scheme 3-2. As clearly demonstrated by the product analysis, heterolytic cleavage of the O–O bond takes place. The stoichiometry of Cu^{I} : CmOOH as 2 : 1 suggests that formally two electrons are transferred from the copper(I) ions to the peroxo moiety to induce the O–O bond heterolysis. That event may produce (μ-hydroxo)dicopper(II) intermediate **A** and cumyl alkoxide CmO^{-}, both of which quickly collapse to give (μ-hydroxo)(μ-alkoxo)dicopper(II) species **2b**. Finally, **3b** or **3b'** is produced by hydrolysis or methanolysis of **2b**.

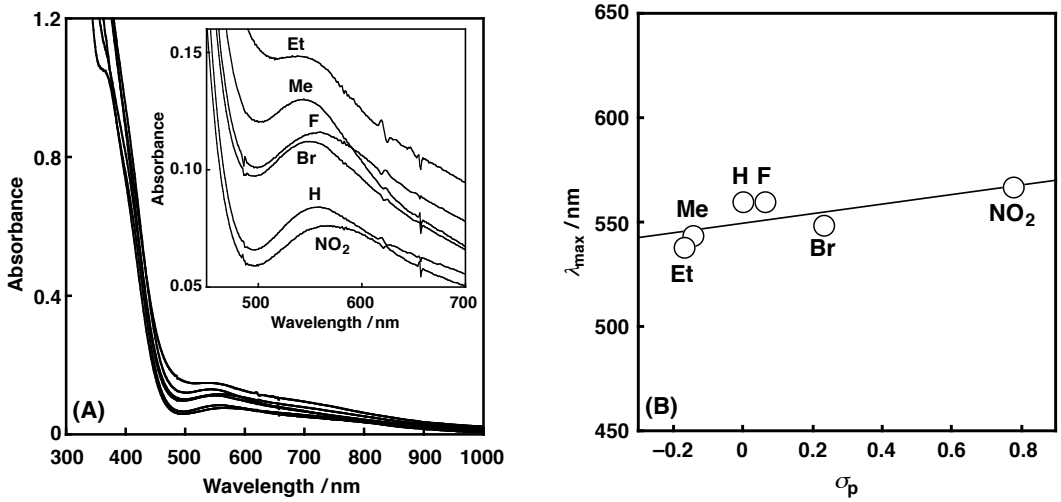

Figure 3-6. (A) UV-vis spectra of the intermediates **2b**^{X} derived from the reaction of **1b** (0.5 mM) and ^{X}CmOOH (0.5 mM; R = Et, Me, H, F, Br, NO_2) in CH_3CN at –40°C under anaerobic conditions. Inset: Expanded UV-vis spectrum at 450–700 nm region. λ_{max} = 538 nm for X = Et, λ_{max} = 544 nm for X = Me, λ_{max} = 560 nm for X = H, λ_{max} = 560 nm for X = F, λ_{max} = 549 nm for X = Br, λ_{max} = 567 nm for X = NO_2. (B) Plot of λ_{max} against the Hammett σ_p values; slope = 23.1 nm/σ_p (unit), R = 0.73.

Further evidence in support of generation of the postulated intermediate **2b** is the fact that essentially similar spectra but having slightly different λ_{max} values were obtained in the reactions of **1b** with a series of cumene hydroperoxide derivatives ^{X}CmOOH (X = Et, Me, Br, F and NO_2) under the same experimental conditions (Figure 3-6(A), λ_{max} = 538 ~ 567 nm; nearly quantitative (> 95 %) formation of the corresponding alcohols ^{X}CmOH was also confirmed by HPLC analysis). Such the difference in λ_{max} of the intermediates **2b** generated by using ^{X}CmOOH may be due to the electronic effects of the *p*-substituents on the LMCT transition from the alkoxide ligand to Cu^{II}. As indicated in Figure 3-6(B), there was a weak correlation between λ_{max} and Hammett σ_p values, where the λ_{max} shifted toward longer wavelength as the electron-withdrawing nature of the *p*-substituent (X) increases.

Conclusions

In this study, the author and his co-workers have investigated the reaction of copper(I) complexes **1a** and **1b** with cumene hydroperoxide derivatives (^{X}CmOOH) to find that the reaction proceeded in a 2 : 1 stoichiometry to induce *heterolytic* O–O bond breaking of the alkyl hydroperoxides. In this case, the corresponding alcohol was obtained as the major product. The result is in sharp contrast to the 1 : 1 reaction between the copper(II) complexes and CmOOH producing the ketone (PhC(O)Me) as the major product via homolytic O–O bond cleavage.

Very recently, Hutchings and co-workers reported a significant result that in the Fe-loaded zeolite (ZSM-5) catalyzed methane-oxidation with H_2O_2, alcohol (methanol) product selectivity is significantly improved by the addition of copper.[13] In this reaction, the primary product is methyl hydroperoxide (MeOOH), which is produced by the direct reaction of methane with a generated dinuclear iron active-oxygen species.[13] Our present study suggests that the role of copper in the Hutchings's methane-oxidation reaction is enhancement of O–O bond heterolysis of the primary product MeOOH to give MeOH as the major product. Mechanistic details of the O–O bond cleavage process and application to catalytic oxidation reactions are now under progress.

References

1. a) Girerd, J.-J.; Banse, F.; Simaan, A. in *Structure and Bonding, Vol. 97*, Springer: Berlin, Heidelberg, **2000**, pp 145-177; b) Costas, M.; Mehn, M. P.; Jensen, M. P.; Que, L., Jr. *Chem. Rev.* **2004**, *104*, 939-986; c) Chavez, F. A.; Mascharak, P. K. *Acc. Chem. Res.* **2000**, *33*, 539-545; d) Hikichi, S.; Akita, M.; Moro-oka, Y. *Coord. Chem. Rev.* **2000**, *198*, 61-87; e) Akita, M.; Hikichi, S. *Bull. Chem. Soc. Jpn.* **2002**, *75*, 1657-1679.
2. a) Zang, Y.; Elgren, T. E.; Dong, Y.; Que, L., Jr. *J. Am. Chem. Soc.* **1993**, *115*, 811-813; b) Ménage, S.; Wilkinson, E. C.; Que, L., Jr.; Fontecave, M. *Angew. Chem., Int. Ed.* **1995**, *34*, 203-205; c) Kim, J.; Larka, E.; Wilkinson, E. C.; Que, L., Jr. *Angew. Chem., Int. Ed.* **1995**, *34*, 2048-2051; d) Lange, S. J.; Miyake, H.; Que, L., Jr. *J. Am. Chem. Soc.* **1999**, *121*, 6330-6331; e) Lehnert, N.; Ho, R. Y. N.; Que, L., Jr.; Solomon, E. I. *J. Am. Chem. Soc.* **2001**, *123*, 8271-8290; f)

Lehnert, N.; Ho, R. Y. N.; Que, L., Jr.; Solomon, E. I. *J. Am. Chem. Soc.* **2001**, *123*, 12802-12816; g) Miyake, H.; Chen, K.; Lange, S. J.; Que, L., Jr. *Inorg. Chem.* **2001**, *40*, 3534-3538; h) Kim, J.; Zang, Y.; Costas, M.; Harrison, R. G.; Wilkinson, E. C.; Que, L., Jr. *J. Biol. Inorg. Chem.* **2001**, *6*, 275-284; i) Jensen, M. P.; Lange, S. J.; Mehn, M. P.; Que, E. L.; Que, L., Jr. *J. Am. Chem. Soc.* **2003**, *125*, 2113-2128; j) Kaizer, J.; Costas, M.; Que, L., Jr. *Angew. Chem., Int. Ed.* **2003**, *42*, 3671-3673; k) M. i. Payeras, A.; Ho, R. Y. N.; Fujita, M.; Que, L., Jr. *Chem. Eur. J.* **2004**, *10*, 4944-4953; l) Rohde, J.-U.; Torelli, S.; Shan, X.; Lim, M. H.; Klinker, E. J.; Kaizer, J.; Chen, K.; Nam, W.; Que, L., Jr. *J. Am. Chem. Soc.* **2004**, *126*, 16750-16761; m) Bukowski, M. R.; Halfen, H. L.; van den Berg, T. A.; Halfen, J. A.; Que, L., Jr. *Angew. Chem., Int. Ed.* **2005**, *44*, 584-587; n) Jensen, M. P.; Costas, M.; Ho, R. Y. N.; Kaizer, J.; M. i. Payeras, A.; Munck, E.; Que, L., Jr.; Rohde, J. U.; Stubna, A. *J. Am. Chem. Soc.* **2005**, *127*, 10512-10525; o) Bautz, J.; Comba, P.; Que, L., Jr. *Inorg. Chem.* **2006**, *45*, 7077-7082; p) Jensen, M. P.; Payeras, A. M. i.; Fiedler, A. T.; Costas, M.; Kaizer, J.; Stubna, A.; Munck, E.; Que, L., Jr. *Inorg. Chem.* **2007**, *46*, 2398-2408; q) Shan, X.; Rohde, J. -U.; Koehntop, K. D.; Zhou, Y.; Bukowski, M. R.; Costas, M.; Fujisawa, K.; Que, L., Jr. *Inorg. Chem.* **2007**, *46*, 8410-8417; r) Fiedler, A. T.; Que, L., Jr. *Inorg. Chem.* **2009**, *48*, 11038-11047.

3. a) MacFaul, P. A.; Arends, I. W. C. E.; Ingold, K. U.; Wayner, D. D. M. *J. Chem. Soc., Perkin Trans. 2* **1997**, 135-146; b) Wada, A.; Ogo, S.; Watanabe, Y.; Mukai, M.; Kitagawa, T.; Jitsukawa, K.; Masuda, H.; Einaga, H. *Inorg. Chem.* **1999**, *38*, 3592-3593; c) Sobolev, A. P.; Babushkin, D. E.; Talsi, E. P. *J. Mol. Catal. A-Chem.* **2000**, *159*, 233-245; d) Ogihara, T.; Hikichi, S.; Akita, M.; Uchida, T.; Kitagawa, T.; Moro-oka, Y. *Inorg. Chim. Acta* **2000**, *297*, 162-170; e) Lobanova, M. V.; Bryliakov, K. P.; Duban, E. A.; Taksum, E. P. *Mendeleev Communications* **2003**, 175-177; f) Lehnert, N.; Fujisawa, K.; Solomon, E. I. *Inorg. Chem.* **2003**, *42*, 469-481; g) Krishnamurthy, D.; Kasper, G. D.; Namuswe, F.; Kerber, W. D.; Sarjeant, A. A. N.; Moenne-Loccoz, P.; Goldberg, D. P. *J. Am. Chem. Soc.* **2006**, *128*, 14222-14223; h) Gosiewska, S.; Permentier, H. P.; Bruins, A. P.; van Koten, G.; Gebbink, R. *Dalton Trans.* **2007**, 3365-3368; i) Seo, M. S.; Kamachi, T.; Kouno, T.; Murata, K.; Park, M. J.; Yoshizawa, K.; Nam, W. *Angew. Chem., Int. Ed.* **2007**, *46*, 2291-2294; j) Namuswe, F.; Kasper,

G. D.; Sarjeant, A. A. N.; Hayashi, T.; Krest, C. M.; Green, M. T.; Moenne-Loccoz, P.; Goldberg, D. P. *J. Am. Chem. Soc.* **2008**, *130*, 14189-14200; k) Namuswe, F.; Hayashi, T.; Jiang, Y. B.; Kasper, G. D.; Sarjeant, A. A. N.; Moenne-Loccoz, P.; Goldberg, D. P. *J. Am. Chem. Soc.* **2010**, *132*, 157-167; l) Stasser, J.; Namuswe, F.; Kasper, G. D.; Jiang, Y.; Krest, C. M.; Green, M. T.; Penner-Hahn, J.; Goldberg, D. P. *Inorg. Chem.* **2010**, *49*, 9178-9190.

4. Kovaleva, E. G.; Lipscomb, J. D. *Science* **2007**, *316*, 453-457.
5. Costas, M.; Chen, K.; Que, L., Jr. *Coord. Chem. Rev.* **2000**, *200-202*, 517-544.
6. a) Kitajima, N.; Katayama, T.; Fujisawa, K.; Iwata, Y.; Morooka, Y. *J. Am. Chem. Soc.* **1993**, *115*, 7872-7873; b) Chen, P.; Fujisawa, K.; Solomon, E. I. *J. Am. Chem. Soc.* **2000**, *122*, 10177-10193; c) Kunishita, A.; Ishimaru, H.; Nakashima, S.; Ogura, T.; Itoh, S. *J. Am. Chem. Soc.* **2008**, *130*, 4244-4245; d) Choi, Y. J.; Cho, K.-B.; Kubo, M.; Ogura, T.; Karlin, K. D.; Cho, J.; Nam, W. *Dalton Trans.* **2011**, *40*, 2234-2241.
7. Tano, T.; Ertem, M. Z.; Yamaguchi, S.; Kunishita, A.; Sugimoto, H.; Fujieda, N.; Ogura, T.; Cramer, C. J.; Itoh, S. *Dalton Trans.* **2011**, *40*, 10326-10336.
8. Burkitt, M. J. *Arch. Biochem. Biophys.* **2001**, *394*, 117-135.
9. a) Adachi, S.; Nagano, S.; Ishimori, K.; Watanabe, Y.; Morishima, I.; Egawa, T.; Kitagawa, T.; Makino, R. *Biochemistry* **1993**, *32*, 241-252; b) Avila, D. V.; Brown, C. E.; Ingold, K. U.; Lusztyk, J. *J. Am. Chem. Soc.* **1993**, *115*, 466-470; c) Baciocchi, E.; Bietti, M.; Salamone, M.; Steenken, S. *J. Org. Chem.* **2002**, *67*, 2266-2270.
10. Yang, L.; Powell, D. R.; Houser, R. P. *Dalton Trans.* **2007**, 955-964.
11. Lucas, H. R.; Li, L.; Sarjeant, A. A. N.; Vance, M. A.; Solomon, E. I.; Karlin, K. D. *J. Am. Chem. Soc.* **2009**, *131*, 3230-3245.
12. A similar spectrum (λ_{max} = 380 nm (ε = 2200 M^{-1} cm^{-1}) and 565 nm (300 M^{-1} cm^{-1}) was observed in the initial stage of the reaction between **1a** and CmOOH under the same experimental conditions (Figure S6), suggesting the formation of a similar dinuclear copper(II) intermediate with μ-OH and μ-OCm bridges in the mononuclear copper(I) system.
13. Hammond, C.; Forde, M. M.; Ab Rahim, M. H.; Thetford, A.; He, Q.; Jenkins, R. L.; Dimitratos, N.; Lopez-Sanchez, J. A.; Dummer, N. F.; Murphy, D. M.;

Carley, A. F.; Taylor, S. H.; Willock, D. J.; Stangland, E. E.; Kang, J.; Hagen, H.; Kiely, C. J.; Hutchings, G. J. *Angew. Chem., Int. Ed.* **2012**, *51*, 5129-5133.

14. Perrin, D. D.; Armarego, W. L. F.; Perrin, D. R.; *Purification of Laboratory Chemicals 4th Edition*, 4th ed., Pergamon Press, Elmsford, NY, **1996**.
15. Kawahara, S.-i.; Uchimaru, T. *Eur. J. Inorg. Chem.* **2001**, *2001*, 2437-2442.
16. a) Finn, M. G.; Sharpless, K. B. *J. Am. Chem. Soc.* **1991**, *113*, 113-126; b) Ueno, T.; Masuda, H.; Ho, C.-T. *J. Agric. Food. Chem.* **2004**, *52*, 5677-5684.

Chapter 4 Copper Complex Supported by an N_2S-Tridentate Ligand Inducing Efficient O-O Bond Heterolytic Cleavage of Alkylhydroperoxide

Introduction

Copper monooxygenases such as peptidylglycine α-hydroxylating monooxygenase (PHM), dopamine β-monooxygenase (DβM) and tyramine β-monooxygenase (TβM) employ two un-coupled, mononuclear copper sites referred to as Cu_M and Cu_H.[1-6] Cu_M serves as the reaction site for dioxygen activation and substrate oxygenation, whereas Cu_H functions as an electron acceptor from the physiological reductant (ascorbate). The Cu_M site is ligated by two histidine imidazoles and one methionine sulfur (N_2S donor set), whereas Cu_H is coordinated by three histidine imidazoles (N_3 donor set).[3, 4] These coordination environments are somewhat unusual, since most of the reaction centers of O_2-activating copper proteins (type-2 and type-3 Cu proteins) consist of nitrogen rich donor groups, whereas the large number of electron transfer proteins (type-1 Cu proteins) involve sulfur-containing ligand environment.[7, 8] Thus, such a unique feature of these copper monooxygenases has long been a target in the synthetic bioinorganic modeling studies.[9-20]

So far, a series of mononuclear copper-dioxygen adducts have been characterized as model compounds of possible reactive intermediates of copper monooxygenases.[21-25] Among them, a mononuclear copper(II)-superoxide complex supported by a simple N_3-ligand L^{N3} (1-[2-(2-pyridyl)ethyl]-1,5-diazacyclooctane derivatives, Figure 4-1) is a unique example, which exhibits both a similar structural feature (distorted tetrahedral copper(II) with end-on superoxide ligand) and a reactivity (aliphatic hydroxylation) to those of the putative reactive intermediate involved in the enzymatic reactions.[26, 27] In this study, the author and his co-workers have synthesised and characterised the copper(I) and copper(II) complexes supported by L^{N2S} (Figure 4-1) in order to get insights into the effects of sulfur atom on the structure and reactivity. Ligand L^{N2S} has the same molecular framework to that of L^{N3}, but one of the alkylamine nitrogen atoms is replaced by a sulfur atom, allowing us to simply access the electronic effects of the

donor atom.

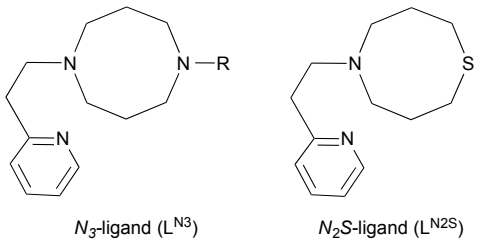

Figure 4-1. Ligand structures.

Experimental

Materials and physical measurements

The reagents and the solvents used in this study, except the ligands and the copper complexes, were commercial products of the highest available purity and were further purified by standard methods, when necessary.[32] Cumene hydroperoxide (CmOOH) used in this study was prepared by a reported procedure,[33] and purified by silica gel column chromatography (eluent: AcOEt–Hexane). ^{18}O-labeled ($Cm^{18}O^{18}OH$) was synthesized using $^{18}O_2$ instead of $^{16}O_2$ by the same procedure.

UV-visible spectra were taken in acetone or in acetonitrile on a Hewlett Packard 8453 photodiode array spectrophotometer equipped with a Unisoku thermostated cell holder designed for low temperature measurements (USP-203). ^{1}H-NMR spectra were recorded on a JEOL ECS 400 or a Varian UNITY INOVA 600MHz. EPR spectra were recorded on a BRUKER E-500 spectrometer at –196 °C equipped with a variable temperature cell holder or a JEOL JES–FA100. A Mn^{II}-maker was used as the reference, and experimental errors in the EPR parameters is ± 0.001. Mass spectra were recorded with a JEOL JMS–700T Tandem MS station or a JEOL JMS–700. ESI-MS (electrospray ionization mass spectra) measurements were performed on a Mariner ESI-TOF instrument. Cyclic voltammetric measurements were performed with a Hokuto Denko HZ-3000 or HZ-7000 in deaerated solvent containing 0.10 M *n*-Bu_4PF_6 as a supporting electrolyte. A GC working (BAS) was polished with BAS polishing alumina suspension and rinsed with acetone before use. The counter electrode was a platinum wire. The measured potentials were recorded with respect to an

$Ag/AgNO_3$ (0.01 M) reference electrode. The cyclic voltammograms for copper(I) complexes were taken inside of the glovebox filled with nitrogen gas at 25ºC. Resonance Raman scattering was excited 441.6 nm from He-Cd laser (KIMMON KOHA, K5651R). Resonance Raman scattering was dispersed by a single polychromator (Ritsu Oyo Kogaku, MC-100) and was detected by a liquid nitrogen cooled CCD detector (HORIBA JOBIN YVON, Symphony 1024 x 128 Cryogenic Front Illuminated CCD Detector). The resonance Raman measurements were carried out using a rotated cylindrical cell thermostated at –80°C or a rotating NMR tube (outer diameter = 5 mm) thermostated at –40 °C by flashing cold nitrogen gas. A 135° back-scattering geometry was used.

Ligand Synthesis

***N*-(Pyridine-2-yl)ethyl-bis(3-hydroxypropyl)amine.** A 200 mL round-bottom flask was charged with 2-(2-aminoethyl)pyridine (4.0 g, 33 mmol), 3-chloro-1-propanol (13 g, 0.13 mol), sodium carbonate (35 g, 0.33 mol), tetrabutylammonium bromide (~5 mg), water (70 mL), and CH_3CN (70 mL). The mixture was refluxed for 2 days. The reaction mixture was cooled to room temperature and extracted with $CHCl_3$ (3 x 50 mL), and the combined organic fractions were dried over Na_2SO_4. After removal of Na_2SO_4 by filtration, evaporation of the solvent gave a brown oil, from which the pure product was isolated by alumina column chromatography (eluent: AcOEt : MeOH = 95 : 5) in 70 % (6.5 g). ^{1}H-NMR ($CDCl_3$) δ 1.67 (4 H, pentet, J = 6.0 Hz, CH_2-CH_2-CH_2), 2.65 (4 H, t, J = 6.0 Hz, N-CH_2-CH_2-CH_2-OH), 2.82 (2 H, t, J = 7.2 Hz, Py-CH_2-CH_2-), 3.00 (2 H, t, J = 7.2 Hz, Py-CH_2-CH_2-), 3.61 (4 H, t, J = 5.6 Hz, -CH_2-OH), 7.15-7.18 (1 H, m, PyH_5), 7.20 (1 H, d, J = 7.6 Hz, PyH_3), 7.66 (1 H, td, J = 1.6 Hz and J = 7.2 Hz, PyH_4), 8.50 (1 H, d, J = 2.4 Hz, PyH_6); HRMS (EI^+) m/z = 238.1680, calcd for $C_{13}H_{22}N_2O_2$ = 238.1681.

***N*-(Pyridine-2-yl)ethyl-bis(3-chloropropyl)amine.** *N*-(Pyridine-2-yl)ethyl-bis(3-hydroxypropyl)amine (0.36 g, 1.3 mmol) in benzene (30 mL) was cooled to 0 ºC. At this temperature, 0.5 mL of thionyl chloride was added dropwise under aerobic conditions. After an initial exothermal reaction, the mixture was refluxed for 4 h, then brought down to room temperature and left

to stand overnight. After cooling down again to 0 °C, a solution of sodium carbonate (10%) was poured until pH became basic. The organic layer was then separated, dried over Na_2SO_4. After removal of Na_2SO_4 by filtration, evaporation of the solvent gave brown oil, from which the pure product was isolated by alumina column chromatography (eluent: AcOEt) in 78 % (0.28 g). ^{1}H-NMR ($CDCl_3$, 400 MHz) δ 1.84 (4 H, pentet, J = 6.4 Hz, CH_2-CH_2-CH_2), 2.59 (4 H, t, J = 6.4 Hz, N-CH_2-CH_2-CH_2-Cl), 2.84 (2 H, t, J = 6.4 Hz, Py-CH_2-CH_2-), 2.91 (2 H, t, J = 6.4 Hz, Py-CH_2-CH_2-), 3.46 (4 H, t, J = 6.4 Hz, -CH_2-Cl), 7.09-7.13 (1 H, m, PyH_5), 7.19 (1 H, d, J = 8.0 Hz, PyH_3), 7.59 (1 H, td, J = 1.6 Hz and J = 7.6 Hz, PyH_4), 8.53 (1 H, d, J = 4.8 Hz, PyH_6); HRMS (EI$^+$) m/z = 274.1003, calcd for $C_{13}H_{20}Cl_2N_2$ = 274.1004.

***N*-(2-(Pyridin-2-yl)ethyl)-1-thia-5-azacyclooctane (L^{N2S}).** *N*-(Pyridine-2-yl)ethyl-bis(3-chloropropyl)amine (0.2 g, 0.55 mmol) was combined with Na_2S (43 mg, 0.55 mmol) in anhydrous ethanol (100 mL) and refluxed for 19 h. The ethanol was then evaporated in vacuo. The residue was taken up with Et_2O (50 mL) and washed with 5 % NaOH aq (20 mL x 3) and then water, and dried over Na_2SO_4. After removal of Na_2SO_4 by filtration, evaporation of the solvent gave yellow oil, from which L^{N2S} was isolated by alumina column chromatography (eluent: AcOEt) in 52 % (67 mg). ^{1}H-NMR ($CDCl_3$, 400 MHz) δ 1.81 (4 H, pentet, J = 6.0 Hz, CH_2-CH_2-CH_2), 2.48 (4 H, t, J = 6.0 Hz, -CH_2-N-CH_2-), 2.64 (4 H, t, J = 6.4 Hz, -CH_2-S-CH_2-), 2.87-2.94 (4 H, m, Py-CH_2-CH_2-), 7.10-7.13 (1 H, m, PyH_5), 7.17 (1 H, d, J = 7.6 Hz, PyH_3), 7.60 (1 H, td, J = 2.0 Hz and J = 8.0 Hz, PyH_4), 8.54 (1 H, d, J = 5.2 Hz, PyH_6); HRMS (EI$^+$) m/z = 236.1348, calcd for $C_{13}H_{20}N_2S$ = 236.1347.

Synthesis of a Copper(I) Complex (1^{N2S}). Since the copper(I) complex is sensitive to air, all the manipulations for the synthesis, crystallization, and stock solution preparation of the copper(I) complex was carried out under N_2 atmosphere inside a glovebox (KOREA KIYON KK-011AS, [O_2] < 1 ppm).

[$Cu^I(L^{N2S})$](PF_6) (1^{N2S}). [$Cu^I(CH_3CN)$](PF_6) (24 mg, 64 μmol) was added to a THF solution of L^{N2S} (15 mg, 64 μmol). After stirring the solution for 30 min at room temperature, insoluble material was removed by filtration. Addition of ether (50 mL) to the filtrate gave yellow-green solids that were isolated by

decantation, washed with ether three times, and dried (45 % yield, 13 mg). Single crystals were obtained for the X-ray analysis by vapor diffusion of ether into a THF solution of the complex. FT-IR (KBr) 841 cm^{-1} (PF_6^-); ESI-MS (pos.) *m*/*z* = 299.3, calcd for $[Cu^I(L^{NNS})]^+$ 299.1; Anal. Calcd for $[Cu^I(L^{NNS})]PF_6$ ($C_{13}H_{20}CuF_6N_2PS$): C, 35.10; H, 4.53; N, 6.30. Found: C, 35.43; H, 4.64; N, 6.30.

Synthesis of Copper(II) Complexes (2^{N2S}•Cl, 2^{N2S}•N_3, 2^{N2S}•NO_2 and 2^{N2S}•OTf_2).

$[Cu^{II}(L^{N2S})(Cl)](BF_4)$ (2^{N2S}•Cl). $Cu^{II}Cl_2$ (8.6 mg, 64 μmol) was added to a CH_3CN solution of L^{N2S} (15 mg, 64 μmol). After stirring the solution for 10 min at room temperature, $NaBF_4$ (7.0 mg, 64 μmol) was added to the solution. Addition of CH_2Cl_2 (30 mL) to the solution gave a white powder that was precipitated by standing the mixture for several minutes. Insoluble material was then removed by filtration. The filtrate was concentrated to give green oily material. Single crystals were obtained for the X-ray analysis by diffusion of *n*–hexane into a CH_2Cl_2 solution of the complex (73 % yield, 20 mg). FT-IR (KBr) 1084 cm^{-1} (BF_4^-); ESI-MS (pos.) *m*/*z* = 334.0, calcd for $[Cu^{II}(L^{N2S})(Cl)]^+$ 334.0; Anal. Calcd for $[Cu^{II}(L^{N2S})(Cl)]BF_4 \cdot 0.1H_2O$ ($C_{13}H_{20.2}BClCuF_4N_2O_{0.1}S$): C, 36.83; H, 4.80; N, 6.61. Found: C, 36.64; H, 4.76; N, 6.60.

$[Cu^{II}(L^{N2S})(N_3)](BF_4)$ (2^{N2S}•N_3). To a methanol solution of L^{N2S} (12 mg, 51 μmol) was added $Cu^{II}SO_4 \cdot 5H_2O$ (13 mg, 51 μmol), when the color of solution turned dark blue. After stirring for 5 min, NaN_3 (3.3 mg, 51 μmol) was added to give the green solution. Then, $NaBF_4$ (5.6 mg, 51 μmol) was added to the solution, and the mixture was stirred for additional 5 min. Insoluble material was then removed by filtration. The filtrate was concentrated to give green oily material. Single crystals were obtained for the X-ray analysis by diffusion of *n*–hexane into a CH_2Cl_2 solution of the complex (67 % yield, 15 mg). FT-IR (KBr) 2078 cm^{-1} (N_3^-), 1073 cm^{-1} (BF_4^-); ESI-MS (pos.) *m*/*z* = 299.2, calcd for $[Cu^I(L^{N2S})]^+$ 299.1; Anal. Calcd for $[Cu^{II}(L^{N2S})(N_3)]BF_4 \cdot 0.13H_2O$ ($C_{13}H_{20.26}BClCuF_4N_5O_{0.13}S$): C, 36.22; H, 4.74; N, 16.25. Found: C, 35.91; H, 4.75; N, 16.56.

$Cu^{II}(L^{N2S})(NO_2)(OTf)$ (2^{N2S}•NO_2). To a methanol solution of L^{N2S} (6.5 mg, 23 μmol) was added $Cu^{II}SO_4 \cdot 5H_2O$ (6.0 mg, 23 μmol), when the color of solution turned dark blue. After stirring for 5 min, $NaNO_2$ (1.6 mg, 23 μmol) was added

to give the green solution. Then, NaOTf (4.0 mg, 23 μmol) was added to the solution, and the mixture was stirred for additional 5 min. Insoluble material was then removed by filtration. The filtrate was concentrated to give green oily material. Single crystals were obtained for the X-ray analysis by diffusion of *n*–hexane into a CH_2Cl_2 solution of the complex (43 % yield, 5.0 mg). FT-IR (KBr) 1477 cm^{-1} (NO_2^-), 1248, 1158 and 1030 cm^{-1} (OTf^-); ESI-MS (pos.) *m*/*z* = 448.2, calcd for $[Cu^{II}(L^{N2S})(OTf)]^+$ 448.0; Anal. Calcd for $Cu^{II}(L^{N2S})(NO_2)(OTf)\cdot 0.5H_2O$ ($C_{14}H_{21}ClCuF_3N_3O_{5.5}S_2$): C, 33.36; H, 4.20; N, 8.34. Found: C, 33.24; H, 3.96; N, 8.30.

$Cu^{II}(L^{N2S})(OTf)_2$ (2^{N2S}•OTf). To a CH_2Cl_2 solution of L^{N2S} (8.0 mg, 34 μmol) was added $Cu^{II}(OTf)_2$ (12 mg, 34 μmol). After stirring for 5 min, insoluble material was then removed by filtration. The filtrate was concentrated to give green oily material. Single crystals were obtained for the X-ray analysis by diffusion of *n*–hexane into a CH_2Cl_2 solution of the complex (74 % yield, 15 mg). FT-IR (KBr) 1262, 1170 and 1035 cm^{-1} (OTf^-); ESI-MS (pos.) *m*/*z* = 448.1, calcd for $[Cu^{II}(L^{N2S})(OTf)]^+$ 448.0; Anal. Calcd for $Cu^{II}(L^{N2S})(NO_2)(OTf)\cdot 0.5H_2O$ ($C_{14}H_{21}ClCuF_3N_3O_{5.5}S_2$): C, 33.05; H, 3.40; N, 4.71. Found: C, 30.13; H, 3.37; N, 4.68.

Product analysis

Decomposition products of cumene hydroperoxide. An acetone solution (3.0 mL) of $\mathbf{1}^{N2S}$ (0.5 mM) was cooled to –85°C, and then an acetone solution of CmOOH (1 equiv) was added to the solution under nitrogen atmosphere. The resulting mixture was stirred for 1 h at –85°C. After warming the solution to room temperature, anisole (0.5 mM) was added as an internal standard, and then decomposition products derived from cumene hydroperoxide were analyzed by using a HPLC system consisting of a Shimadzu LC-6A chromatographic pump and an on-line Shimadzu UV-vis spectrophotometric detector. Reverse phase chromatography was performed on an ODS column (Cosmosil $5C_{18}$-AR-II, 250 mm x 4.6 mm, Nacalai tesque) at room temperature with an acetonitrile-water (40 : 60) mixed solvent as mobile phase at a constant flow rate of 0.5 mL min^{-1}. The yields of products were determined by comparing the integrated peak areas of

the products with that of the internal standard (anisole) using calibration lines.

Hydroxylated ligand (L^{N2SO}). An acetone solution (3.0 mL) of $\mathbf{1}^{N2S}$ (12 mg, 27 μmol) was cooled to –85°C using a Unisoku thermostated cell holder designed for low temperature measurement. Then, an acetone solution of CmOOH (2 equiv) was added to the solution under nitrogen atmosphere. The resulting mixture was stirred for 1 h at –85°C, and then gradually warmed up to room temperature. A mixture of organic materials was obtained by treating the reaction mixture with an NH_3 aq and subsequent extraction by $CHCl_3$. The combined organic layer was dried over Na_2SO_4. After removal of Na_2SO_4 by filtration, evaporation of the solvent gave a yellow oil. ^{1}H-NMR (400 MHz, $CDCl_3$) δ 2.03 (2 H, pentet, J = 6.0 Hz, CH_2-CH_2-CH_2), 2.18 (2 H, pentet, J = 6.0 Hz, CH_2-CH_2- CH_2-), 2.62 (2 H, m, -CH_2-S-CH_2-), 2.74 (2 H, m, -CH_2-S-CH_2-) 2.77-2.84 (4 H, m, N-CH_2-CH_2-), 3.32 (2 H, m, Py-CH_2-CH_2-), 3.50 (2 H, m, Py-CH_2-CH_2-), 7.16-7.20 (1 H, m, PyH_5), 7.46-7.51 (1 H, m, PyH_3), 7.67 (1 H, td, J = 2.0 Hz and J = 8.0 Hz, PyH_4), 8.54 (1 H, d, J = 5.2 Hz, PyH_6); HRMS (FAB$^+$) m/z = 253.1378, calcd for $C_{13}H_{21}N_2OS$ ($[L^{N2SO}+H]^+$) = 253.1375. FT-IR (neat) 1077, 1104 cm^{-1} (S=O).

X-ray crystal structure determination

Each single crystal obtained was mounted on a CryoLoop (Hampton Research Co.) with a mineral oil, and all data of X-ray diffraction were collected at –170 ºC on a Rigaku R-AXIS-RAPID diffractmeter using filtered Mo-Kα radiation. The structures were solved by direct methods SIR 92 or SIR 2008 and expanded using Fourier techniques.[34,35] The non-hydrogen atoms were refined anisotropically by full-matrix least-squares on F^2. The hydrogen atoms were attached at idealized positions on carbon atoms and were not refined. All structures in the final stages of refinement showed no movement in the atom positions. The calculations were performed using Single-Crystal Structure Analysis Software, version 4.0. CCDC. 959052, 959053, 959054, 959055 and 959056.

Results and Discussion

Synthesis and characterization

Ligand L^{N2S} was synthesized in three steps as shown in Scheme 4-1. Treatment of 2-(2-aminoethyl)pyridine and 3-chloro-1-propanol in CH_3CN gave a bis(3-hydroxypropyl)amine derivative, which was then converted to the dichloro derivative by the reaction with $SOCl_2$. Ring closure using Na_2S gave ligand L^{N2S} in a reasonable yield.

Scheme 4-1

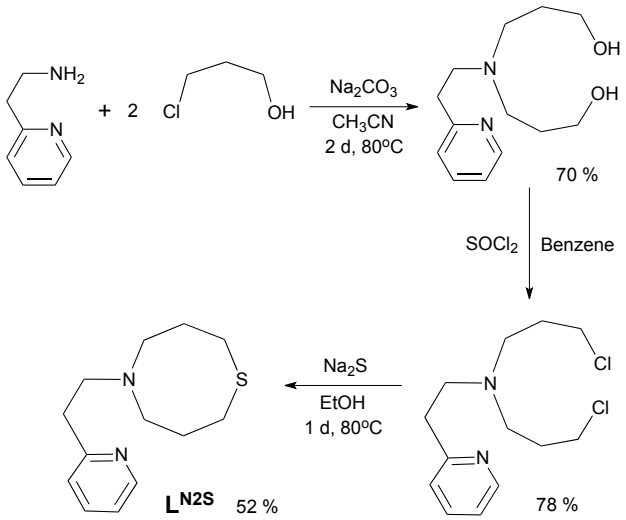

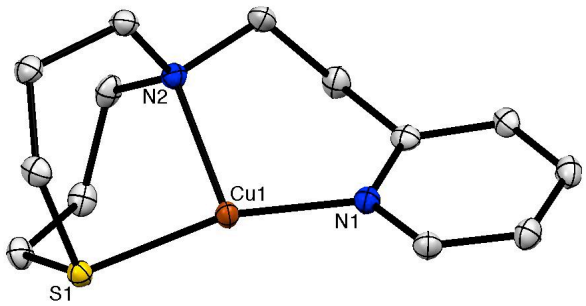

Figure 4-2. ORTEP drawing of $\mathbf{1}^{N2S}$ showing 50 % probability thermal ellipsoids. Counter anion (PF_6^-) and hydrogen atoms are omitted for clarity.

Copper(I) complex $[Cu^{I}(L^{N2S})](PF_6)$ ($\mathbf{1}^{\mathbf{N2S}}$) was prepared by the reaction of L^{N2S} with an equimolar amount of $[Cu^{I}(CH_3CN)_4](PF_6)$ in THF. The crystal structure of 1^{N2S} is shown in Figure 4-2. The crystallographic data and selected bonds lengths and angles of $\mathbf{1}^{\mathbf{N2S}}$ are presented in Tables 4-1 and 4-2, respectively.

Table 4-1. X-ray Crystallographic Data of Copper(I) Complexes $\mathbf{1}^{\mathbf{N2S}}$.

Compound	$\mathbf{1}^{\mathbf{N2S}}$
formula	$C_{13}H_{20}CuF_6N_2PS$
formula weight	444.88
crystal system	monoclinic
space group	$P2_1/n$ (#14)
a, Å	9.0976(3)
b, Å	15.0804(6)
c, Å	12.5185(5)
α, deg	90
β, deg	105.9955(9)
γ, deg	90
V, Å^3	1650.6(1)
Z	4
F(000)	904.00
D_{calcd}, g/cm^{-3}	1.790
T, K	103
crystal size, mm	0.500 x 0.400 x 0.400
μ (Mo$K\alpha$), cm^{-1}	16.071
$2\theta_{max}$, deg	54.9
no. of reflns measd	3774
no. of reflns obsd	3774 (All reflections)
no. of variables	217
R1 [a]	0.0302
wR2 [b]	0.1122
GOF	1.031

[a] $R1 = \Sigma \, ||F_o| - |F_c|| \, / \, \Sigma \, |F_o|$. [b] $wR2 = [\, \Sigma \, w \, (|F_o^2| - |F_c^2|)^2 \, / \, \Sigma \, w \, (F_o^2)^2]^{1/2}$

Table 4-2. Selected Bond Lengths (Å) and Angles (deg) of $\mathbf{1}^{N2S}$

	$\mathbf{1}^{N2S}$		
Cu(1)–S(1)	2.2028(4)	Cu(1)–N(1)	1.9295(13)
Cu(1)–N(2)	2.1662(13)		
S(1)–Cu(1)–N(1)	163.02(4)	S(1)–Cu(1)–N(2)	94.37(4)
N(1)–Cu(1)–N(2)	102.60(6)		

$\mathbf{1}^{N2S}$ exhibits a slightly distorted T-shape structure ligated by the two nitrogen atoms, N(1) and N(2), and one sulfur atom S(1) of the supporting ligand [Cu(1)–N(1), 1.930 Å; Cu(1)–N(2), 2.166 Å; Cu(1)–S(1), 2.203 Å]. The sum of the three angles around the copper center [∠S(1)–Cu(1)–N(1), ∠S(1)–Cu(1)–N(2), ∠N(1)–Cu(I)–N(2)] is equal to 360°, indicating that the copper ion and the three donor atoms exist in the same plane. The copper(I) complex $\mathbf{1}^{N3}$ supported by L^{N3} exhibited a similar T-shape structure, demonstrating that the molecular framework of the ligands can highly stabilize such a three coordinate T-shape structure of copper(I).[26, 27] Although the precise structure of the reduced enzyme is not known, the EXAFS data have suggested that the reduced Cu_M is 3-coordinate or 4-coordinate with a weakly bound water molecule, where the Cu_M–S_{Met} distance is 2.24 Å.[4] In this context, $\mathbf{1}^{N2S}$ represents a good structural model of reduced Cu_M, even though the Cu–S distance in $\mathbf{1}^{N2S}$ (2.203 Å) is slightly shorter than that in the enzyme (2.24 Å).

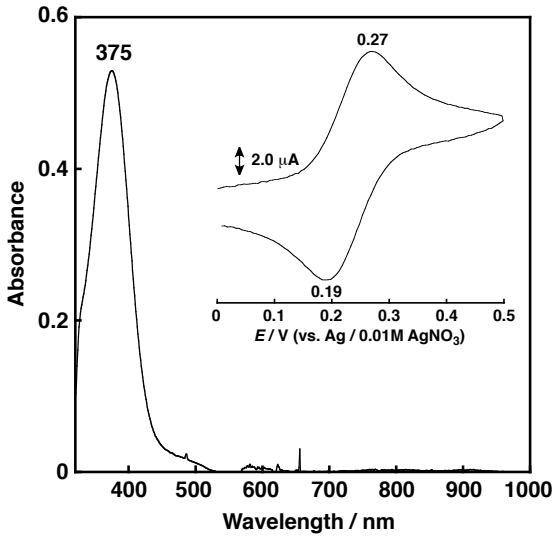

Figure 4-3. UV-vis spectrum of $\mathbf{1}^{\mathbf{N2S}}$ (0.5 mM) in acetone at 25°C. Inset: Cyclic voltammogram of $\mathbf{1}^{\mathbf{N2S}}$ (1.0 mM) in acetone containing 0.1 M $TBAPF_6$; working electrode GC, counter electrode Pt, reference electrode Ag/ 0.01 M $AgNO_3$, scan rate 50 mV/s.

$\mathbf{1}^{\mathbf{N2S}}$ showed a relatively intense absorption band at 375 nm (ε = 1058 M^{-1} cm^{-1}) ascribable to a Cu^{I} to S charge transfer (MLCT) (Figure 4-3), and exhibited a reversible Cu^{I}/Cu^{II} redox couple at 0.23 V *vs*. $Ag/AgNO_3$ in acetone (Figure 4-3, inset) that is higher than that of 1^{N3} (0.11 V for R = $-CH_2CH_2Ph$) under the same conditions.[27]

Copper(II) complexes $\mathbf{2}^{\mathbf{N2S}}\bullet\mathbf{X}$ (X = coordinating counter anion; Cl, N_3, NO_2, OTf) were also prepared as the model compounds of resting enzymes in the copper(II) oxidation state. The crystal structures of $\mathbf{2}^{\mathbf{N2S}}\bullet\mathbf{Cl}$, $\mathbf{2}^{\mathbf{N2S}}\bullet\mathbf{N_3}$, $\mathbf{2}^{\mathbf{N2S}}\bullet\mathbf{NO_2}$ and $\mathbf{2}^{\mathbf{N2S}}\bullet\mathbf{OTf}$ have been determined as shown in Figures 4-3 and 4-4. The crystallographic data and the selected bond lengths and angles are summarized in Tables 4-3 and 4-4.

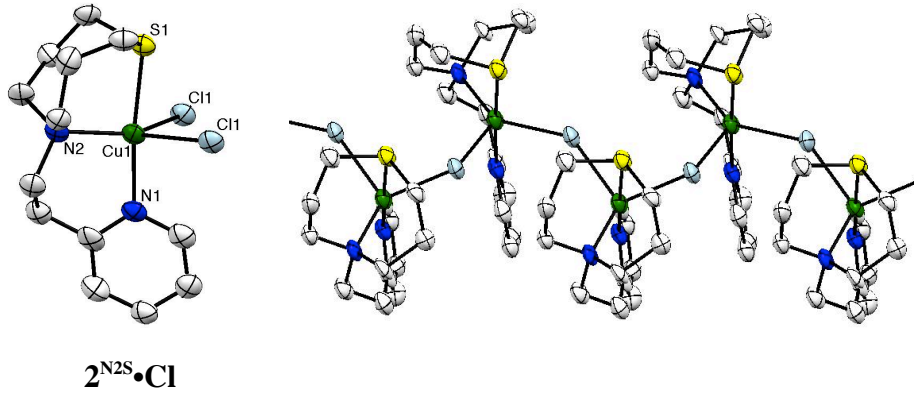

2^{N2S}•Cl

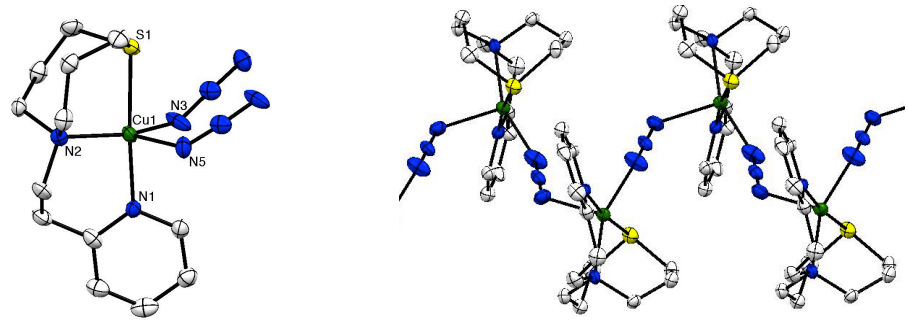

2^{N2S}•N_3

Figure 4-3. ORTEP drawings of 2^{N2S}•**Cl**, 2^{N2S}•N_3 and its linear chain structure showing 50 % probability thermal ellipsoids. Non-coordinated counter anion (BF_4^-) and hydrogen atoms are omitted for clarity.

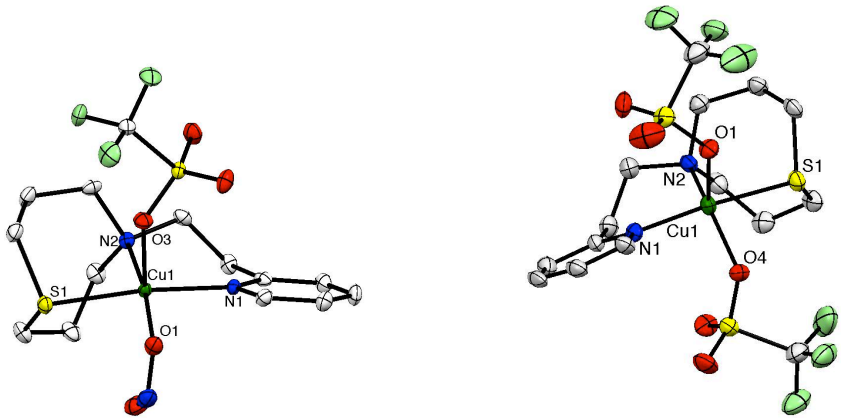

2^{N2S}•NO_2 2^{N2S}•**OTf**

Figure 4-4. ORTEP drawings of 2^{N2S}•NO_2 and 2^{N2S}•**OTf** showing 50 % probability thermal ellipsoids. Hydrogen atoms are omitted for clarity.

Table 4-3. X-ray Crystallographic Data of Copper(II) Complexes 2^{N2S}•Cl, 2^{N2S}•N_3, 2^{N2S}•NO_2 and 2^{N2S}•OTf.

Compound	2^{N2S}•Cl	2^{N2S}•N_3
formula	$C_{13}H_{20}BClCuF_4N_2S$	$C_{26}H_{40}B_2Cu_2F_8N_{10}S_2$
formula weight	422.18	857.49
crystal system	monoclinic	monoclinic
space group	$P2_1/c$ (#14)	$P2_1/n$ (#14)
a, Å	10.430(2)	19.271(2)
b, Å	22.179(5)	7.1058(4)
c, Å	7.084(2)	25.114(2)
α, deg	90	90
β, deg	92.797(3)	103.692(2)
γ, deg	90	90
V, Å^3	1636.6(5)	3341.2(4)
Z	4	4
F(000)	860.00	1752.00
D_{calcd}, g/cm^{-3}	1.713	1.704
T, K	103	103
crystal size, mm	0.600 x 0.200 x 0.100	0.400 x 0.400 x 0.100
m (MoKa), cm^{-1}	16.627	14.808
$2q_{max}$, deg	55.0	55.0
no. of reflns measd	15561	31522
no. of reflns obsd	3744 (All reflections)	7660 (All reflections)
no. of variables	228	491
R1 [a]	0.1626	0.0561
wR2 [b]	0.4008	0.1528
GOF	1.000	1.142

[a] $R1 = \Sigma \, ||F_o| - |F_c|| \, / \, \Sigma \, |F_o|$. [b] $wR2 = [\, \Sigma \, w \, (|F_o^2| - |F_c^2|)^2 \, / \, \Sigma \, w \, (F_o^2)^2]^{1/2}$

Table 4-3. X-ray Crystallographic Data of Copper(II) Complexes 2^{N2S}•Cl, 2^{N2S}•N_3, 2^{N2S}•NO_2 and 2^{N2S}•OTf (continued).

Compound	2^{N2S}•NO_2	2^{N2S}•OTf
formula	$C_{14}H_{22}CuF_3N_3O_6S_2$	$C_{15}H_{20}CuF_8N_2O_6S_3$
formula weight	513.01	598.05
crystal system	triclinic	monoclinic
space group	*P*-1 (#2)	*P*21/c (#14)
a, Å	7.6907(4)	7.172(2)
b, Å	8.7410(5)	20.845(4)
c, Å	15.2512(7)	15.117(3)
α, deg	84.088(2)	90
β, deg	78.235(2)	103.769(4)
γ, deg	74.662(2)	90
V, Å^3	966.66(8)	2195.0(7)
Z	2	4
F(000)	526.00	1212.00
D_{calcd}, g/cm^{-3}	1.713	1.810
T, K	103	103
crystal size, mm	0.400 x 0.300 x 0.100	0.500 x 0.200 x 0.200
μ (Mo$K\alpha$), cm^{-1}	14.124	13.673
$2\theta_{max}$, deg	54.9	55.0
no. of reflns measd	9398	21107
no. of reflns obsd	4363 (All reflections)	5020 (All reflections)
no. of variables	262	298
R1 [a]	0.0377	0.0749
wR2 [b]	0.1430	0.2053
GOF	1.188	1.083

[a] $R1 = \Sigma \, ||F_o| - |F_c|| \, / \, \Sigma \, |F_o|$. [b] $wR2 = [\, \Sigma \, w \, (|F_o^2| - |F_c^2|)^2 \, / \, \Sigma \, w \, (F_o^2)^2]^{1/2}$

Table 4-4. Selected Bond Lengths (Å) and Angles (deg) of 2^{N2S}•Cl, 2^{N2S}•N_3, 2^{N2S}•NO_2 and 2^{N2S}•OTf.

2^{N2S}•Cl

Cu(1)–Cl(1)	2.388(3)	Cu(1)–Cl(1)*	2.572(3)
Cu(1)–S(1)	2.310(3)	Cu(1)–N(1)	2.016(8)
Cu(1)–N(2)	2.068(8)		

Cl(1)–Cu(1)–Cl(1)*	98.50(9)	Cl(1)–Cu(1)–S(1)	85.52(9)
Cl(1)–Cu(1)–N(1)	90.0(3)	Cl(1)–Cu(1)–N(2)	140.2(3)
Cl(1)*–Cu(1)–S(1)	81.65(9)	Cl(1)*–Cu(1)–N(1)	94.3(3)
Cl(1)*–Cu(1)–N(2)	119.9(3)	S(1)–Cu(1)–N(1)	173.4(3)
S(1)–Cu(1)–N(2)	89.6(3)	N(1)–Cu(1)–N(2)	96.9(3)

2^{N2S}•N_3

Cu(1)–S(1)	2.3306(13)	Cu(1)–N(1)	2.036(4)
Cu(1)–N(2)	2.078(4)	Cu(1)–N(5)*	2.265(4)
Cu(1)–N(3)	2.029(4)		

S(1)–Cu(1)–N(1)	173.24(10)	S(1)–Cu(1)–N(2)	88.85(11)
S(1)–Cu(1)–N(5)*	91.71(11)	S(1)–Cu(1)–N(3)	86.51(13)
N(1)–Cu(1)–N(2)	96.98(14)	N(1)–Cu(1)–N(5)*	90.39(14)
N(1)–Cu(1)–N(3)	86.78(15)	N(2)–Cu(1)–N(5)*	102.36(13)
N(2)–Cu(1)–N(3)	155.92(15)	N(5)*–Cu(1)–N(3)	101.39(15)

2^{N2S}•NO_2

Cu(1)–S(1)	2.3343(10)	Cu(1)–O(1)	2.012(2)
Cu(1)–N(1)	2.037(3)	Cu(1)–N(2)	2.076(3)
Cu(1)–O(5)	2.343(3)		

S(1)–Cu(1)–O(1)	85.01(8)	S(1)–Cu(1)–N(1)	172.73(7)
S(1)–Cu(1)–N(2)	89.03(8)	S(1)–Cu(1)–O(3)	89.65(10)
O(1)–Cu(1)–N(2)	172.02(10)	O(1)–Cu(1)–O(3)	83.29(10)
O(3)–Cu(1)–N(1)	92.05(15)	O(3)–Cu(1)–N(2)	102.01(13)
O(1)–Cu(1)–N(1)	88.17(10)	N(1)–Cu(1)–N(2)	97.52(10)

2^{N2S}•OTf

Cu(1)–S(1)	2.2860(15)	Cu(1)–O(1)	2.247(4)
Cu(1)–O(4)	2.118(4)	Cu(1)–N(1)	2.006(5)
Cu(1)–N(2)	2.040(6)		

S(1)–Cu(1)–O(1)	84.84(11)	S(1)–Cu(1)–O(4)	84.78(12)
S(1)–Cu(1)–N(1)	171.15(16)	S(1)–Cu(1)–N(2)	90.42(14)
O(1)–Cu(1)–O(4)	95.93(15)	O(1)–Cu(1)–N(1)	92.12(16)
O(1)–Cu(1)–N(2)	109.86(17)	O(4)–Cu(1)–N(1)	87.27(18)
O(4)–Cu(1)–N(2)	153.25(16)	N(1)–Cu(1)–N(2)	98.4(2)

All the copper(II) complexes exhibit five-coordinate structures with $\tau = 0.01 \sim 0.55$,[28] among which **2^{N2S}•OTf** and **2^{N2S}•NO_2** exhibit a monomeric structure (Figure 4-4), but **2^{N2S}•Cl** and **2^{N2S}•N_3** form coordination polymer chain structures, where one of the coordinated counter anions (Cl^- and N_3^-) acts as the bridging ligand (Figure 4-3). Thus, the structure and chemical properties were examined using **2^{N2S}•OTf**.

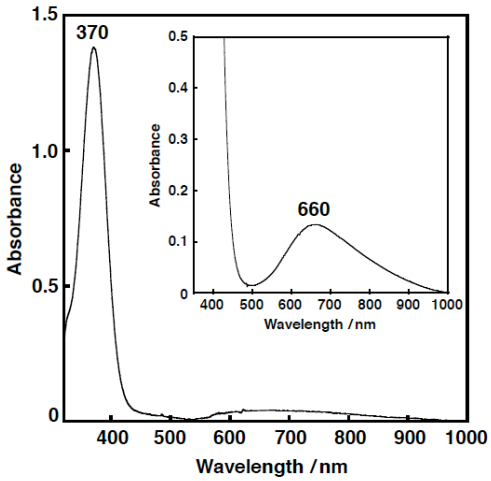

Figure 4-5. The UV-vis spectrum of $\mathbf{2}^{\mathbf{N2S}}$•OTf (0.25 mM) in acetone at –85°C. λ_{max} = 370 nm (ε = 5520 M^{-1} cm^{-1}). Inset: An expanded UV-vis spectrum of $\mathbf{2}^{\mathbf{N2S}}$•OTf (0.60 mM). λ_{max} = 660 nm (ε = 222 M^{-1} cm^{-1}).

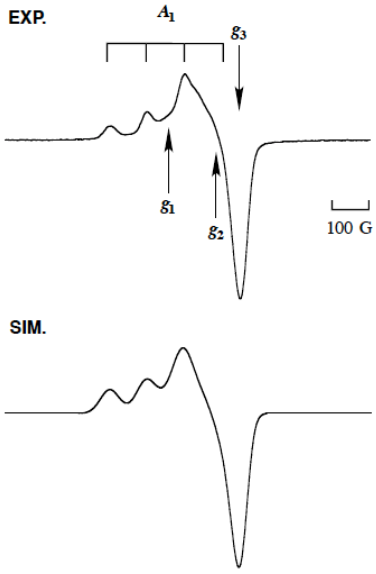

Figure 4-6. The EPR spectrum (EXP, top) of $\mathbf{2}^{\mathbf{N2S}}$•**OTf** (0.5 mM) in acetone at –196 °C, and its computer simulation spectrum (SIM, bottom) with the parameters of g_1 = 2.275, g_2 = 2.100, g_3 = 2.015, A_1 = 150 G, A_2 = 59 G, and A_3 = 16 G.

Copper(II) complex $\mathbf{2}^{\mathbf{N2S}}$•**OTf** exhibits a distorted square pyramidal structure coordinated by N(1), N(2), S(1) and O(4) in the equatorial plan and O(1)

occupying the axial position (τ = 0.30), which is in accord with the observed ligand filed absorption band at 660 nm (ε = 222 M^{-1} cm^{-1}, Figure 4-5) and a typical EPR signals of Cu^{II} with a tetragonal geometry (Figure 4-6, the EPR parameters are provided in the figure caption). The structural feature is quite different from that of the copper(II) complexes supported by L^{N3}, which enforces the copper(II) center having a four-coordinate distorted tetrahedral geometry.[26, 27] Thus, the replacement of the donor atom from nitrogen to sulfur resulted in a significant change in the coordination geometry of the copper(II) complexes. In this case, Cu–S distance is 2.286 Å, which is longer than that in the copper(I) complex (2.203 Å). Such an elongation of the Cu^{II}–S bond demonstrates the strong preference of the Cu^{I}–S bond. However, the Cu^{II}–S distance in the model complex (2.286 Å) is much shorter than that in the resting state (copper(II) oxidation state) of the enzyme, that is 2.68 Å, although the coordination geometry is similar each other.[3]

Reactivity

First, the reaction of $\mathbf{1}^{N2S}$ and O_2 was examined in acetone at low temperature (–85 °C). However, no spectral change was observed. Even at room temperature or in other solvents such as THF and CH_2Cl_2, $\mathbf{1}^{N2S}$ showed no reactivity toward O_2. This result is in sharp contrast to the high O_2-reactivity of $\mathbf{1}^{N3}$, which gives a mononuclear copper(II)-superoxide complex.[26,27] Such a big difference in the O_2-reactivity between the two ligand systems could be attributed to the higher oxidation potential of $\mathbf{1}^{N2S}$ (0.23 V) as compared to that of $\mathbf{1}^{N3}$ (0.11 V). As mentioned above, the Cu–S distance in the enzyme is much longer, especially in the copper(II) oxidation state, which may cause less copper(I)-stabilizing effect of the sulfur donor atom in the enzymatic system. Therefore, Cu_M can activate O_2 for the substrate oxygenation reaction even in the presence of Met ligand.

On the other hand, $\mathbf{1}^{N2S}$ smoothly reacted with cumene hydroperoxide (CmOOH) in a 1 : 1 ratio to give CmOH (cumyl alcohol) as the major product (98 %) together with a trace amount of acetophenone (PhC(O)Me). In the case of $\mathbf{1}^{N3}$, only 44 % of CmOH was obtained together with a small amount of PhC(O)Me (6.0 %), and 50 % of CmOOH was recovered. Thus, the

stoichiometry in the $\mathbf{1}^{\mathbf{N3}}$ case was 2 : 1.

We have recently examine the reactivity of a series of copper complexes using CmOOH as a prove for searching the O–O braking pattern in the copper-peroxide adducts.[29,30] It has been demonstrated that copper(I) complexes supported by nitrogen ligands react with CmOOH in a 2 : 1 ratio to induce the heterolytic O–O bond cleavage of the peroxide to give CmOH as the major product. In this case, each copper(I) complex formally act as an one-electron donor to induce totally two-electron reduction of CmOOH, thus providing the heterolytic cleavage product, CmOH, in a ~50 % yield based on the copper(I) starting material (Stoichiometry of Cu : CmOOH is 2 : 1).[30] Thus, $\mathbf{1}^{\mathbf{N3}}$ (N_3-donor ligand) giving CmOH in a ~50 % yield, is involved in this category.

In this respect, the reactivity of $\mathbf{1}^{\mathbf{N2S}}$ (N_2S-donor ligand) is different, showing the 1 : 1 stoichiometry to give CmOH in a ~100 % yield based on the copper(I) starting material. Such a unique reactivity of $\mathbf{1}^{\mathbf{N2S}}$ can be attributed to the presence of the sulfur atom. In order to get insight into the effect of the sulfur atom, the reaction was examined by UV-vis, resonance Raman and EPR spectra as follows.

Figure 4-7 shows the UV-vis spectral change for the reaction of $\mathbf{1}^{\mathbf{N2S}}$ and an equimolar amount of CmOOH in acetone. After about 1000 s, an intermediate **A** exhibiting characteristic absorption bands at 336, 465 and 625 nm was developed (Figure 4-7, solid line). This intermediate was gradually converted to another intermediate **B** having absorption bands at 336, 415, and 635 nm (Figure 4-7, dashed line). When the solution was warmed up to room temperature, the absorption bands in the visible region completely disappeared, suggesting formation of a copper(I) product **C** (Figure 4-7, dotted line). The EPR spectrum of the final reaction solution was essentially EPR silent, being consistent with the formation of a copper (I) complex.

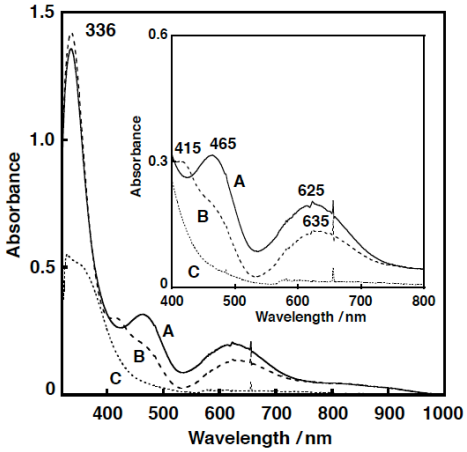

Figure 4-7. The UV-vis spectra of Intermediate A (solid line; 1000 s after the reaction of $\mathbf{1}^{N2S}$ (0.5 mM) with an equimolar amount of CmOOH in acetone at –85°C), B (dashed line; 1h after the reaction), and C (dotted line; after warming up to 30°C).

Then, the reaction was examined by resonance Raman spectrum at the low temperature. As shown in Figure 4-8, isotope-sensitive Raman bands were observed at 887, 827 and 610 cm^{-1}, which shifted to 794 and 603 cm^{-1}, when ^{18}O-labeled CmOOH was employed. The Raman bands at 887 and 827 cm^{-1} could be attributed to the O–O bond stretching vibration of a cumylperoxide adduct intermediate **A** and the band at 610 cm^{-1} may be due to its Cu–O stretching vibration.[31]

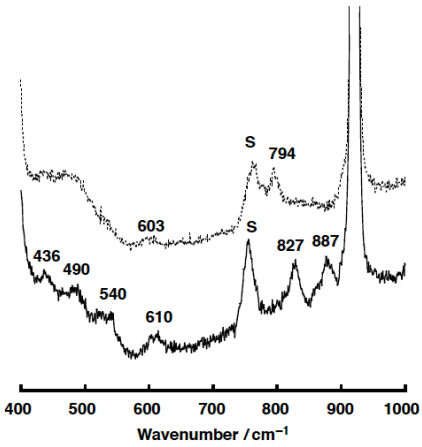

Figure 4-8. Resonance Raman spectra of the intermediate derived from the reaction of $\mathbf{1}^{N2S}$ (3.0 mM) with CmOOH (3.0 mM) generated by using $Cm^{16}O_2H$ (solid line, below) and $Cm^{18}O_2H$ (dotted line, above) obtained with λ_{max} = 441.6 nm in CH_3CN at –40°C; s denotes the solvent band.

Scheme 4-2

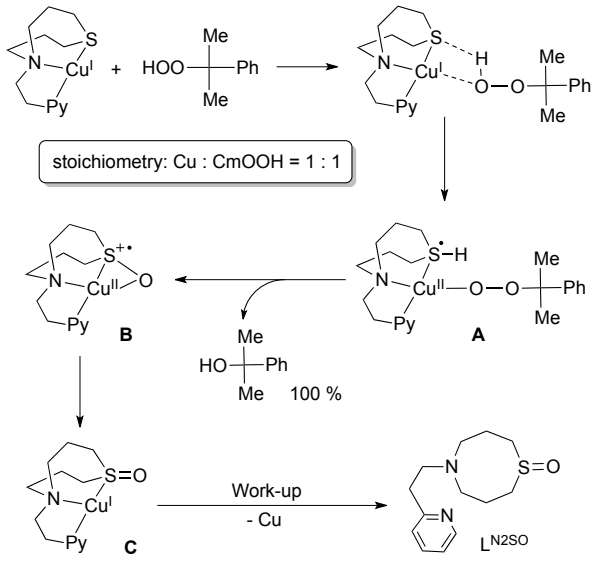

On the basis of these results, a possible reaction mechanism is proposed in Scheme 4-2. Association of the copper(I) complex $\mathbf{1}^{\mathbf{N2S}}$ and CmOOH may induce proton-coupled electron-transfer (PCET) to generate intermediate **A**, where a proton of CmOOH is transferred to the sulfur atom and an electron is transferred from copper(I) to the sulfur atom. In this case, an empty d orbital of the sulfur atom can accommodate the electron provided from copper(I). Then, nucleophilic attack of the sulfur atom to the proximal oxygen leads to S–O bond formation with concomitant proton migration to the distal oxygen atom. Eventually, O–O bond heterolytic cleavage takes place to give intermediate **B** and CmOH. Then, electronic rearrangement of **B** occurs upon warming to give a copper(I) complex **C** with an oxygenated ligand.

The sulfoxide ligand L^{N2SO} was obtained nearly quantitatively after the work-up treatment of the reaction mixture with NH_4OH aq (demetalation). The formation of L^{N2SO} was confirmed by the ^{1}H-NMR, IR and ESI-mass spectra (see Experimental section), and the isotope labeling experiment using $Cm^{18}O_2H$ confirmed that the oxygen atom incorporated to the ligand was originated from CmOOH used (Figure 4-9). Although mechanistic details of the enzymatic reaction remain obscure, such a role of sulfur ligand could be involved to enhance the O–O bond cleavage of the peroxide intermediate in the copper monooxygenases.

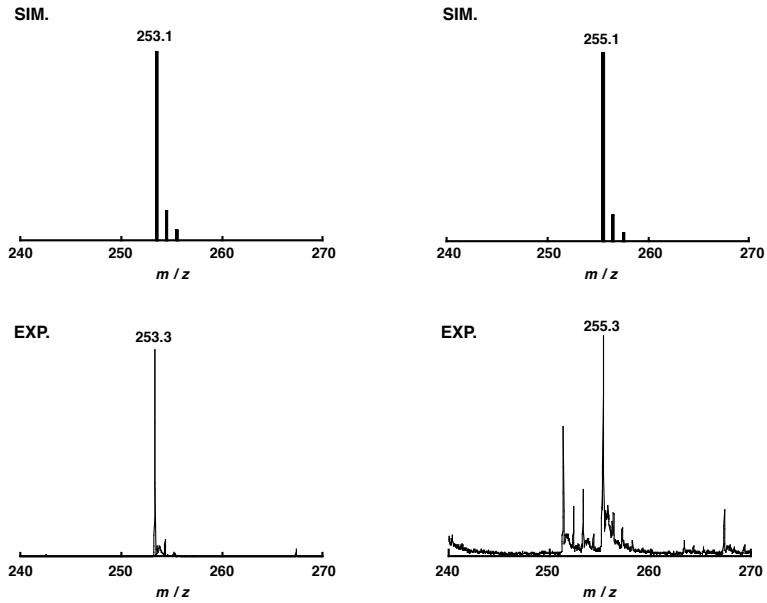

Figure 4-9. Experimental (bottom) and simulated (top) peak envelopes in the positive-ion ESI-MS spectra of the ligand oxidation product derived from the reaction mixture of $\mathbf{1}^{\mathbf{N2S}}$ and CmOOH in acetone. (left) with $Cm^{16}O_2H$ and (right) with $Cm^{18}O_2H$.

Conclusions

In summary, copper(I) and copper(II) complexes of N_2S ligand (L^{N2S}) have been synthesised and characterised in order to get insights into the effects of sulfur atom of Met ligand in the enzyme active site. Structural examinations have suggested that the sulfur coordination in the present model system is stronger than that in the enzymatic system, causing higher stability of the copper(I) oxidation state toward O_2. Nonetheless, reactivity study using cumene hydroperoxide has clearly indicated that the sulfur atom helps the O–O bond heterolysis of the peroxide intermediate. Such an effect of sulfur must be important to facilitate the enzymatic reactions. The present result also suggests that the sulfur atom of the Met ligand in the enzymatic system can be oxygenated to sulfoxide during the catalytic cycles. In other words, posttranslational modification of the Met sulfur could occur in the enzyme active site.

Acknowledgment

This chapter was reproduced from Dalton Transactions, 2013, under revision, with permission from the Royal Society of Chemistry.

Reference

1. Klinman, J. P. *Chem. Rev.* **1996**, *96*, 2541-2562.
2. Prigge, S. T.; Mains, R. E.; Eipper, B. A.; Amzel, L. M. *Cell. Mol. Life Sci.* **2000**, *57*, 1236-1259.
3. Prigge, S. T.; Kolhekar, A. S.; Eipper, B. A.; Mains, R. E.; Amzel, L. M. *Science*, **1997**, *278*, 1300-1305.
4. Blackburn, N. J.; Rhames, F. C.; Ralle, M.; Jaron, S. *J. Biol. Inorg. Chem.* **2000**, *5*, 341-353.
5. Blackburn, N. J.; Hasnain, S. S.; Pettingill, T. M.; Strange, R. W. *J. Biol. Chem.* **1991**, *266*, 23120-23127.
6. Hess, C.; Klinman, J. P.; Blackburn, N. J. *J. Biol. Inorg. Chem.* **2010**, *15*, 1195-1207.
7. Solomon, E. I.; Baldwin, M. J.; Lowery, M. D. *Chem. Rev.* **1992**, *92*, 521-542.
8. Solomon, E. I.; Tuczek, F.; Root, D. E.; Brown, C. A. *Chem. Rev.* **1994**, *94*, 827-856.
9. Casella, L.; Gullotti, M.; Bartosek, M.; Pallanza, G.; Laurenti, E. *J. Chem. Soc., Chem. Commun.* **1991**, 1235-1237.
10. Alzuet, G.; Casella, L.; Laura Villa, M.; Carugo, O.; Gullotti, M. *J. Chem. Soc., Dalton Trans.* **1997**, 4789-4794.
11. Champloy, F.; Benali-Cherif, N.; Bruno, P.; Blain, I.; Pierrot, M.; Reglier, M.; Michalowicz, A. *Inorg. Chem.* **1998**, *37*, 3910-3918.
12. Ohta, T.; Tachiyama, T.; Yoshizawa, K.; Yamabe, T.; Uchida, T.; Kitagawa, T. *Inorg. Chem.* **2000**, *39*, 4358-4369.
13. Kodera, M.; Kita, T.; Miura, I.; Nakayama, N.; Kawata, T.; Kano, K.; Hirota, S. *J. Am. Chem. Soc.* **2001**, *123*, 7715-7716.
14. Aboelella, N. W.; Gherman, B. F.; Hill, L. M. R.; York, J. T.; Holm, N.; Young, V. G.; Cramer, C. J.; Tolman, W. B. *J. Am. Chem. Soc.* **2006**,

128, 3445-3458.

15. Zhou, L.; Powell, D.; Nicholas, K. M. *Inorg. Chem.* **2006**, *45*, 3840-3842.
16. Zhou, L.; Powell, D.; Nicholas, K. M. *Inorg. Chem.* **2007**, *46*, 7789-7799.
17. Lee, Y.; Lee, D.-H.; Narducci Sarjeant, A. A.; Zakharov, L. N.; Rheingold, A. L.; Karlin, K. D. *Inorg. Chem.* **2006**, *45*, 10098-10107.
18. Hatcher, L. Q.; Lee, D. H.; Vance, M. A.; Milligan, A. E.; Sarangi, R.; Hodgson, K. O.; Hedman, B.; Solomon, E. I.; Karlin, K. D. *Inorg. Chem.* **2006**, *45*, 10055-10057.
19. Lee, D.-H.; Hatcher, L. Q.; Vance, M. A.; Sarangi, R.; Milligan, A. E.; Narducci Sarjeant, A. A.; Incarvito, C. D.; Rheingold, A. L.; Hodgson, K. O.; Hedman, B.; Solomon, E. I.; Karlin, K. D. *Inorg. Chem.* **2007**, *46*, 6056-6068.
20. Park, G. Y.; Lee, Y.; Lee, D.-H.; Woertink, J. S.; Sarjeant, A. A. N.; Solomon, E. I.; Karlin, K. D. *Chem. Commun.* **2010**, *46*, 91-93.
21. Itoh, S. *Curr. Opin. Chem. Biol.* **2006**, *10*, 115-122.
22. Mirica, L. M.; Ottenwaelder, X.; Stack, T. D. P. *Chem. Rev.* **2004**, *104*, 1013-1045.
23. Lewis, E. A.; Tolman, W. B. *Chem. Rev.* **2004**, *104*, 1047-1076.
24. Itoh, S. in *Copper-Oxygen Chemistry*, eds. Karlin, K. D. and Itoh, S. John Wiley & Sons, Hoboken, **2011**, vol. 4, pp. 225-282.
25. Peterson, R. L.; Kim, S.; Karlin, K. D. in *Comprehensive Inorganic Chemistry II*, eds. Reedijk, J. and P. K., Elsevier, Oxford, **2013**, vol. 3, pp. 149-177.
26. Kunishita, A.; Kubo, M.; Sugimoto, H.; Ogura, T.; Sato, K.; Takui, T.; Itoh, S. *J. Am. Chem. Soc.* **2009**, *131*, 2788-2789.
27. Kunishita, A.; Ertem, M. Z.; Okubo, Y.; Tano, T.; Sugimoto, H.; Ohkubo, K.; Fujieda, N.; Fukuzumi, S.; Cramer, C. J.; Itoh, S. *Inorg. Chem.* **2012**, *51*, 9465-9480.
28. Addison, A. W.; Rao, T. N.; Reedijk, J.; van Rijn, J.; Verschoor, G. C. *J. Chem. Soc., Dalton Trans.* **1984**, 1349-1356.
29. Tano, T.; Ertem, M. Z.; Yamaguchi, S.; Kunishita, A.; Sugimoto, H.;

Fujieda, N.; Ogura, T.; Cramer, C. J.; Itoh, S. *Dalton Trans*. **2011**, *40*, 10326-10336.

30. Tano, T.; Sugimoto, H.; Fujieda, N.; Itoh, S. *Eur. J. Inorg. Chem*. **2012**, 4099-4103.
31. Kunishita, A.; Ishimaru, H.; Nakashima, S.; Ogura, T.; Itoh, S. *J. Am. Chem. Soc*. **2008**, *130*, 4244-4245.
32. Perrin, D. D.; Armarego, W. L. F.; Perrin, D. R. *Purification of Laboratory Chemicals*, 4th ed.: Pergamon Press: Elmsford, NY, **1996**.
33. Finn, M. G.; Sharpless, K. B. *J. Am. Chem. Soc*. **1991**, *113*, 113-126.
34. Altomare, A.; Cascarano, G.; Giacovazzo, C.; Guagliardi, A.; Burla, M.; Polidori, G.; Camalli, M. *J. Appl. Crystallogr*. **1994**, *27*, 435-436.
35. Burla, M. C.; Caliandro, R.; Camalli, M.; Carrozzini, B.; Cascarano, G. L.; Caro, L. D.; Giacovazzo, C.; Polidori, G.; Siliqi, D.; Spagna, R. *J. Appl. Crystallogr*. **2007**, *40*, 609-613.
36. Adachi, S.; Nagano, S.; Ishimori, K.; Watanabe, Y.; Morishima, I.; Egawa, T.; Kitagawa, T.; Makino, R. *Biochemistry* **1993**, *32*, 241-252.
37. Baciocchi, E.; Bietti, M.; Salamone, M.; Steenken, S. *J. Org. Chem*. **2002**, *67*, 2266-2270.

Concluding Remarks

In this thesis, the author has described his studies on control of oxygen–oxygen bond cleavage of copper-peroxide complexes. Particular attention has been focused on the effects of the ligand-denticity (tridentate vs. tetradentate), oxidation-state of copper ion (Cu^{I} vs. Cu^{II}), and heteroatoms of the supporting ligand (nitrogen vs. sulfur) on the oxygen–oxygen bond breaking pattern of the peroxide complexes.

The results and findings in this work are summarized as follows:

In chapter 1, redox properties of a mononuclear copper(II) superoxide complex, $(L)Cu^{II}$-$OO^{\bullet}$, have been examined toward several types of external substrates in order to get further insight into the intrinsic reactivity of the end-on superoxide copper(II) complex. Based on the reactivity toward a series of one-electron reductants, the reduction potential of $(L)Cu^{II}$-$OO^{\bullet}$ was estimated, and confirmed the reduction of the oxidation state from superoxide to peroxide by the quantification of generated H_2O_2. In the reaction of TEMPO-H (2,2,6,6-tetramethylpiperidine-*N*-hydroxide), a simple HAT (hydrogen atom transfer) reaction took place to give the corresponding hydroperoxide complex LCu^{II}-OOH, whereas the reaction with phenol derivatives gave the corresponding phenolate adducts, presumably via an acid-base reaction between the superoxide ligand and the phenols. The reaction of $(L)Cu^{II}$-$OO^{\bullet}$ with a series of triphenylphosphine derivatives gave the corresponding triphenylphosphine oxides via an electrophilic ionic substitution mechanism. These reactivities of $(L)Cu^{II}$-$OO^{\bullet}$ which is sharp contrast to those of a similar end-on superoxide copper(II) complex supported by a tetradentate TMG_3tren ligand (1,1,1-Tris{2-[N^2-(1,1,3,3-tetramethylguanidino)]ethyl}amine, Maiti, D. *et al*. *Angew*. *Chem*., *Int*. *Ed*. **2008**, *47*, 82-85), colud be attributed to the different geometry of the superoxide complesxes.

In chapter 2, copper(II) complexes supported by tridentate ligand bpa [bis(2-pyridylmethyl)amine] and tetradentate ligand tpa [tris(2-pyridylmethyl)amine], respectively, react with cumene hydroperoxide (CmOOH) in the presence of base in CH_3CN to provide the corresponding copper(II) cumylperoxide complexes, the formation of which has been confirmed by resonance Raman and ESI-MS analyses using ^{18}O-labeled CmOOH. UV-vis and EPR spectra as well as DFT calculations

providing their structural information. Both cumylperoxide copper(II) complexes are fairly stable at ambient temperature, but decompose at a higher temperature (60 °C) in CH_3CN. Detailed product analyses and DFT studies indicate that the self-decomposition involves O–O bond homolytic cleavage of the peroxide moiety, concomitant hydrogen-atom abstraction from the solvent is partially involved. In the presence of 1,4-cyclohexadiene (CHD), the cumylperoxide complexes react smoothly at 30 °C to give benzene as one product. Detailed product analyses and DFT studies indicate that reaction with CHD involves concerted O–O bond homolytic cleavage and hydrogen-atom abstraction from the substrate, with the oxygen atom directly bonded to the copper(II) ion (proximal oxygen) involved in the C–H bond activation step.

In Chapter 3, the reaction of copper(I) complexes and cumene hydroperoxides has been examined to demonstrate that heterolytic O–O bond cleavage of the peroxides proceeds predominantly to give the corresponding alcohols (cumyl alcohols) as the major product, where the stoichiometry of Cu^I : peroxide is 2 : 1. The result is in sharp contrast to the 1 : 1 reaction between the copper(II) complexes and cumene hydroperoxide, providing ketone (acetophenone) as the major product via homolytic O–O bond cleavage.

Finally in chapter 4, in order to develop N_2S coordination environment which mimics the enzyme active site, the author has synthesized and characterized copper complexes supported by a new type of sulfur-containing ligand (L^{N2S}), which is related to an N_3-tridentate ligand (L^{N3}) used in chapter 1. Structural study has suggested that sulfur-coordination in the model system is much stronger than that in the enzyme system, causing higher stability of the copper(I) oxidation state toward dioxygen. On the other hand, reactivity study has demonstrated a notable electronic effect of sulfur donor atom in the reaction with cumene hydroperoxide, inducing efficient heterolytic O–O bond cleavage.

These new findings in this thesis not just contribute to a comprehensive understanding of enzymatic reaction mechanism, but also provide a stimulus for development of new environmentally-friendly methods for industrial large-scale applications of transition-metal-catalyzed substrate oxidation reactions.

List of Publications

Original Paper

1. Reactivity of Copper(II)-Alkylperoxo Complexes
   Tetsuro Tano, Mehmed Z. Ertem, Satoru Yamaguchi, Atsushi Kunishita, Hideki Sugimoto, Nobutaka Fujieda, Takashi Ogura, Christopher J. Cramer and Shinobu Itoh
   Dalton Trans. **2011**, *40*, 10326-10336.

2. Heterolytic Alkyl Hydroperoxide O–O Bond Cleavage by Copper(I) Complexes
   Tetsuro Tano, Hideki Sugimoto, Nobutaka Fujieda and Shinobu Itoh
   Eur. J. Inorg. Chem. **2012**, 4099-4103.

3. Redox Properties of a Mononuclear Copper(II)-Superoxide Complex
   Tetsuro Tano, Yuri Okubo, Atsushi Kunishita, Minoru Kubo, Hideki Sugimoto, Nobutaka Fujieda, Takashi Ogura and Shinobu Itoh
   Inorg. Chem. **2013**, *52*, 10431-10437.

4. Copper Complex Supported by an N_2S-Tridentate Ligand Inducing Efficient Heteroytic O–O Bond Cleavage of Alkylhydroperoxide
   Tetsuro Tano, Kaoru Mieda, Hideki Sugimoto, Talashi Ogura and Shinobu Itoh
   Dalton Trans. under revision.

Supplementary

1. Nickel(II) Complexes of tpa Ligands with 6-Phenyl Substituents (Ph_ntpa). Structure and H_2O_2-Reactivity
   Tetsuro Tano, Yoshitaka Doi, Masayuki Inosako, Atsushi Kunishita, Minoru Kubo, Hirohito Ishimaru, Takashi Ogura, Hideki Sugimoto and Shinobu Itoh
   Bull. Chem. Soc. Jpn. **2010**, *83*, 530-538.

2. Oxygenation Chemistry at a Mononuclear Copper(II) Hydroquinone System with O_2
   Kae Tabuchi, Mehmed Z. Ertem, Hideki Sugimoto, Atsushi Kunishita, Tetsuro Tano, Nobutaka Fujieda, Christopher J. Cramer and Shinobu itoh

Inorg. Chem. **2011**, *50*, 1633-1647.

3. Active Site Models for Cu_A Site of Peptidylglycine α-Hydroxylating Monooxygenase and Dopamine β-Monooxygenase
   Atsushi Kunishita, Mehmed Z. Ertem, Yuri Okubo, Tetsuro Tano, Hideki Sugimoto, Kei Ohkubo, Nobutaka Fujieda, Shunichi Fukuzumi, Christopher J. Cramer and Shinobu Itoh
   Inorg. Chem. **2012**, *51*, 9465-9480.

4. Flavonolate Complexes of M^{II} (M = Mn, Fe, Co, Ni, Cu, and Zn). Structural and Functional Models for the ES (Enzyme–Substrate) Complex of Quercetin 2,3-Dioxygenase
   Ying-ji Sun, Qian-Qian Huang, Tetsuro Tano and Shinobu Itoh
   Inorg. Chem. **2013**, *52*, 10936-10948.

Acknowledgments

The author would like to express his gratitude to Professor Shinobu Itoh for his kind guidance, excellent suggestions, and encouragement throughout this work.

The author is deeply grateful to Professor Kazuya Kikuchi and Professor Shunichi Fukuzumi for their helpful comments.

The author is deeply grateful to Associate Professor Hideki Sugimoto and Assistant Professor Nobutaka Fujieda for their useful suggestions.

The author desires to his heartily thanks to Professor Christopher J. Cramer and Dr. Mehmed Z. Ertem of University of Minnesota for his cooperation of theoretical calculations.

The author is deeply grateful to Professor Takashi Ogura and Dr. Satoru Yamaguchi, Dr. Minoru Kubo and Ms. Kaoru Mieda of University of Hyogo for their cooperation in resonance Raman measurements.

The author is deeply grateful to Professor Shunichi Fukuzumi and Dr. Kei Ohkubo (Osaka University) for his cooperation in EPR measurements.

The author desires to express his sincere thanks to Dr. Atsushi Kunishita for his useful suggestion.

The author thanks all technicians in Laboratory for Instrumental Analysis, Graduate School of Engineering, Osaka University for some kinds of analysis (NMR, Mass Spectrometry and Elemental Analysis).

Thanks are also given to all member of Bio-Functional Chemistry (BFC) Laboratory at Division of Advanced Science and Biotechnology, Graduate School of Engineering, Osaka University for valuable suggestions and kindly friendship.

Finally, the author acknowledges continuous encouragement and assistant given by his father, Nobuyoshi Tano, his mother, Toshiko Tano, his brother, Yosuke Tano, and his friends.

Tetsuro Tano
Division of Advanced Science and Biotechnology
Graduate School of Engineering
Osaka University

Osaka, Japan
January, 2014